

UNIVERSITA' DEGLI STUDI DI FIRENZE
Facoltà di Scienze Matematiche, Fisiche e Naturali



“Structural investigation of nanostructures electrodeposited on Silver single crystals”

Dottorato di Ricerca
in Scienze Chimiche
XXIII ciclo

**Tesi di
Elisa Lastraioli**

Tutore:
Prof. Maria Luisa Foresti

Coordinatore:
Prof. Andrea Goti

Settore disciplinare: CHIM 02

SUMMARY

1	INTRODUCTION	1
1.1	Introduction to Nanotechnology and Nanostructures	2
1.2	Sulfur based nanostructured compound semiconductors	3
1.3	Metallic and bimetallic nanostructures as catalysts for Oxygen Reduction Reaction	5
1.4	Object of the thesis	7
1.4.1	Underpotential Deposition	11
1.4.2	Electrochemical Atomic Layer Epitaxy	12
1.4.3	Surface Limited Redox Replacement	14
1.4.4	Self Assembled Monolayers	14
2	OUTLINE	19
	Electrodeposition on Silver single crystals	19
2.1	Preparation of semiconductor thin films by ECALE method	19
2.1.1	Structural investigation of the first layer of Sulfur-based semiconductor: STM study of the structure of the first layer of Sulfur deposited at underpotential on Ag(100) and Ag(110)	19
2.1.2	Electrodeposition and structural analysis of CdS thin films on Ag(100) and Ag(110)	31
2.1.3	Electrodeposition of PbS on Ag(111)	36

2.2	Electrodeposition of metal mono and multilayers on Ag(111)	46
2.2.1	Electrodeposition of Cadmium Sulfide on Ag(111) for the obtainment of Cadmium single layers	48
2.2.2	Electrodeposition of Cobalt Sulfide and Iron sulfide on Ag(111) for the obtainment of Cobalt and Iron single layers respectively	52
2.2.3	Surface Limited Redox Replacement (SLRR) method for Cobalt single layer deposition	57
2.3	Electrodeposition Confined into nanosized patterns and Catalysis towards Oxygen Reduction	59
2.3.1	Electrodeposition of Cadmium Sulfide into a patterned hexadecanethiol Self Assembled Monolayer obtained by microcontact printing	59
2.3.2	Confined Electrodeposition of CdS in the Holes Left by the Selective Desorption of 3-Mercapto-1-propionic Acid from a Binary Self-Assembled Monolayer Formed with 1-Octanethiol	63
2.3.3	Confined Electrodeposition of Cadmium Sulfide in the Holes Left by the Selective Desorption of 3-Mercapto-1-propionic Acid from a Binary Self-Assembled Monolayer Formed with 1-Dodecanthiol	73
2.3.4	Cobalt deposition into the pattern obtained by selective desorption of the short chain-thiol from a binary alkanethiol SAM and catalysis towards oxygen reaction reaction	81
	Electrodeposition on Gold single crystal	91
2.4	Electrodeposition of Palladium on Au(111)	91
2.5	Structural analysis of a SAM of 4-Mercaptopyridine on Au(111) covered by one monolayer of Palladium.	98
3	CONCLUSIONS AND PERSPECTIVES	104
4	REFERENCES	107

1 INTRODUCTION

The possibility of driving the preparation of nanostructures, controlling their dimension and composition, is one very important objective towards future improvements of present-day research in several fields.

Until now, research on nanostructures has contributed to the development of a number of current and emerging technologies and in addition to the progress of nanoscience.

The great interest in nanometer-scale materials stems from the fact that their optical, electrical, magnetic, or mechanical properties are often very different from those of the same materials in the bulk phase and, what is more important, they can be tuned by changing the physical dimensions of the material.¹

In microelectronics, smaller has always meant more components per chip, a faster response, lower material consumption, lower cost, lower power consumption and improved performance. The trend towards miniaturization also involves important applications, including energy, photonics, nanobiotechnology, devices and sensors.

In this context, this thesis is directed to the realization, by means of electrodeposition, of nanometric and subnanometric materials with potential important applications like photovoltaic and catalysis.

Known methods of surface limited electrodeposition, alone and combined with the use of appropriately designed templates, led to the obtainment of different kinds of nanostructures: single atomic layers, nanostructured thin films and islands. These nanostructures have been divided into two main classes: Sulfur based compound semiconductors and metallic nanostructures, both of which have been accurately characterized by means of electrochemical techniques and Scanning Probe Microscopy.

An accurate structural study of the first layer of Sulfur on Silver single crystals, performed with in-situ Scanning Tunneling Microscopy, opens the thesis and introduces the topic of thin films of Sulfur based compound semiconductors, which always have Sulfur as a first layer.

Then, metal single and multilayer preparation on Ag(111) is described for several metals. In addition to Underpotential Deposition (UPD), the method of Surface Limited Redox Replacement elaborated by Adžić has been successfully applied for those elements that can not be deposited at underpotential. Moreover, for metals which do not present UPD on Silver, a novel method of deposition of single and multiple layers has been elaborated.

After the preparation of layers and multilayers of metals and semiconductors on the whole Silver surface, the same techniques have been employed for the electrodeposition confined into suitable nanostructured templates. Templates are insulating layers with natural or artificial holes in which deposition occurs. Two kinds of thiol based Self Assembled Monolayers (SAMs) have been used as templates: patterns originated by stamps with microcontact printing (μ CP) and templates originated by selective desorption of one component from binary SAMs. Using these templates, metallic electrodeposited nanostructures have been opportunely designed and tested as catalysts towards an important electrocatalytic reaction: the Oxygen reduction reaction (ORR). In particular, electrodeposition of non-noble metals, supposed to have synergic catalytic activity with Silver towards ORR, was performed in order to study the catalytic properties of different bimetallic catalysts and to stress the role of the surface morphology and structure.

1.1 Introduction to Nanotechnology and Nanostructures

Nanotechnology is defined as design, fabrication and application of nanostructures, and the fundamental understanding of the relationship between physical properties or phenomena and material dimensions. In particular, design and fabrication of nanostructures are the essential aspects of nanotechnology, since studies on new physical properties and applications of nanostructures are possible only when nanostructures are made available with the desired size, morphology, structure and chemical composition.

Nanotechnology deals with materials or structures – like clusters, crystallites, layers or molecules - in nanometer scales, typically ranging from subnanometers to several hundreds of nanometers.

The intense academic and industrial interest in nanostructured materials stems from the remarkable variations in fundamental electrical, optical and magnetic properties that occur as one progresses from an ‘infinitely extended’ solid to a particle of material consisting of a countable number of atoms. Their uniqueness is due partially to the very large percentage of atoms at interfaces and partially to quantum confinement effects, that make possible to tune their properties by changing the physical dimensions of the material. Some of these properties are already known. For example, band gaps of semiconductors can be tuned by varying material dimension. There may be many more unique physical properties not yet known. These new physical properties or phenomena promise new advancement in technology. For example, ultra-strong and ultra-light multifunctional materials may be made from hierarchical nanostructures. Nanotechnology also promises the possibility of creating nanostructures of metastable phases with non-conventional

properties including superconductivity and magnetism. Yet, another very important aspect of nanotechnology is the miniaturization of current and new instrument, sensors and machines that will greatly impact the world we live in. Examples of possible miniaturization are: computers with infinitely great power, biosensors, nanorobots.

Their great potential of improving performance and capabilities of materials, make the nanostructures important in a number of applications, from nanoscale electronics and optics, to nanobiological systems and nanomedicine, to new materials, and therefore it requires the contribution from multidisciplinary teams of physicists, chemists, material scientists, engineers, molecular biologists, pharmacologists and others to work together on (i) synthesis and processing of nanomaterials and nanostructures, (ii) understanding the physical properties related to the nanometer scale, (iii) design and fabrication of nano-devices or devices with nanomaterials as building blocks, and (iv) design and construction of novel tools for characterization of nanostructures and nanomaterials.

Synthesis and processing of nanomaterials and nanostructures constitute the essential aspect of nanotechnology. Studies on new physical properties and applications of nanomaterials and nanostructures are possible only when they are made available with desired size, morphology, structure and chemical composition.

Work on the fabrication and processing of nanomaterials and nanostructures started long time ago, far earlier than nanotechnology emerged as a new scientific field. Such research has been drastically intensified in the last decade, resulting in overwhelming literatures in many journals across different disciplines. The research on nanotechnology is evolving and expanding very rapidly.

Between the different methods of preparation of nanostructures, *electrodeposition* is a well-suited technique, for several reasons. It is a low temperature technique, thereby minimizes grain growth, and allows a very high degree of control over the amount of material deposited through the Faraday's laws, which relate the amount of material deposited to the amount of charge passed, or surface limited processes.

Two main classes of nanostructures, prepared by electrodeposition, are treated in this thesis: Sulfur based nanostructured compound semiconductors and metallic nanostructures as catalysts for ORR.

1.2 Sulfur based nanostructured compound semiconductors

The compound semiconductors result from the combination of two or more elements. Thus, unlike Silicon, which is an intrinsic semiconductor and, hence, is characterized by well defined electronic properties, they yield materials with optoelectronic and electronic properties included in a vast range. For this reason,

they can be used in operations which are beyond the physical limits of Silicon electronic properties. For example, the higher mobility of electrons allows the use of higher frequencies. Moreover, some compound semiconductors are able to work in very severe conditions as regards to the temperature or the high presence of radiations.

Epitaxy enhances all properties of the compound semiconductors. An important prerequisite for epitaxial growth is an ordered substrate, such as the surface of a single crystal. Another important prerequisite is a good match between the lattice constant of the compound and that of the substrate. A significant example is offered by the growth of quantum dots of Cadmium Selenide (CdSe) on Au(111) as compared with the analogous growth on Pd(111). In the first case, the very low mismatch (ca. 0.6%) between the lattice constant of CdSe and Au(111) leads to the formation of CdSe(0001), whereas, in the latter case the high mismatch (4.1%) causes the formation of an amorphous deposit². However, the most important prerequisite for epitaxy seems to be the method used for the compound growth. From this point of view, the most suitable methods are those based on layer-by-layer growth, such as those involving self-limiting chemical reactions. In general, these methods can be referred to as “Atomic Layer Epitaxy” (ALE), a term often used to indicate processes based on the reaction of molecular species from the gas phase. The same self-limiting mechanism of growth can also take place when the reactants are ionic species in solution, and in this case the methods are known as SILAR (Successive Ionic Layer Adsorption and Reaction)³ and ECALE (Electrochemical ALE)⁴.

The use of single crystals increases the probability for epitaxial growth, since the high-order structure of the first UPD layer, that is, the layer of the first element deposited on the metal used as a substrate, favors the ordered deposition of the second layer and of the successive ones. In other words, the crystallinity of the substrate is at least partially transferred to the compound during the growth. As a matter of fact, all Cadmium and Zinc Sulfides obtained on Ag(111) exhibit crystalline structures and have good semiconductor properties.^{5,6,7,8}

For example, binary semiconductors are considered important technological materials because of their potential applications in optoelectronic devices, solar cells, IR detectors and lasers.⁹ Binary compounds of group IIB and group VIA elements, commonly referred to as II-VI compounds, have important technological applications. Thin films of these compounds are usually prepared by vacuum evaporation, chemical vapor deposition, sputtering and spray pyrolysis methods¹⁰, while here we present the advantageous method of electrodeposition. The crucial point in material electrodeposition is to control the dimensions of the electrodeposited structures. Of course, compound electrodeposition also requires composition control, that is to say the right stoichiometric ratio. Combining dimensional and composition control allows the attainment of compound semiconductor thin films, which is our field of interest. The semiconductive layers

of electronics and optoelectronics devices, must be, as possible, crystalline and, still better, epitaxial. In fact, small amounts of stress can shift the luminescent properties, and a small number of defects can provide recombination centers that lower the device's efficiency.

Moreover, a good deal of importance towards Sulfur based compound semiconductors is warranted by the renewed interest toward their application in solar cells and thermoelectric materials.

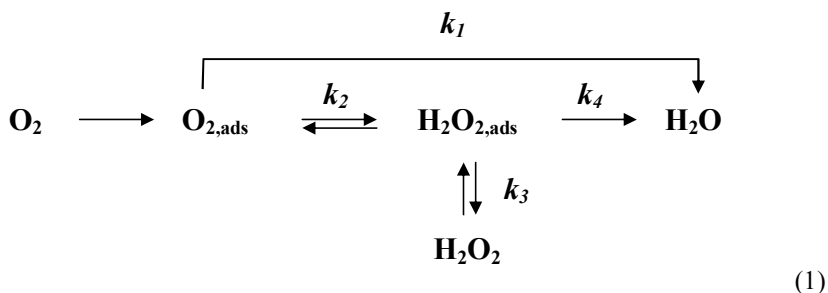
At the present, the task for renewable energy resources is stimulating the research for new materials allowing to set up low cost and high conversion efficiency solar cells. Lowering the costs of raw materials, as well as increasing attention paid to the environmental consequences of the industrial production, drive the development and the choice of materials on the basis of their chemical composition. Sulfur based compound semiconductors are good candidates for photovoltaic systems, either in terms of reduction of costs and of increase of efficiency. The so-called thin film, or second generation, solar cell containing Cu(In,Ga)Se_2 (CIGS) and CdTe are already on the market. These reach a maximum efficiency of about 20% and are presently representing about 12 % of the photovoltaic market. However, elements with which these materials are built raise troubles concerning the rarity of the resources (Indium) and environmental pollution (Selenium). Comparative compound semiconductors are thus considered, in order to achieve the best performance, without including toxic or rare elements in their bulk compositions.

1.3 Metallic and bimetallic nanostructures as catalysts for Oxygen Reduction Reaction

Oxygen reduction reaction (ORR) is regarded as one of the most important electrocatalytic reactions in electrochemical energy conversion systems and in several industrial processes. However, the high overpotential for the ORR requires an intensive use of expensive catalysts such as Platinum. In spite of many attempts in the last decade to create non-Platinum catalyst for low temperature ($<200^\circ\text{C}$) air cathodes, Platinum remains the catalyst of choice at least for acid-based fuel cells.

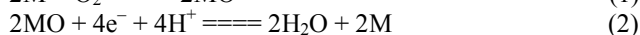
The situation in alkaline electrolyte is rather different from acid electrolyte, and many opportunities are offered for non-Platinum catalysts for the ORR.

Although there are numerous reaction pathways and schemes proposed for the ORR, it appears that the one presented below is the most appropriate for the ORR on the Platinum group and IB group metals:^{11,12,13,14,15,16}



On the basis of this reaction scheme, three reaction pathways are possible. One is direct four-electron O_2 reduction to water (rate constant k_1) where first electron transfer is immediately followed by breaking of the O-O bond (no peroxo intermediates). The second possible pathway is two electron reduction to H_2O_2 (rate constant k_2), which can be either a final product (rate constant k_3) or further be reduced to H_2O (rate constant k_4), i.e. the so called *serial four-electron pathway*. The analysis for the ORR on Pt(hkl) and Au(hkl) single-crystal surfaces supports the serial reaction pathway.^{11,12,13,14,15,16} The same pathway with a very small (0.5–2.5%) peroxide formation is most likely operative on Ag(hkl) in KOH.¹¹ On the contrary, analogous analysis carried out in acidic medium shows that the four-electron pathway takes only place at the highest overpotentials, whereas at the lowest overpotentials only the two-electron pathway, with 100% of H_2O_2 , occurs.¹⁶ Moreover, at the same temperature and overpotentials, the kinetics of the ORR always increases in the order $(100) \leq (111) \leq (110)$, indicating that the reaction is structure-sensitive.

A promising strategy is the use of bimetallic catalysts, such as Cobalt-Palladium, that have been shown to reach the performance of Platinum. While the elementary steps of the Oxygen reduction are not yet firmly established, thermodynamic analyses suggest that the ORR at a metal (M) electrode can be viewed as consisting of an initial dissociative chemisorption step (1) followed by the four-electron reduction of the oxide to water (2).



Analysis of thermochemical data for these two reactions spanning a wide range of metals indicates that elements, which form stable bonds to O, perform well for O_2 bond scission and poorly for O atom reduction. Conversely, metals that reduce adsorbed O atoms efficiently, are ineffective with respect to O_2 bond scission. Based on these observations, a simple guideline for the development of bimetallic catalysts has been proposed: combine a metal that is good at O-O bond scission with a second metal that reduces adsorbed O atoms efficiently.^{17,18} Besides the experimental evidence of catalytic activity of the Silver-Cobalt mixtures spotted on glassy carbon substrates,¹⁷ theoretical predictions based on ab-initio-derived thermodynamic

guidelines indicate that other silver-based bimetallic catalysts could be employed.¹⁸ Both Refs 17 and 18 refer to the acidic medium. However, according to Ref. 19 the same adsorbed intermediates are provided for the Oxygen reduction mechanism both in acidic and in alkaline medium, thus suggesting that the guidelines reported in Refs 17 and 18 could be extended to the alkaline medium.

With the aim of completely remove Platinum and replace it with less expensive materials, guidelines for the design of bimetallic electrocatalysts for cathodes for Direct Alcohol Fuel Cell (DAFC), in which the Oxygen reduction takes place, have been proposed assuming a simple mechanism where one metal breaks the Oxygen-Oxygen bond of molecular O₂ and the other metal acts to reduce the resulting adsorbed atomic Oxygen.^{17,18} Besides the experimental evidence of catalytic activity of the Silver-Cobalt mixtures,¹⁷ the theoretical predictions indicate that other Silver-based bimetallic catalysts could be employed either for Cobalt and for Iron.¹⁸ The catalytic properties of Silver have been reported long ago.^{14,20,21,22,23} For practical catalysts the morphology-activity relationship is a topic of fundamental and technological significance. Reference 24 reports the strong morphology dependence of the catalytic activity of Palladium toward the ORR and with more than 100 references represents a good state-of-art on ORR catalysis. Well-ordered metal layers can be obtained by exploiting surface phenomena such as Underpotential Deposition (UPD).²⁵ UPD layers can also be used as template for the spontaneous deposition of a more noble metal monolayer, and the procedure can be repeated to form a multilayer of the noble metal.^{26,27} UPDs are also used for the formation of compounds by the Electrochemical Atomic Layer Epitaxy (ECALE) technique.⁴

In this thesis, the research activity focused on the Oxygen reduction reaction is based on the use of Silver substrates as cathodes. The intent is to study the catalytic effect of Silver substrates electrochemically modified at nanometer scale through the surface alloying with metals able to exert synergic effects on the catalytic properties of Silver, and to stress the role of the surface morphology and structure. Well-ordered layers of such metals will be obtained by exploiting surface phenomena such as Underpotential Deposition (UPD) and Surface Limited Redox Replacement (SLRR), described in the following paragraphs 1.4.1 and 1.4.3. In addition, a new deposition method – Selective Electrodesorption Based Atomic Layer Deposition (SEBALD) – is described in the section 2.2.

1.4 Object of the thesis

The object of the present thesis is the electrochemical preparation of nanostructures on Silver single crystals, with their electrochemical and microscopic characterization. Atomic Force Microscopy (AFM) was used to characterize

morphology and nanometer range structure, whereas Scanning Tunneling Microscopy was used to determine atomic structures. There is a wide range of nanostructures in electrochemistry, including metal clusters, islands, wires and layers. Here, we refer either to the deposition of monoatomic layers of different elements forming a compound or to metal nanostructured islands, according to the different applications for which they have been designed. Namely, two main classes of nanostructures, described in the paragraphs 1.2 and 1.3, have been electrodeposited on Silver: well ordered nanostructured thin films of compound semiconductors and metallic nanolayers and nanoclusters. In addition, the evaluation of the catalytic activity towards Oxygen reduction of the latter ones has been performed.

The following paragraphs of the Introduction contain a brief description of each of the following surface limited electrodeposition methods used to prepare nanostructures on Silver:

-Underpotential Deposition (UPD)

-Electrochemical Atomic Layer Epitaxy (ECALE)

-Surface Limited Redox Replacement (SLRR)

-Selective Electrodesorption Based Atomic Layer Deposition (SEBALD)

All these methods of electrodeposition have been used either on the whole Silver surface and on surfaces covered by nanostructured templates to obtain confined deposits where a further control on the lateral growth was added to the vertical one. Templates have been obtained using thiol based Self Assembled Monolayers (SAMs), which are described in the last paragraphs of the Introduction (1.4.4.1 and 1.4.4.2). It must be noted that the SEBALD method has been first proposed in this thesis and it is still under study.

Most of the work was done on Silver single crystals and is divided in the first three sections of the *Outline* of the thesis. The development of each part has been driven by different purposes and applications, that are here briefly explained:

-2.1 Preparation of semiconductor thin films by ECALE method.

The binary sulfides prepared by ECALE are generally grown starting from a Sulfur layer deposited at underpotential. The use of single crystals increases the probability for epitaxial growth, since the high-order structure of the first UPD layer, that is, the layer of the first element deposited on the metal used as a substrate, favors the ordered deposition of the second layer and of the successive ones. In other words, the crystallinity of the substrate is at least partially transferred to the compound during the growth. Since the crystalline structure of metal sulfides obtained on Ag(111) is often responsible of their good semiconductor properties: the possibility to control the deposition of the first layer is of fundamental importance for the quality of the final product.

Therefore, the study of Sulfur based semiconductor thin films prepared by ECALE on Ag(111) starts with the accurate study of the very early stage of their preparation, that is the electrodeposition of the first layer of Sulfur on Silver single crystals. The structure of the Sulfur UPD layer on Ag(111) was thoroughly investigated by Scanning Tunneling Microscopy (STM).²⁸ The analogous investigation carried out on Ag(100) and Ag(110) in this thesis aims to complete the picture of the Sulfur UPD on Silver. A deep characterization in terms of geometry and coverage of the Sulfur adlayers formed in the underpotential region was done with in-situ Electrochemical STM and Chronocoulometry.

The semiconductor compounds grown by ECALE in this thesis are Lead Sulfide (PbS) and Cadmium Sulfide (CdS). The deposition of PbS, developed on the whole Silver surface, required the settlement of the experimental conditions for electrodeposition. On the contrary the experimental conditions for the ECALE deposition of CdS were already well known on Ag(111), but not on the other two low index faces. For this reason, an electrochemical and structural investigation was carried out on CdS thin films grown by ECALE on Ag(110) and Ag(100) in order to complete the overview of CdS on Silver. Results from a structural analysis carried out by Surface X-ray Diffraction revealed a strong influence of the substrate structure on the film order. Indeed, the wurtzite structure was found on Ag(100), while on Ag(110) the contemporary presence of two CdS allotropic structures (wurtzite and zincblende) was observed. Film thickness and surface roughness were determined by X-ray reflectivity. CdS deposition by ECALE was performed again in this thesis. It was used to develop the new SEBALD method (section 2.2) and as an “electrodeposition probe” for the study of electrodeposition within nanostructured templates (section 2.3).

-2.2 Electrodeposition of metal mono and multilayers on Ag(111).

The possibility of synergic effects of some metals on the catalytic activity of Silver led us to study the way to perform controlled deposition of Cobalt or Iron on Silver. In fact, these metals cannot be deposited at underpotential on Silver, and any attempt to control the deposition at overpotential, even at potentials slightly negative to the Nernst value, didn't allow an effective control. To this purpose, two possible methods to control electrodeposition, have been taken into account.

The first one is the new “SEBALD” method, here elaborated and characterized, that needs two steps. First, the deposition of one or more layers of a metal sulfide compound is done by the ECALE method. The successive cathodic stripping of Sulfur leaves the metallic element on the surface. The method can also be used to obtain metal layers of controlled thickness. In fact, the basic ECALE cycle can be also repeated to increase the thickness of the sulfide, so that the successive selective desorption of Sulfur leaves increasing amounts of metals. This method has been valuated and characterized with the well-known compound CdS, and then applied to the new compound studied, Cobalt Sulfide (CoS) and Iron Sulfide (FeS).

The second method of controlled electrodeposition is the Surface Limited Redox Replacement (SLRR), elaborated by Adžić and explained in the paragraph 1.4.3, that was used for the deposition of Cobalt on Silver.

-2.3 Electrodeposition Confined into nanosized patterns and Catalysis towards Oxygen Reduction Reaction

Electrodeposition on Silver, within the holes of patterned thiol Self Assembled Monolayers (SAMs), was performed using the same methods performed on the whole surface. Various sized and shaped patterns of the insulating layer gave rise to different nanostructures. A first type of SAM patterned by microcontact printing was used to perform electrodeposition of CdS limited to stripes. A second type of pattern was originated by selective desorption of one component of binary SAMs. These templates were first characterized using CdS as an electrodeposition probe and then used for metal electrodeposition. The study of metallic nanostructures obtained with this method on Silver aims to design, develop and value a series of Platinum free catalysts for cathodes of Direct Alcohol Fuel Cells (DAFCs). Electrodeposition of nanostructured layers and clusters of non-noble metals (Cobalt and Iron) on Silver, exploiting surface limited phenomena like Underpotential Deposition (UPD) and Surface Limited Redox Replacement (SLRR), was performed on the surface covered by templates.

The contents described until now can be summarized in the following draft:

			Method used	Metals/ compounds deposited
What is deposited	Metal layers	Metals that give UPD on Ag	UPD	Cd, Zn.
		Metals that do not give UPD on Ag	“Selective Electrodeposition Based Atomic Layer Epitaxy” ⇒	Cd, Co, Fe.
			“Surface Limited Redox Replacement” of metal monolayer ⇒	Co.
	Nanostructured Semiconductors		⇒ ECALE	PbS, CdS, CoS.

All methods of surface limited electrodeposition above are used for the obtainment of different nanostructures:





		Method used	Metals/ compounds deposited
Structure of the deposit	On the whole surface	UPD	S, Zn.
		SLRR	Co.
		SEBALD	Co, Fe.
		ECALE	CdS, PbS, CoS.
	Confined in nanotemplates	  μ CP stripes 530nm large	CdS.
		 binary SAMs  Islands covering 12-22-30-39% of the total area	CdS, Zn, Co.

Table I Draft of the thesis

At the end of the thesis, the sections 2.4 and 2.5 are dedicated to a project carried out in an external laboratory (University of Ulm, Germany).

The same concepts of Underpotential Deposition and SAM formation are applied to Au(111). More precisely, the Underpotential Deposition of Palladium on Au(111) was followed by in-situ STM, with the determination of the structures of the first two layers of Palladium. After that one layer of Palladium was deposited on Au(111), the morphology of a SAM of 4-Mercaptopyridine formed on it was studied by in-situ STM.

1.4.1 Underpotential Deposition

Underpotential Deposition (UPD) is the well-known phenomenon²⁵ whereby the deposition of one element occurs at a potential preceding the Nernstian equilibrium value. Actually, Underpotential Deposition occurs when the depositing element is able to somehow interact with the substrate, so that the deposition of the layer in direct contact with the substrate occurs at a potential preceding bulk deposition, that

is, the deposition of the element on itself. Underpotential Deposition is a surface-limited phenomenon, so that the resulting deposit is generally limited to an atomic layer. This circumstance is easily confirmed by the independence of the height of the corresponding voltammetric peak upon the bulk concentration of the depositing element and, thus, ensures atomic-level control in the deposit.

Moreover, when UPD is performed on a single-crystal face, as done in this thesis, the resulting deposit is generally epitaxial, namely it is strongly affected by the crystallographic orientation of the substrate.

In the present thesis, different techniques are used to study the conditions and characterize the phenomenon of Underpotential Deposition. An accurate analysis by cyclic voltammetry, Scanning Tunneling Microscopy and Chronocoulometry has been performed to study the deposition of the first layer of Sulfur on the low index faces of Silver. Then, Underpotential Deposition of some metals on the first layer of Sulfur on Ag(111) have been characterized by cyclic voltammetry and, in some cases, by AFM.

1.4.2 Electrochemical Atomic Layer Epitaxy

The Electrochemical Atomic Layer Epitaxy (ECALE) method was proposed by Stickney⁴ to obtain a low-cost production of structurally well-ordered compound semiconductors on polycrystalline and single crystal Gold substrates. Its name comes from the evident analogy with the Atomic Layer Epitaxy (ALE) techniques, from which ECALE differs because of the use of potential in place of temperature to limit deposition. The method is based on the alternate Underpotential Deposition of atomic layers of the elements that form the compound, in a cycle that can be repeated as many times as desired. Each cycle of deposition forms a monolayer of compound, and the number of cycles determines how thick the deposit will be. The ECALE procedure requires the separate UPD of both elements which form the compound, with each deposition being followed by rinsing the cell with an inert electrolyte. The negative free energy change involved in the formation of the compound is the principal reason for the occurrence of the UPD of the metal on the non metal previously deposited, and viceversa. The major advantage of this method is that the individual steps of each cycle can be examined and optimized independently. This means that the conditions for deposition can be adjusted according to potentials, pH, reactants, the times of deposition and so on. These conditions are strictly dependent on the compound that must be obtained, and on the substrate used. Once the deposit is formed, the amount of the elements deposited in a given number of cycles is quantitatively determined from the charge involved in the anodic stripping of the metallic element and the cathodic stripping of the non-

metallic element. Plots of the charges for metal and Sulfur measured in the stripping as a function of the number of cycles are linear, suggesting a layer-by-layer growth. Of course, the use of single crystal substrates increases the probability of the epitaxial growth. ECALE has been used to produce a wide variety of well-ordered semiconductor deposits under ambient pressure and temperature.

In this thesis, the method was employed for the growth of metal sulfur thin films on Ag(111). The different compounds were obtained by depositing alternate layers of Sulfur and metal at underpotential. Almost all depositions were carried out using ammonia buffer solutions of pH about 9.6 as supporting electrolyte. A complexing agent such as ammonia is necessary to keep metals in solution at this relatively high pH, which, on the other hand, is preferred to not alter the sulfur deposits.

Experimental arrangement

An automated deposition apparatus consisting of Pyrex solutions reservoirs, solenoid valves, a distribution valve and a flow-cell was used under the control of a computer. The electrochemical cell was a Kel-F cylinder with about a 10 mm inner diameter delimited by the working electrode on one side and the counter electrode on the other side (Figure 1). The inlet and the outlet for the solutions were placed on the side walls of the cylinder. The counter electrode was a gold foil, and the reference electrode was a Ag/ AgCl/ KCl sat placed on the outlet tubing. Both the distribution valve and the cell were designed and developed in the workshop of our Department.



Figure 1 Scheme of the flow electrochemical cell with the inlet for solutions (a), the counter electrode (b), the outlet for solutions (c), the reference electrode (d) and the working electrode (e).

1.4.3 Surface Limited Redox Replacement

The method, proposed by Adžić et al. for metal deposition²⁶, consists in the replacement of an ordered metal layer obtained by UPD by a more noble metal.

The first step of the technique involves the formation of the UPD adlayer of a metal M on a substrate S at underpotential. In the second step, the adlayer of metal M is replaced by a more noble metal P in an electroless deposition process. The replacement of M occurs via an irreversible and spontaneous redox process in which the UPD layer is oxidatively dissolved by cations of more noble metals, which are simultaneously reduced and deposited. The substrate metal S has to be more noble than the metal undergoing deposition (P) in order to avoid its oxidation.

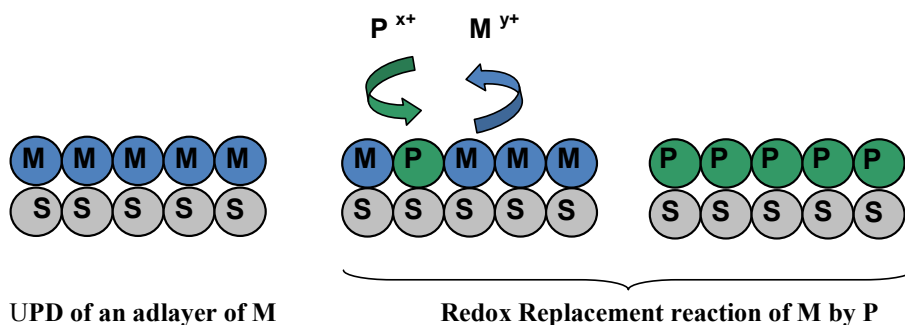


Figure 2 Scheme of Surface Limited Redox Replacement

1.4.4 Self Assembled Monolayers

Self assembled monolayers (SAMs) are organic assemblies formed by the spontaneous adsorption of molecular constituents from solution or gas phase onto solid surfaces. The adsorbates organize spontaneously, and sometimes epitaxially, into crystalline or semicrystalline structures. The molecules or ligands that form SAMs have a chemical functionality, or “headgroup”, with a specific affinity for a substrate. There are a number of headgroups that bind to specific metals, metal oxides and semiconductors. The most extensively studied class of SAMs is derived from the adsorption of alkanethiols on Gold, Silver, Copper, Palladium, Platinum, and Mercury.²⁹ The high affinity of thiols for the surfaces of noble and coinage metals allows the generation of well-defined organic surfaces with useful and highly alterable chemical functionalities displayed at the exposed interface.

SAMs are the most elementary form of a nanometer-scale organic thin-film material, their thickness is typically 1-3 nm, and therefore are nanostructures. SAMs are well-suited for studies in nanoscience and technology because (i) they are easy to prepare, (ii) they form on objects of all sizes and are critical components for stabilizing and adding function to nanostructures, (iii) they can couple the external environment to the electronic (current-voltage responses, electrochemistry) and optical (local refractive index, surface plasmon frequency) properties of metallic structures, and (iv) they link molecular-level structures to macroscopic interfacial phenomena, such as wetting, adhesion and friction.

In this thesis, SAMs formed on Silver have been used as insulating nanostructured layers for confined electrodeposition (section 2.3). They were formed by microcontact printing and by selective desorption of binary SAMs, which are explained in the following paragraphs.

Moreover, a heteroaromatic thiol SAM was object of study in the section 2.5. A study of stability and morphology of the SAM on Gold and Palladium was performed.

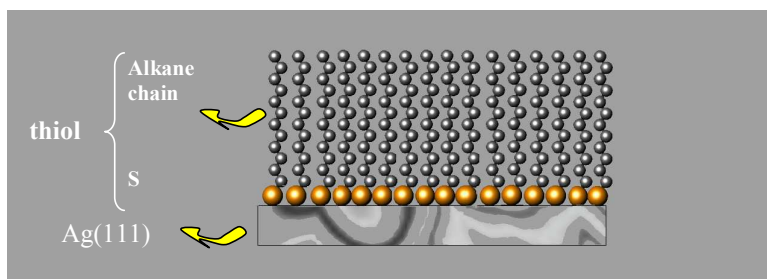


Figure 3 Structure of an alkanethiol SAM on Ag(111)

Aromatic and heteroaromatic SAMs

In recent years, aromatic thiol SAMs have received attention because of their high conductivity and strong structural rigidity, compared to conventional alkanethiol SAMs, making them interesting for molecular electronics and electrode modification.^{30,31,32}

It has been realized that the electronic properties of SAMs strongly depend on molecular orientations, adsorption conditions, and intermolecular interactions. Therefore, the control of the structural ordering of aromatic thiol SAMs has become a crucial issue in tailoring various SAM properties.

Moreover, SAMs of thiols containing aromatic or heterocyclic groups have the capacity to immobilize biological molecules or protein on surfaces^{33,34,35} and, when containing functionalized headgroups, SAMs can be used to detect metal ions in very low concentrations.³⁶ A recent application of functionalized SAMs, when end groups can coordinate ions of metals in solution, is the deposition of a metal layer

on top of the SAM. This process of metallization of the SAM has been successfully developed by Kolb and coworkers using several kind of substrates and thiols.^{37,38} Selective adsorption of metal ions on the pyridine end group is followed by the reduction of the complexed metal, giving rise to islands of metal on top of the SAM. One chapter of the thesis is dedicated to the study of a heteroaromatic thiol SAM. We have characterized the structure and electrochemical behavior of 4-mercaptopyridine SAM on Au(111) covered by one layer of Palladium using EC-STM and cyclic voltammetry.

1.4.4.1 Microcontact Printing

Microcontact printing (μ CP) is a widely used top-down approach to create patterns. It consists of a high-resolution technique used to transfer a pattern from an elastomeric stamp to a solid substrate by conformal contact. The method was introduced by Whitesides and co-workers,^{39,40} who brought a polymer inked with alkanethiols into contact with a Gold substrate to form a striped SAM in the area of contact. Since long chain thiols act as insulators, this arrangement can represent a starting point for the attainment of nanocircuits.

Chapter 2.3.1 describes the use of μ CP for the formation of a hexadecanethiol (HDT) striped SAM on Ag(111). It acts as a template for the confined electrolyrodeposition of CdS within the submicrometric stripes of HDT deposited on Ag(111).^{41,42}

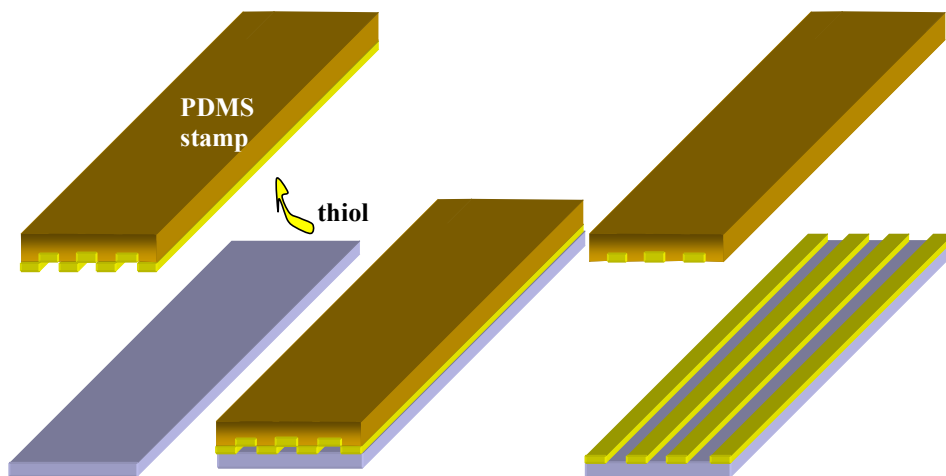


Figure 4 Scheme of μ CP technique

1.4.4.2 Binary SAMs and selective desorption of one component for preparation of templates

Monolayers comprising a well-defined mixture of molecular structures are called “mixed” SAMs. There are three easy methods for synthesizing mixed SAMs: (i) coadsorption from solutions containing mixtures of thiols ($\text{RSH} + \text{R}'\text{SH}$), (ii) adsorption of asymmetric disulfides (RSSR'), and (iii) adsorption of asymmetric dialkylsulfides (RSR').

The adsorption of mixtures of thiols ($\text{RSH} + \text{R}'\text{SH}$) allows the formation of SAMs with widely varying compositions,⁴³ as shown in the section 2.3. The mole fraction of a specific adsorbate in the SAM does not necessarily reflect the same mole fraction of the adsorbate in solution. Experimental conditions can bias the relative ratio of the molecular components constituting the SAM: for example, the choice of solvent can modify the relative mole fractions of adsorbates in SAMs formed from a mixture of polar and non polar molecules.⁴⁴ Similarly, SAMs composed of two different alkanethiols having different chain lengths exhibit phase separation at the nanometer scale on Gold and Silver surfaces that allows the engineering of ordered, two-dimensional systems with Angstrom-level control over thickness and structure simply varying the composition of the mixture.^{45,46,47,48,49,50,51,52,53} The domain distribution of the two thiols of the binary mixture strongly depends on the difference in chain length.⁵⁴

In particular, an almost homogeneous phase is formed when thiols have comparable length; otherwise, they form separate phases as shown by STM investigations.^{55,56,57,58,59,60} Since the desorption potential is progressively more negative the longer the alkanethiol chain is, the application of a suitable potential will allow the desorption of the shortest thiol chain. The selective desorption of the shortest chain thiol leaves a domain of free electrode surface available for the subsequent readsorption of different thiols,^{61,62} thus suggesting a possible use as a template for electrodeposition.

This is what has been done in the section 2.3 of the thesis, in which the adsorption of two mixed SAMs on Ag(111) have been accurately studied with electrochemical techniques and AFM. The systems 1-octanethiol/3-mercaptopropionic acid (chapter 2.3.2) and 1-dodecanethiol/3-mercaptopropionic acid (chapters 2.3.3-2.3.4) were studied and used as templates for confined electrodeposition.

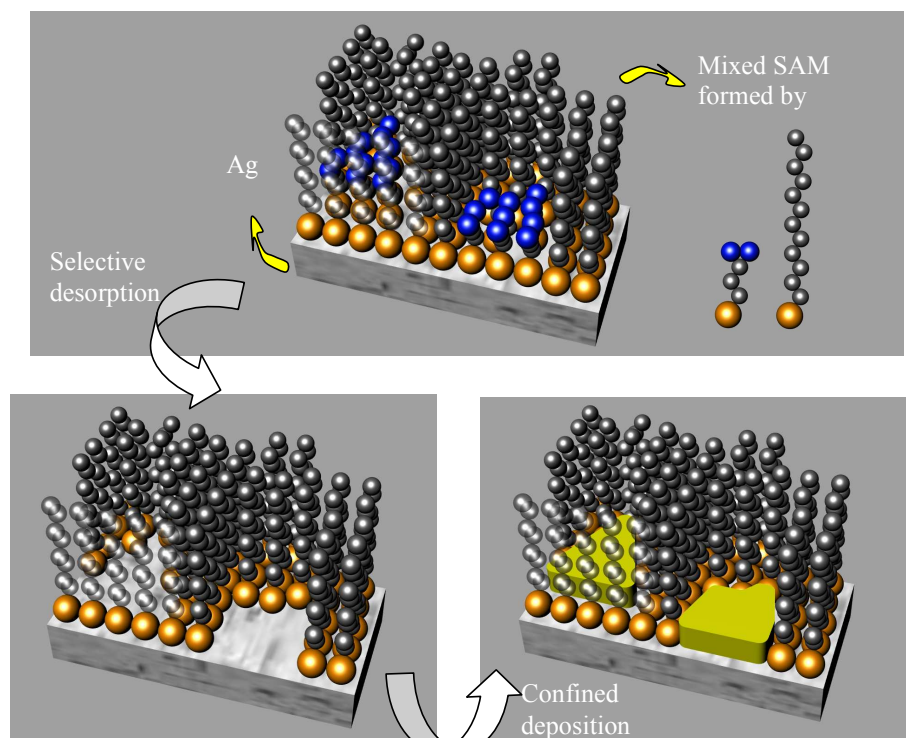


Figure 5 Scheme of electrodeposition confined within mixed SAM based templates

2 OUTLINE

Electrodeposition on Silver single crystals:

2.1 Preparation of semiconductor thin films by ECALE method

2.1.1 Structural investigation of the first layer of Sulfur-based semiconductor: STM study of the structure of the first layer of Sulfur deposited at underpotential on Ag(100) and Ag(110)

Introduction

The present chapter aims to detail the formation of the first layer of Sulfur at underpotential on Ag(100) and Ag(110), that is the very first stage of deposition of metal sulfides grown by ECALE. While the structure of the Sulfur UPD layer on Ag(111) was thoroughly investigated in our laboratory by scanning tunneling microscopy (STM),²⁸ the analogous investigation carried out on Ag(100) and Ag(110), here presented, aims to complete the picture of Sulfur UPD on Silver.

STM is a powerful tool for structural investigations since it allows the study of the structure of the species grown at the very early stages of deposition.

The STM investigation of Sulfur UPD on Ag(111) revealed two main structures depending on the applied potential: a $(\sqrt{3} \times \sqrt{3})R30^\circ$ at potentials positive to -1.1 V/SCE and a $(\sqrt{7} \times \sqrt{7})R19.1^\circ$, marked by a transition peak, at -0.89 V/SCE. The latter structure confirmed previous results obtained by Rovida in UHV⁶³. A complete survey of the behavior of molecular S₂ on Ag(111) in UHV was recently proposed by M. Yu et al.⁶⁴ who used different techniques, such as STM, LEED, XPS and NIXSW, to obtain surface characterization and further structural information. Interestingly, they proposed the same $(\sqrt{7} \times \sqrt{7})R19.1^\circ$ structure for both Sulfur and methanethiolate formed on the surface. And, in fact, the phase

formed by Sulfur on a Silver surface is important as a starting point to determine the structural organization of thiols and, in general, of molecules adsorbed by the thiol group onto a specific surface⁶⁵. Moreover, a Sulfur adlayer deposited on Silver is an appropriate substrate to investigate adsorbed organic molecules, since the weak van der Waals interactions of the S-molecule drive self-ordering processes better than strong molecule-surface interactions that hinder molecule mobility⁶⁶.

Apart from the electrochemical measurements reported by White and co-workers^{67,68}, there are few papers concerning STM measurements on Ag(100) and on Ag(110) surfaces.

Sulfur adsorption was already object of STM in-situ studies on other metal single crystals, such as Gold and Copper. On these metals, the process was studied on faces (111)^{69,70,71} and (100)^{72,73}.

In the following, electrochemical measurements and electrochemical scanning tunneling microscopy (EC-STM) results obtained for the underpotential deposition of Sulfur from Na₂S solution in 0.1 M NaOH on Ag(100) and on Ag(110) are presented. The cyclic voltammogram on Ag(100) presents two broad peaks, whereas three partial overlapping peaks and a sharper one are observed on Ag(110). STM measurements carried out during the whole UPD process show that progressively more compact structures are formed as the applied potential is scanned toward more positive potentials. More precisely, p(2x2), c(2x6) and c(2x2) were found on Ag(100) at E = -1.25, -1.0 and -0.9 V, respectively. Less definite conclusions can be drawn for the structures of Sulfur overlayers on Ag(110). However, the experimental findings are consistent with an incomplete p(2x1) at potentials preceding the sharp peak, and with a c(2x2) structure at E = -0.9 V vs Ag/AgCl, KCl_{sat}. The coverage values calculated on the basis of the hypothesized structures have been compared with the values obtained from chronocoulometric measurements at the most positive potentials investigated.

Thus, the experimental coverage $\theta = 0.5$ coincides with the coverage calculated for the c(2x2) structure found on Ag(110) at E = -0.9 V by STM, whereas the experimental coverage $\theta = 0.42$ suggests that a mixture of structures c(2x6) and c(2x2) is formed on Ag(100).

Experimental Section

Merck Suprapure NaOH and Aldrich analytical reagent grade Na₂S were used without further purification. The water used was obtained from mineral water by distilling it once and then distilling it again using alkaline permanganate while constantly discarding the heads. The solution was freshly prepared because aged sulfide solutions yielded in situ STM images of polysulfide chains on Silver that were not observed when using freshly prepared solutions.

Suitable Silver single crystals were prepared in our laboratory. The solidification of melted silver was force started from a seed according to the Bridgman technique. Globe-shaped single crystals of 12 mm diameter were prepared, and after identifying the desired crystallographic orientation, the face of interest was isolated by cutting with a slow saw. Mechanical polishing with progressively finer papers and then with alumina powder of different grades, down to 0.3 μm (Buehler Micropolish) allowed us to obtain a mirror-like surface⁷⁴.

Before each measurement, a clean and oxide free surface was ensured by chemical polishing using a following a procedure elaborated by Hamelin⁷⁵ based on a Japanese patent⁷⁶. It consists in the surface oxidation of silver by means of a solution 0.15M CrO_3 and 0.1M HCl . After polishing, the electrode is soaked first in a concentrated ammonia solution for about 5 minutes, and then in concentrated sulphuric acid for about 20 minutes. Finally, it is thoroughly rinsed with water.

Terraces of sufficiently large size were obtained by annealing the crystals in an inert gas atmosphere at 500 $^\circ\text{C}$.

The in-situ STM measurements were performed with a Molecular Imaging STM (Pico SPM). The tips used were prepared from 0.25 mm diameter tungsten wire (Aldrich) by electrochemical etching in a 2 M NaOH solution, or by cutting a Pt-Ir (80:20) wire. To minimize faradaic current at the tip-electrolyte interface, the tips were covered with Apiezon wax.

In this paper, the topography images are 512x512 pixels obtained with constant-current mode and without further filtration, unless otherwise indicated in the legend. Experimental conditions like tunneling current (I_T) and bias voltage (U_B) are given in the figure captions; positive bias voltages indicate that the tip is positive respect to the sample.

An electrochemical cell in Kel-F was specifically designed and adapted to the STM commercial instrument. The cell has fairly uncommon features: a Ag/AgCl reference electrode, a stable connection through the lower surface of the crystal for the working electrode and a circular Pt counter electrode (Figure 1). The same electrochemical cell and crystals were used for both the voltammetric and STM studies. All potentials are referred to a Ag/AgCl , KCl_{sat} reference electrode.

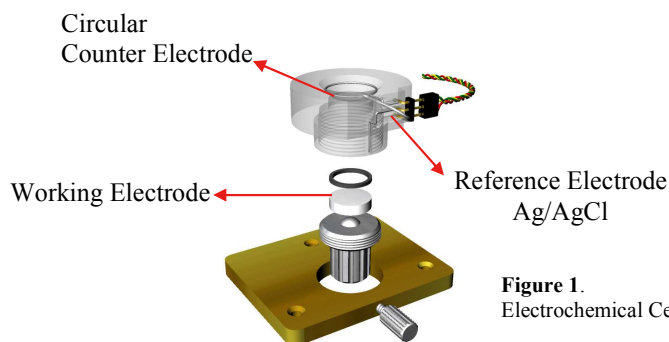


Figure 1.
Electrochemical Cell.

Results and Discussion

Cyclic Voltammetry. A voltammetric study was performed with the electrochemical cell and the crystals described above. Cyclic voltammograms were performed in 1 mM Na₂S and 0.1 M NaOH solutions (pH = 13) in the Sulfur UPD region. This high pH value was chosen to avoid hydrogen evolution that could mask the negative peaks due to Sulfur UPD and to ensure the presence of only one Sulfur-containing species in the solution, i.e. HS⁻.

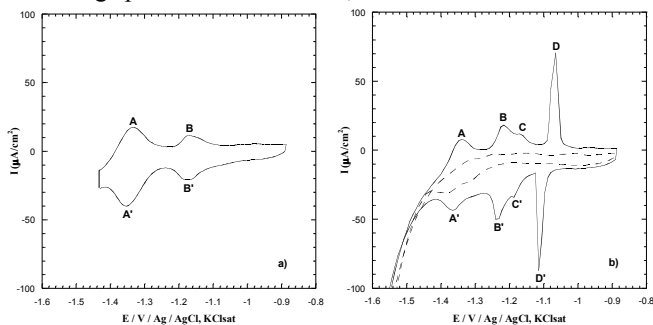


Figure 2. Cyclic voltammograms of Ag(100) (a) and Ag(110) (b) in 1 mM Na₂S in 0.1 M NaOH solutions. Scan rate 50mV/sec. The dashed line in (b) refers to the supporting electrolyte NaOH on Ag(110).

It must be noted that the voltammograms obtained in the STM cell are similar to those reported in the literature^{67,67}, thus suggesting that no leakage of Cl⁻ occurs during experiments.

Cycling the potential between -1.45 and -0.9 V on Ag(100) yields only two broad anodic peaks at -1.32V (A) and -1.15V (B) with the corresponding cathodic peaks A' and B' (Figure 1a). On the contrary, cycling the potential between -1.55 and -0.9 on Ag(110) yields three partially overlapping anodic peaks at -1.34 (A), -1.22 (B), -1.17 (C) and a sharper one at -1.06 V (D) with the corresponding cathodic peaks A', B', C' and D' (solid curve in Figure 1b).

It is worthwhile to note that on Ag(110) and Ag(100) the underpotential deposition of Sulfur occurs at more negative potentials than on Ag(111)^{67,77}, in agreement with the more negative value of the potential of zero charge (pzc) of these faces. (The potential of zero charge of the faces (111), (100) and (110), as measured in an apspecifically adsorbed electrolyte such as KPF₆, are -0.695, -0.865 and -0.975 V/SCE respectively⁷⁸).

Apart from the values of the potential, the shape of Sulfur UPD on Ag(110) is similar to the one reported for Ag(111). In particular, the very narrow and sharp shape of peak D seems to indicate a two-dimensional phase transition similar to that proposed for Ag(111) on the basis of a chronocoulometric investigation.⁷⁹ An analogous chronocoulometric investigation carried out for Ag(110) didn't give satisfying results. However, the presence of two-dimensional phase transitions taking place in electrode processes was determined by cyclic voltammetry, by scanning the potential in the UPD region from low to moderately high scan rates (ν) and measuring the current peak, I_p , the peak's half-width, $\Delta E_{p/2}$, (i.e. the width, in millivolts, at the peak's half-height) and the difference, ΔE_p , between the reduction and oxidation peak potentials⁸⁰. In the presence of two-dimensional growth mechanism, plotting $\log I_p$, $\log \Delta E_{p/2}$ and $\log \Delta E_p$ against $\log \nu$ should yield slopes of 0.6, 0.4 and 0.4 respectively. The analysis carried out on the UPD region of Sulfur on Ag(110) yielded the expected slope values (Figure 3).

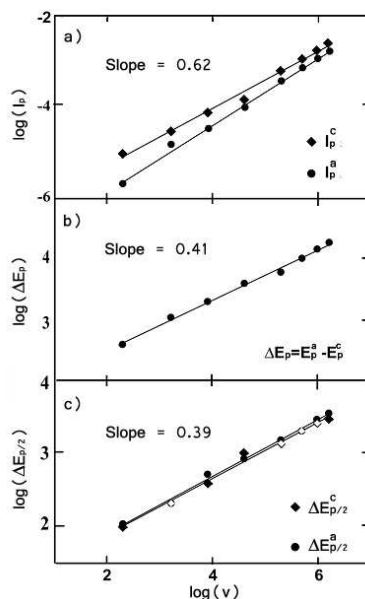


Figure 3. Scan rate (ν) analysis of S UPD on Ag(110) based on the procedure reported in Reference 21

Chronocoulometric Measurements. The charges involved in the UPD region were accurately calculated using potential-step chronocoulometry. To this end, the applied potential was stepped from a variable initial potential to a fixed final potential $E_f = -1.5$ V, at which Sulfide desorption is rapid and almost complete, and the resulting current was analogically integrated over time. The initial potential E was progressively varied from -1.5 to -0.9 V in 25 mV increments. The rest time at

potential E was made long enough to ensure the attainment of adsorption equilibrium.

Plotting the cathodic charge density $Q(E,t)$ vs time t showed an abrupt rise followed by a modest linear increase in time due to the current of hydrogen evolution, that is constant at E_f . Linear extrapolation of these plots to $t=0$ yielded the charge density, Q_0 , corrected for the faradaic contribution due to hydrogen evolution. The curves indicated by circles in Figure 4 show the plotting of Q_0 vs E obtained for Ag(100) (a) and for Ag(110) (b). Note that for Ag(110) the charge plot (Fig. 4b) shows a slight inflection corresponding to the transition from peak A to peaks (B+C) of Figure 1b and two well-defined plateaus corresponding to the potential region between peaks C and D and to the region positive to peak D, respectively. Apart from the potential range, this behavior is identical to the one observed on Ag(111) and reported before⁹. Dashed lines in Figure 4 are the Q_0 vs E plots provided by 0.1 M NaOH under otherwise identical conditions.

The vertical distances between the plateaus of both the circles curves and their corresponding dashed ones give the charges involved in the Sulfur UPD region. These charges are $163 \mu\text{C cm}^{-2}$ for Ag(100) and $137 \mu\text{C cm}^{-2}$ for Ag(110). Retaining the results previously obtained on Ag(111)⁸¹, we assumed that at the most positive potentials investigated an almost complete charge transfer of two electrons per Sulfide ions occurred. Thus, considering that the area of the surface unit cell for Ag(100) is 8.35 \AA^2 and that for Ag(110) is 11.81 \AA^2 , the respective coverage values are $\theta = 0.42$ and $\theta = 0.50$. The coverage obtained on Ag(111) with the same procedure was $\theta = 0.43$ ²⁸

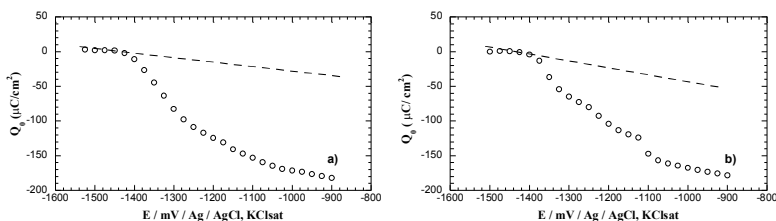


Figure 4. Chronocoulometric charge vs potential curves for Ag(100) (a) and Ag(110) (b) 0.1 M NaOH in the absence (dashed lines) and in the presence of 1 mM Na_2S (circles).

STM Investigation of Sulfur on Ag(100). The Silver (100) crystal, prepared as described above, was brought into contact with the electrolyte at a potential of -1.5 V at which Sulfur was not adsorbed, and then the potential was scanned in the positive direction.

Because of the closeness of Hydrogen evolution to the beginning of Sulfur deposition, it was not possible to image the bare silver substrate before deposition to have a direct relationship between structure and substrate. Therefore, all STM

images reported hereafter refer to the default instrument calibration. However, the distances reported in the text as well as in the profiles of Figure 6 have been calculated on the basis of the calibration determined in a separate experiment on graphite HOPG.

The large scale morphology of the surfaces remained nearly unchanged whether in the absence or presence of sulfur in solution. In both cases the surface appeared to be composed of atomically smooth terraces separated by atomic steps.

The atomically resolved topography of a little silver terrace covered by the Sulfur adlayer clearly indicates its square geometry, whose measured lattice constants are 0.57 ± 0.01 and 0.58 ± 0.01 nm (Figure 5).

Such values are close to double the lattice constant of Ag(100), in agreement with a 0.25 coverage $p(2 \times 2)$, in which Sulfur atoms are situated in equivalent highly coordinated 4-fold sites. This structure will be referred as phase I, whose schematic representation will be shown later in Figure 6.

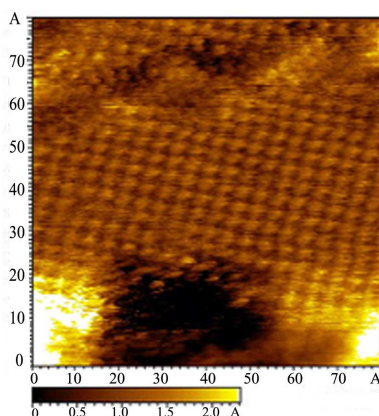


Figure 5. 8 nm x 8 nm STM image of Ag(100) in 1 mM Na₂S, 0.1 M NaOH. Electrode potential $E = -1.25$ V, $I_T = 1.2$ nA, $U_B = 0.71$ V.

A positive potential scan beyond peak B of Figure 2a, led to a phase transition that resulted in a more dense structure (referred to phase II in Figure 6) in which atoms are ordered in pairs of spots forming parallel rows.

The STM image in Figure 6 shows various domains of phase II meeting perpendicularly. Profile a shows that the distance between two S atoms in a row is 0.57 ± 0.01 nm whereas in profile b the distance between aligned pairs is 0.41 ± 0.01 nm within a pair and 0.83 ± 0.01 nm between two adjoining rows.

Thus, single rows are made up of pairs of atoms spaced from each other 2 times the Silver lattice constant ($2r_{Ag}$) and are composed of atoms that are distant $\sqrt{2}r_{Ag}$ from each other.

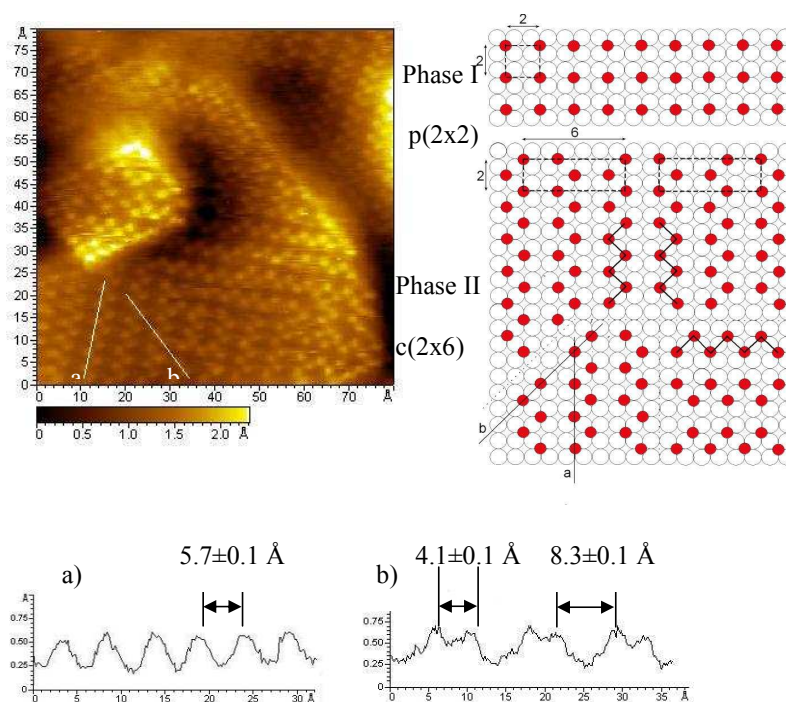


Figure 6. Left: 8 nm x 8 nm STM image of Ag(100) in 1 mM Na₂S, 0.1 M NaOH. Electrode potential $E = -1.0$ V, $I_T = 4.5$ nA, $U_B = 0.18$ V. (a) and (b) are cross-section profiles of the lines in the image. Right: Schematic ball-model structures of sulfur phases I and II on Ag(100). In the model for phase II perpendicular rows made up of paired spots are connected and profiles a and b are drawn.

The proposed structure of geometry c(2x6) and coverage 0.33, again considers atoms sitting in alternating 4-fold sites, confirmed by the constant intensity of the brightness of the spots.

Imaging of both structures I and II in a single experiment (Figure 7) allowed us to compare their lattice directions and dimensions. Figure 5 shows the transition phase due to the potential step from -1.0 V to -1.25 V. It can be noted that the direction of the main rows in phase II is the same as that in phase I. Both Figures 4 and 5 show that phase II forms two domains rotated by 90° with respect to each other, as can be expected for a rectangular adlattice on the square substrate.

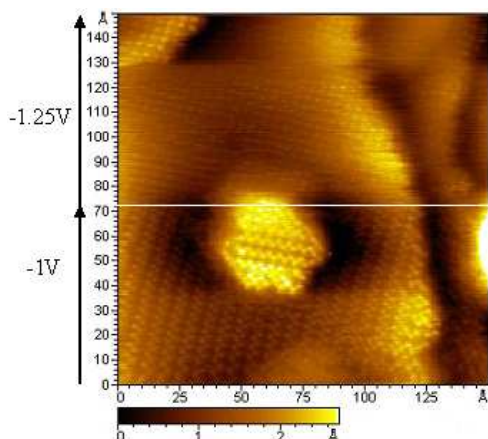


Figure 7. 15 nm x 15 nm STM image of Ag(100) in 1 mM Na₂S, 0.1 M NaOH. Electrode potential: lower part: $E = -1.0$ V, phase II; upper part: $E = -1.25$ V, phase I. $I_T = 4.5$ nA, $U_B = 0.43$ V.

Increasing the potential to -0.9 V reveals large areas of a compact adlayer are observable (Fig. 8). These areas are rotated 45° compared to the phase II layer and have a shorter S-S distance which would indicate a $c(2 \times 2)$ structure corresponding to 0.5 coverage (see the schematic representation in Fig. 8).

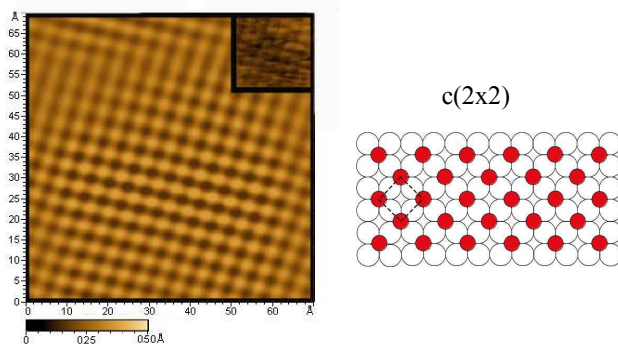
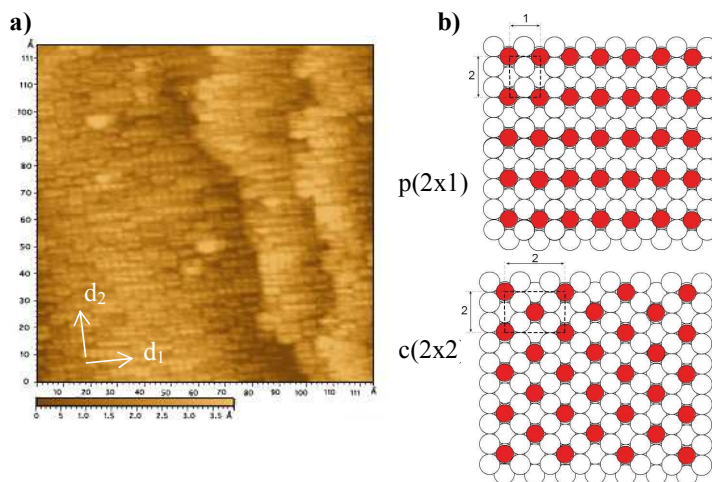


Figure 8. On the left: 7 nm x 7 nm STM image of Ag(100) in 1 mM Na₂S, 0.1 M NaOH. $E = -0.9$, $I_T = 1$ nA, $U_B = 0.20$ V. The image is band-pass filtered, and an inset of the original image is placed in the upper right corner. Right: Schematic ball-model structure of Sulfur phase $c(2 \times 2)$ on Ag(100).

It must be noted that on Cu(100) the sulfur adlayer forms structures analogous to those formed on Ag(100), with the exception that the Copper lattice constant is too small to allow for the formation of the $c(2 \times 2)$ phase⁷². On the contrary, the $c(2 \times 2)$ structure is formed on Au(100) whose lattice constant is equal to that of Ag(100).⁷³

STM Investigation of Sulfur on Ag(110). It is well-known that single crystal surfaces characterized by low density elementary cells result in more stepped surfaces. Among the low Miller index faces of Silver, for example, the achievement of atomically flat terraces decreases with the order of atomic density: $\text{Ag}(111) > \text{Ag}(100) > \text{Ag}(110)$ ⁷⁵. The problems connected with silver surface preparation explain why STM investigations are more frequently carried out on $\text{Ag}(111)$ and $\text{Ag}(100)$ than on $\text{Ag}(110)$. Furthermore, the study of the early stages of deposition is complicated by the overlapping of Hydrogen evolution that is catalyzed by Sulfur. Therefore, STM measurements performed at $E = -1.2$ V show $\text{Ag}(110)$ surfaces already covered by the earliest aligned sulfur deposits. Figure 9a shows rows of incomplete Sulfur deposits, interrupted by several vacancies. From that image, the measurement of the distances between Sulfur atoms within a row and between two adjoining rows yields 0.42 ± 0.01 nm in the direction indicated by arrow d_1 and 0.57 ± 0.02 nm in the direction indicated by arrow d_2 . The position of the crystallographic axes of $\text{Ag}(110)$ underneath the Sulfur layer cannot be unambiguously identified. In fact, the uncovered surface of silver (110) could be imaged only at very negative potentials where hydrogen evolution hinders STM measurements. However, such distances are close to the characteristic lattice constants of $\text{Ag}(110)$, respectively twice the Ag-Ag nearest neighbors distance $2r_{\text{Ag}}$ and the distance between two (110) troughs ($\sqrt{2}r_{\text{Ag}}$). For this reason, we can reasonably suppose the formation of an incomplete structure of geometry $p(2 \times 1)$, as depicted in Figure 9b.



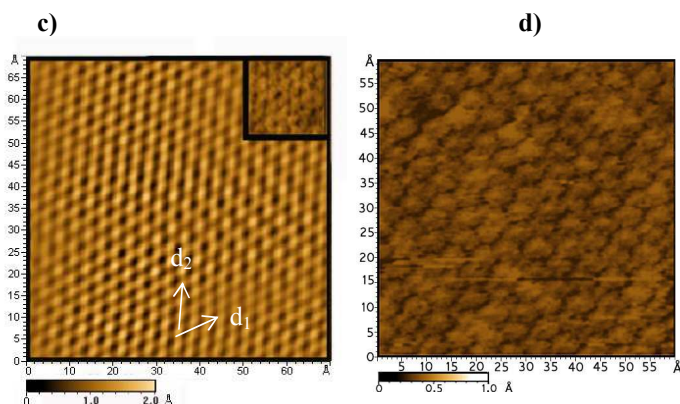


Figure 9. (a) Atomically resolved 12 nm x 12 nm STM image of Ag(110) in 1 mM Na₂S, 0.1 M NaOH. $E = -1.2$ V, $I_T = -1.5$ nA, $U_B = 0.41$ V. (b) Schematic ball-model structure of Sulfur phases p(2x1) and c(2x2) on Ag(110) (c) 7 nm x 7 nm STM image of Ag(110) in 1 mM Na₂S, 0.1 M NaOH. $E = -1.0$ V, $I_T = -1.5$ nA, $U_B = 0.21$ V. The image is band-pass filtered, and an inset of the original image is placed in the upper right corner. (d) 6 nm x 6 nm STM image of Ag(110) in 1 mM Na₂S, 0.1 M NaOH. $E = -0.9$ V, $I_T = 1.0$ nA, $U_B = 0.43$ V.

Before peak D of Figure 2b, the adlayer still appears formed by parallel lines conserving the same direction even at more positive potentials.

A compact and uniform structure was observed only after the sharp peak D at $E = -1.0$ V (Fig. 9c). Such a structure does not conserve the rectangular geometry of p(2x1); conversely, it is a pseudo-hexagonal one. Parts a and c of Figure 9 refer to the same sample at $E = -1.2$ and $E = -1.0$ V, respectively. We can observe a slight rotation of about 8° of d_2 direction and a larger rotation of about 30° for d_1 from Figure 9a to 9c. Distances between atoms from Figure 9c are 0.57 ± 0.02 nm along the d_1 direction and 0.51 ± 0.02 nm along the d_2 direction. The more defined structure formed after peak D of Figure 2b can also be observed in the image taken at -0.9 V (Figure 9d).

It should be noted that the impossibility of unambiguously determining the relationship of the sulfur adlayer with the crystallographic directions of the substrate makes us not completely sure the structure hypothesized for the compact layer. However, the above findings are consistent with a c(2x2) structure with a coverage $\theta = 0.5$ (Figure 9b). Considering a two electron exchange per Sulfide ion, the calculated value of transferred charge is $136 \mu\text{C}/\text{cm}^2$, in excellent agreement with the experimental value of $137 \mu\text{C}/\text{cm}^2$ obtained by the charge versus time plot within the potential range -1.5 V / -0.9 V (Figure 4), which covers nearly the whole adsorption process.

Conclusion

Our STM study of Sulfur adsorption on Ag(100) and Ag(110) in 0.1 M NaOH electrolyte revealed new information about the surface structure of an intriguing electrochemical system.

The cyclic voltammogram performed in a Sulfur ion solution on Ag(100) presents two broad peaks in the UPD region. STM measurements revealed the existence of three different structures dependent on the applied potential. The first structure is $p(2 \times 2)$ with $\theta = 0.25$ at a potential of -1.25 V, i.e. slightly after the first peak. The second structure is $c(2 \times 6)$ with $\theta = 0.33$ at a potential of -1.0 V, i.e. slightly after the second peak. Finally, by increasing the potential to -0.9 V, i.e. slightly before the bulk Silver Sulfide formation, the latter structure was observed to coexist with an even more compact structure $c(2 \times 2)$ with $\theta = 0.5$. The hypothesis of mixed $c(2 \times 6)$ and $c(2 \times 2)$ structures is consistent with the coverage $\theta = 0.42$ obtained from chronocoulometric measurements that only yield average values.

Three partially overlapping peaks and a sharper one are observed on Ag(110). It should be noted that the impossibility of unambiguously determining the relationship of the Sulfur adlayer with the crystallographic directions of the substrate makes us not completely sure of the structures hypothesized for the Sulfur adlayers on this face. However, the STM study revealed that after the second peak, at -1.2 V, a significant amount of Sulfur is already deposited on the surface, forming interrupted lines that are consistent with the formation of an incomplete structure of geometry $p(2 \times 1)$. At $E = -0.9$ V, i.e., after the sharp peak, the structure does not conserve the rectangular geometry of $p(2 \times 1)$ but changes into a pseudohexagonal one. The distances between Sulfur atoms suggest a $c(2 \times 2)$ structure with a coverage of $\theta = 0.5$, in good agreement with chronocoulometric measurements.

2.1.2 Electrodeposition and structural analysis of CdS thin films on Ag(100) and Ag(110)

Introduction

In our laboratory, ECALE method has already been employed to produce well-ordered deposits of Cadmium Sulfide (CdS) on Ag(111) that have proved to be crystalline and to have good semiconductor properties.^{5,6,77}

Up to now the electrodeposition of CdS on Silver by ECALE was investigated only on Ag(111) single crystal electrodes, and no information had been reported about the influence of substrates surface lattice on the crystallographic structure of the film.

This chapter reports the electrochemical and structural investigation carried out on CdS thin films grown by ECALE on Ag(110) and Ag(100).

The charge values measured in the anodic and cathodic strippings of CdS indicate that the amount of Cadmium and Sulfur deposited in a given number of cycles is a function of the number of cycles employed which is consistent with layer-by-layer growth. The charges associated with each layer of Cadmium and Sulfur, give the right 1:1 stoichiometric ratio between the elements, indicating the formation of a compound. Results from a structural analysis carried out by Surface X-ray Diffraction revealed a strong influence of the substrate structure on film order. Indeed, the wurtzite structure was found on Ag(100), while on Ag(110) the contemporary presence of two CdS allotropic structure (wurtzite and zinblende) was observed. Film thickness and surface roughness were determined by X-ray reflectivity.

Experimental Section

Reagents and electrochemical preparation For the electrochemical growth we used, without any further purification, Merck analytical reagent grade $3\text{CdSO}_4 \cdot 8\text{H}_2\text{O}$, Fluka analytical reagent grade Na_2S and Merck analytical reagent grade KClO_4 . Moreover, double distilled water, Merck analytical reagent grade HClO_4 (65%) and NH_4OH (33%) were used to prepare solutions of pH 9.6 ammonia buffer. The solutions were freshly prepared just before the beginning of each series of measurements.

Suitable Silver single crystals were prepared in our laboratory. Silver single crystal spheres were grown in a graphite crucible according to the Bridgman technique. They have been oriented and cut along the crystallographic direction in order to obtain Ag(110) and Ag(100) oriented electrode. Surface were then polished with emery paper (BuehlerMet SiC) and successively finer grades of alumina powder down to 0.05 μm (Buehler Micropolish II).⁷⁴ Before each measurement, the electrode was chemically polished using a patented procedure based on CrO_3 .^{75,76}

An automated deposition apparatus consisting of Pyrex solution reservoirs, solenoid valves, a distribution valve and a flow-cell was used under the control of a computer. The electrolytic cell was a Teflon cylinder with about a 6.7 mm inner diameter and a 40 mm outer diameter, whose inner volume, 0.5 ml, was delimited by the working electrode on one side and the counter electrode on the other side. The inlet and the outlet for the solutions were placed on the side walls of the cylinder. The counter electrode was gold foil, and the reference electrode was an Ag/AgCl/sat. KCl placed on the outlet tubing. Both the distribution valve and the cell were designed and realized in the workshop of our Department.⁷⁷ If not otherwise specified, all potentials are referred to the Ag/AgCl(sat KCl) electrode.

Surface X-ray diffraction and X-ray reflectivity The experiments were carried out at the ID03 beamline of the European Synchrotron Radiation Facility (ESRF) in Grenoble. SXRD and XRR measurements were performed on a six circle diffractometer in vertical geometry. Samples were mounted on the diffractometer stage enclosed in a mylar bag filled with Nitrogen to prevent surface damage by Oxygen and Ozone. X-ray energy was chosen to be 12.4 keV corresponding to a wavelength 1.00 Å.

Intensities of the CdS (001) specular rod were corrected considering the illuminated surface area, the polarization of the incident beam and the Lorentz factor. Modeling and simulation of the CdS (001) CTRs are described in the next section.

Reflectivity curve were fitted using the software PARRAT32⁸², a general purpose program developed at the HMI Institute of Berlin. The code is based on the Parrat formalism⁸³ and includes a roughness factor in the fitting parameter calculated according to Nevot and Croce.⁸⁴

Results and Discussion

Sulfur and Cadmium UPD deposition The formation of the first layer of Sulfur on Ag(111), Ag(100) and Ag(110) has been already extensively investigated using cyclic voltammetry^{67,67} and STM.^{28,85} Electrochemical measurements show that Sulfur UPD deposition processes differ significantly on the three Silver faces and, accordingly, in-situ STM experiments evidenced the presence of different ordered

Sulfur structures depending on the substrate orientation. Moreover, on Ag(110) and Ag(100) the UPD processes occur at more negative potentials than on Ag(111). In fact, on both faces the Sulfur UPD layer can be obtained (in pH=13 solutions) by applying a potential $E=-0.8V$, whereas on Ag(111) it was obtained at $E=-0.68V$.

For the purposes of the present work, Cd deposition was investigated by cyclic voltammetry both on the bare Ag substrate and on Silver covered by a Sulfur UPD layer (Fig. 1). In the latter case, after Sulfur UPD deposition, the cell was washed with ammonia buffer to eliminate HS^- while keeping the potential at the value of potential of Sulfur deposition. Then, the potential was shifted to $-0.1V$ and the ammonia buffer was replaced by a 5mM $CdSO_4$ in pH 9.6 buffer solution.

Figure 1 shows the UPD process of Cadmium on the three low-index faces of Silver and on the same faces covered by a Sulfur UPD layer. It must be underlined that the figure only reports a single reduction/oxidation peak for each system examined, whereas, on Sulfur-covered Silver, Cadmium underpotential deposition yields two consecutive UPD peaks. However, on Ag(100) the second UPD peak could be well observed only during the anodic scan, whereas the second reduction peaks partly merges with the first one and partly is masked by Cadmium bulk deposition. For this reason we limited the potential range of Fig. 1 to the one corresponding to the first UPD peak. Comparison between the different faces allows to verify that the potential of the reduction/oxidation peaks of Cadmium UPD process on the bare silver follows the trend of atomic density of the different faces. More precisely, the UPD process occurs at more positive potentials on the most compact (111) face and then it follows the order $(111) > (100) > (110)$. This is not surprising since this is also the trend of chemisorption processes on the same faces to which a UPD process could be assimilated. On Sulfur-covered Silver substrates all underpotential deposition/re-oxidation processes are expected to follow the same trend and to occur at still more positive potentials due to the more attractive interaction of Cadmium with Sulfur than with Silver. Indeed, this is generally verified with the exception of Cadmium deposition on Sulfur-covered Ag(100) that is practically coincident with the deposition of Cadmium on the bare Ag(100). This occurrence is an intriguing exception that deserves a deeper investigation, better by means of surface technique such as STM. Tentatively, on the basis of the structural STM investigation that revealed the presence of only one structure of S on Ag(111) and on Ag(110),^{28,85} but a mixture of two different structures on Ag(100), we can assume that a certain degree of “disorder” on Ag(100)⁸⁵ could be responsible of a negative shift of potential for the deposition process. However, once the Cadmium monolayer is formed, its re-dissolution process ranges again with the other faces.

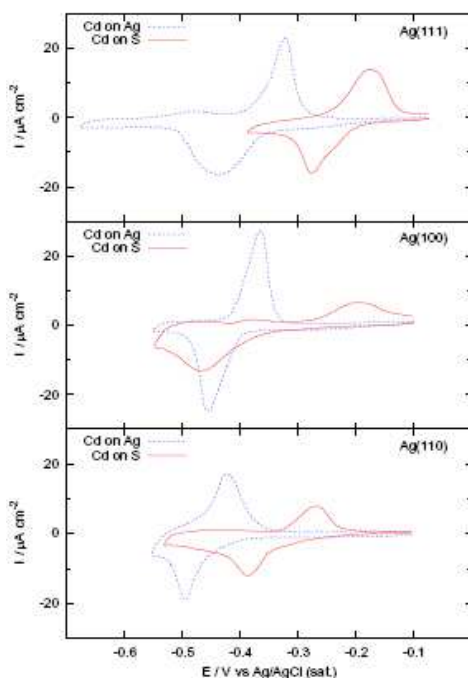


Figure 1 Cyclic voltammograms of Cd on S-covered and bare Ag(111) Ag(100) and Ag(110) from 5 mM CdSO_4 in ammonia buffer pH=9.6 solutions. Scan rate 10mV/sec.

ECALE deposition and electrochemical characterization The experimental sequence of the ECALE cycle necessary to obtain CdS on Ag(110) and Ag(100) was:

- Deposition of Sulfur at -0.68V
- Washing of the cell with supporting electrolyte
- Deposition of Cadmium at -0.6V
- Washing of the cell with supporting electrolyte

This basic sequence is repeated as many times as is necessary to obtain thicker deposits. As usual the amount of the Cadmium and Sulfur deposited in a given number of cycles was estimated from the charge involved in the anodic stripping of Cadmium followed by the cathodic stripping of S.

As already observed for CdS deposition on Ag(111) the stripping potential of Cadmium from CdS shifts as the number of deposition cycles increases, thus indicating that the compound is becoming more stable as the deposit's thickness

increases. The S layers remaining after Cadmium stripping, except for the first layer, behave like bulk Sulfur: hence, during the subsequent reductive stripping, they are reduced at more positive potentials than the first Sulfur layer.

The average charge deposited in each cycle is approximately $85\mu\text{C cm}^{-2}$. This value is calculated by plotting the charges obtained in the stripping of Cd and S as a function of the number of ECALE cycle.

Structural characterization Two stable allotropic structure of CdS are known: wurtzite and zinblende. In previous works on CdS thin films grown by ECALE on Ag(111) only the Wurtzite structure was found.^{5,8}

Since the film structure can be strongly influenced by the substrate lattice, the crystallographic structures of CdS films grown on Ag(100) and Ag(110) are expected to be different respect to the previous findings on Ag(111).

X-ray diffraction experiments were carried out on samples prepared with 30 ECALE cycles deposition on Ag(100) and Ag(110) substrates as described above.

The wurtzite structure was found on Ag(100), while on Ag(110) the contemporary presence of two CdS allotropic structure (wurtzite and zinblende) was observed.

2.1.3 Electrodeposition of PbS on Ag(111)

Introduction

Lead sulfide (PbS) is a binary semiconductor that has received considerable attention because of its variety of applications. In fact, due to its direct band gap of 0.37 eV and absorption coefficient which continuously increase from the infrared through the visible region, PbS has been used in infrared detectors since the mid 1940s.⁸⁶ Like most heavy metal chalcogenides, it seems to be a promising sensor material, particularly for nitrogen oxides.⁸⁷ The techniques commonly used to produce PbS thin films are: electrodeposition,^{88,89} successive ionic layer absorption and reaction (SILAR)^{90,91} and chemical bath deposition (CBD).⁹² A few attempts have been made to investigate the PbS by ECALE method.^{93, 94, 95} This chapter concerns the preparation of PbS grown by ECALE method and its electrochemical and morphological characterization.

In this chapter, the preparation of PbS thin films by ECALE on Ag(111) is described. The electrochemical analysis includes the investigation of the underpotential deposition processes of both Lead and Sulfur, and the characterization of deposits obtained with different deposition cycles to confirm the attainment of the right stoichiometric ratio between Lead and Sulfur. The morphological analysis has been performed by AFM for deposits formed with 50 and 75 deposition cycles and at different times of exposition to the atmosphere.

Experimental

For electrochemical deposition of thin semiconductor films, analytical reagent grade was used, without further purification. Merck $\text{Pb}(\text{NO}_3)_2$ and Aldrich Na_2S were used as sources of Pb and S respectively. HClO_4 (Merck) and NH_4OH (Merck) were used to prepare the pH 9.6 ammonia buffer, whereas $\text{CH}_3\text{COONa}\cdot 3\text{H}_2\text{O}$ (Merck) and CH_3COOH (Merck) were used to prepare the pH 5.0 acetic buffer used as supporting electrolyte. The water used was obtained from mineral water by distilling it once and then, re-distilling it again in alkaline permanganate medium while constantly discarding the heads. The solutions were freshly prepared just before the beginning of each series of measurements.

An automated deposition apparatus, consisting of Pyrex solution reservoirs, solenoid valves, a distribution valve and a flow-cell, which was connected to a computer, was

used. Both the distribution valve and the cell were designed and realized in the workshop of the Department of Chemistry of Florence University. The electrolytic cell was a Teflon cylinder with about 7 mm inner diameter and 42 mm outer diameter, whose inner volume, 0.5 ml, was delimited by the working electrode (WE) on one side and the counter electrode (CE) on the other side. The inlet and the outlet for the solutions were placed on the side walls of the cylinder. The CE was Platinum foil, and the reference electrode (RE) was Ag/AgCl/sat. KCl placed on the outlet tube. The distance between reference and working electrodes introduces resistive contributions that cannot be compensated. However, this cell design with the counter electrode facing the working electrode ensures a high homogeneity of the deposits. The silver single crystals were prepared according to the Bridgeman technique and polished by a CrO₃ based procedure.^{74,75,76}

AFM images were taken with a commercial instrument (PicoSPM, Molecular Imaging) in contact mode with commercial Si₃N₄ cantilever (Nanosensors, Wezlar-Blankenfeld).

Results and Discussion

The growth of PbS multilayer by ECALE exploits the UPD processes of Pb on S and of S on Pb. The negative Gibbs energy change involved in the formation of the compound is the principal reason for the occurrence of the UPD of Pb on the previously deposited S or vice-versa. However, the first atomic layer is formed on the substrate; hence, it is necessary that at least one of the elements forming the compound is deposited on single crystal Ag(111) by a surface limited process. In principle, the semiconductor might be obtained by depositing either the metal or the chalcogen as the first layer. Therefore, for the study of the deposition of the PbS multilayers, the elements were initially examined individually to determine the appropriate conditions for the deposition of the semiconductor.

Formation of Pb and S atomic layers The Pb_{UPD} layer on Ag (111) was performed from 5.0 mM Pb(NO₃)₂ solutions in acetic buffer of pH 5, by scanning the potential from -0.2 V to -0.45 V (Fig. 1). Two well-defined and narrow peaks were observed at -0.35 (B1) and -0.29 V (B2) related to the deposition and dissolution of Pb monolayer, respectively. Here, the difference between the cathodic and anodic peak is somewhat greater than expected, probably due to the uncompensated resistance. However, the shape of cyclic voltammogram of Fig. 1 is consistent to that reported in the literature for the UPD process of lead in acetate medium which is a strong adsorbing electrolyte. In fact, as stressed in Ref.⁹⁶ (and references therein), the electrolyte composition and the presence of adsorbing anion have a significant influence on the UPD process.

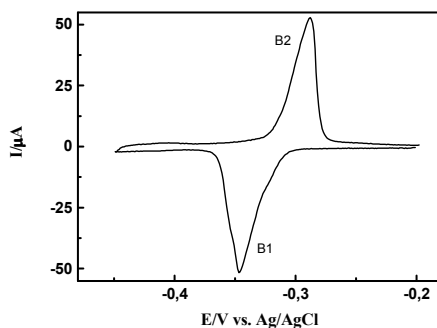


Fig. 1. Cyclic voltammogram of 5.0 mM $\text{Pb}(\text{NO}_3)_2$ in pH 5.0 acetate buffer on Ag(111) substrate, $\nu = 10 \text{ mV s}^{-1}$.

The constancy of the anodic stripping curves of Pb deposited at -0.45V and at different accumulation times ensures that the process is surface limited (Fig. 2).

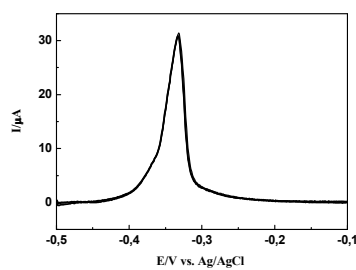


Fig. 2 Coincidence of the stripping curves of Pb_{UPD} deposited at -0.45V for 45, 60 and 90 s.

Integration of this re-dissolution peak yields a charge value of $332 \mu\text{C cm}^{-2}$, which is very close to the value, about $320 \mu\text{C cm}^{-2}$, calculated for a hexagonal Pb monolayer with a near-neighbor distance of 3.4 \AA upon assuming a two electron charge transfer. This near-neighbor distance is that which corresponds to the potential region immediately preceding bulk deposition: at more positive potentials it has been found to slightly and progressively increase.⁹⁶

The underpotential deposition of sulfur on Ag(111) in ammonia buffer has already been extensively investigated and utilized by our group for the attainment of both binary and ternary sulfides.^{77,97,98,99,100}

Here, it is worthwhile to report that the pH 5 acetic buffer necessary to keep lead in solution could cause a partial re-dissolution of a S monolayer deposited on Ag(111). Curve *a* in Fig.3 is the stripping curve of S_{UPD} in ammonia buffer after the electrode has been previously kept for 2 minutes at -0.1V in acetic buffer.

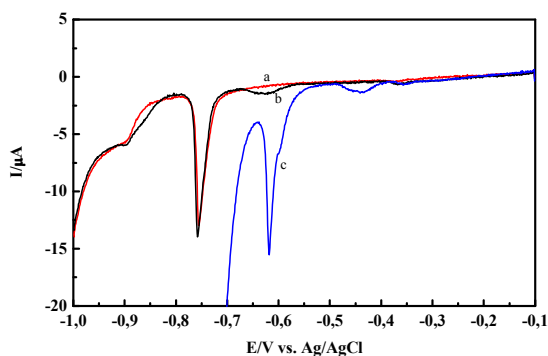


Fig. 3 Stripping curve of S_{UPD} in ammonia buffer after the electrode has been previously kept for 2 minutes at $-0.1V$ in acetic buffer (curve *a*). Stripping curve of S_{UPD} without the washing step with acetic buffer (curve *b*) and stripping curve of S_{UPD} performed in acetic buffer (curve *c*).

For comparison, the figure also reports the curves obtained without the washing step with acetic buffer (curve *b*) and that performed in acetic buffer (curve *c*). Both curves *a* and *c* show a bump in correspondence of the potential of bulk sulfur dissolution. Taking into account the expected shift of the potential due to the different pH, the bump seems to be connected with a partial re-dissolution of the S monolayer induced by acidic medium.

A more favorable situation is encountered when Pb is chosen as the first element to be deposited on Ag. In fact, in this case all S layers are deposited on Pb, and the much more negative free energy change involved in PbS formation, $-23.6 \text{ kcal mol}^{-1}$, than in Ag_2S , $-9.72 \text{ kcal mol}^{-1}$, should eliminate the problem of a possible partial re-dissolution of S.

Next, the underpotential deposition of S on a Pb-covered Ag (111) was examined. Figure 4 shows the oxidative underpotential deposition of sulfur on a Pb-covered Ag(111) as obtained by scanning the potential from -1.0 to -0.70 V in $2.5\text{mM Na}_2\text{S}$ solutions in ammonia buffer.

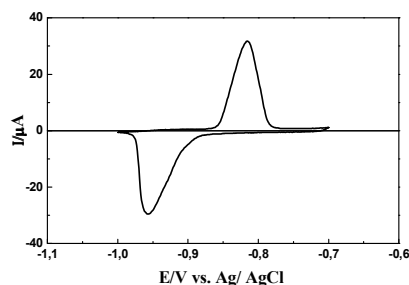


Fig. 4. Cyclic voltammogram of 2.5 mM Na_2S in pH 9.6 ammonia buffer on a Pb/Ag(111), $v = 10 \text{ mVs}^{-1}$.

As expected, due to the more negative free energy change, the sulfur UPD process on the Pb-covered Ag(111) occurs at more negative potentials than on Ag(111).⁹⁷ Therefore, the potential chosen for the deposition of S was -0.7 V. Stripping curves of S deposited at -0.7 V for different times showed that the UPD process is completed after 60 s.

The basic ECALE cycle for PbS deposition is then:

- deposition of Pb at -0.45V for 60 s
- washing at -0.45V with acetic buffer
- deposition of S at -0.7V for 60s
- washing at -0.7V with ammonia buffer

The cycle is then repeated as many times as necessary to obtain thicker deposits.

Electrochemical characterization As usual, the first characterization of the compound obtained is the electrochemical characterization⁷⁷ which is carried out, in-situ, by scanning the potential to values where the deposits are destroyed. The charge involved in the stripping of the single elements gives the amount of deposition. The first PbS layer was then examined by scanning the potential towards positive values to dissolve Pb and successively towards negative potentials to dissolve S. Between the two scans, the cell was rinsed with the supporting electrolyte to eliminate the dissolved lead ions thus avoiding lead re-deposition. Curve *b* in Figure 5 is the stripping curve of Pb from this first PbS monolayer, whereas curve *a* is the stripping curve of Pb directly deposited on Ag(111) as in Fig. 2. As expected, more energy is required to strip Pb from PbS than from the silver substrate. As a consequence, the solid curve is shifted towards more positive potentials.

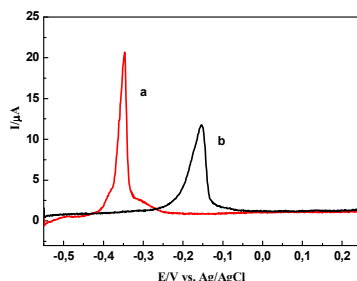


Fig. 5 Stripping curve of Pb from the first PbS monolayer (b); stripping curve of Pb directly deposited on Ag(111) (a), $v = 5 \text{ mVs}^{-1}$.

However, the charge involved in the stripping of Pb from PbS, $296 \mu\text{C cm}^{-2}$, amounts to about 92% of that, $332 \mu\text{C cm}^{-2}$, measured in the stripping of Pb deposited on silver. This could be explained either with a partial destruction of Pb monolayer operated by S deposition or, on the contrary, with the not complete re-dissolution of Pb. The second hypothesis could be supported by the comparison between the stripping curve of the sulfur remaining after lead dissolution (curve *a* in Fig.6) and the stripping curve of sulfur directly deposited on Ag(111) (curve *b* in Fig. 6).

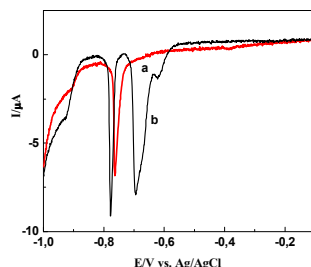


Fig. 6 Stripping curve of the sulfur remaining after lead dissolution (b) and the stripping curve of sulfur directly deposited on Ag(111) (a), $v = 5 \text{ mVs}^{-1}$.

The splitting of curve *b* into two peaks is due to the fact that after lead dissolution the amount of remaining sulfur exceeds that corresponding to a UPD layer on Ag(111), and this excess is stripped at the potential of bulk Sulfur. Finally, the S stripped at the more negative potential is the UPD peak, but the comparison with the curve *a* indicates that the Ag(111) substrate has been somehow modified either by the formation of a Pb adlayer or even by the formation of a Pb-Ag alloy.¹⁰¹

The presence of different sites also seems to be suggested by the presence of the small bump preceding the “bulk” S stripping peak. However, only qualitative

hypotheses can be formulated on the basic voltammograms that should be supported by more suitable surface analysis tools.

The charge associated to this UPD peak, $66 \mu\text{C cm}^{-2}$, plus the charge involved in the “bulk” peak, $260 \mu\text{C cm}^{-2}$, gives a charge value, $326 \mu\text{C cm}^{-2}$, very close to that, $332 \mu\text{C cm}^{-2}$, involved in the stripping of Pb_{UPD} layer deposited on the bare $\text{Ag}(111)$.

The charge involved in the stripping of deposits obtained with different numbers of basic ECALE cycles gives the amount of the elements deposited for that number of cycles. The stripping curves of deposits obtained with 2, 5, 10 and 15 cycles are reported in Fig. 7.

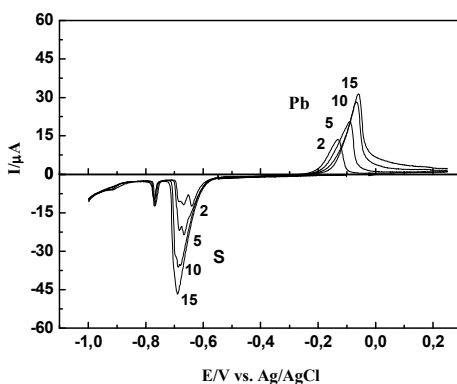


Fig. 7. Linear-sweep voltammograms for the Pb oxidative stripping, and for the S reductive stripping of PbS films deposited with 2, 5, 10 and 15 ECALE cycles, $\nu = 5 \text{ mV s}^{-1}$.

As usual, the stripping process of the first element (in our case Pb) becomes progressively more difficult as the number of deposition cycles increases. As has been shown before⁷⁷ this is not due to the slow kinetics of the dissolution process but rather to an increasing stability of the compound that determines a potential shift of the peaks. Once all of the first element has been stripped away, the remaining layers of the second element (in our case S) behave as a bulk deposit. Therefore they are stripped at the bulk potential except for the first layer, i.e. the layer in contact with the silver substrate. The charge involved in this first layer is constant, regardless of the number of cycles employed. Therefore, this first layer can be considered as the UPD layer.

The behavior described is general and it is fulfilled also by changing the order of the stripping processes. Of course if S is stripped as the first element, the potential shifts in the opposite direction still indicating an increasing stability involved in the compound formation.

Note that the bump observed in Fig. 6 is replaced by a well-defined peak for the deposits obtained with 2 and 5 cycles. However, for deposits obtained with 15

cycles, the two “bulk” peaks merge, thus indicating that the dissolution process is no longer able to distinguish between different sites. Of course this fine structure of the “bulk” S deposit is only observed at low scan rates.

The charges involved in Pb stripping for a given number of cycles coincide with the corresponding charges of sulfur, thus indicating the right 1:1 stoichiometric ratio. Moreover, the plots of the charges for Pb and S stripping as a function of the number of cycles are linear with an average charge per cycle of approximately $83 \mu\text{C cm}^{-2}$, suggesting layer-by-layer growth. This behavior is also observed for other semiconductors obtained by ECALE method.⁷⁷

Morphological characterization The morphological analysis carried out by ex-situ AFM measurements on prepared samples obtained with 50, 75, 100 and 125 ECALE cycle revealed that all samples consisted of homogeneous films of PbS small clusters. However, when exposed to the atmosphere, these clusters tend to enlarge. The morphological evolution of PbS deposits as a function of the exposure time in air was then investigated. The analysis was performed on deposits formed with 50 e 75 deposition cycles and at different times of exposition to the atmosphere. Fig. 8 shows $5 \times 5 \mu\text{m}$ AFM images of a 50-cycle sample as obtained after 1, 16, 40 and 160 hours.

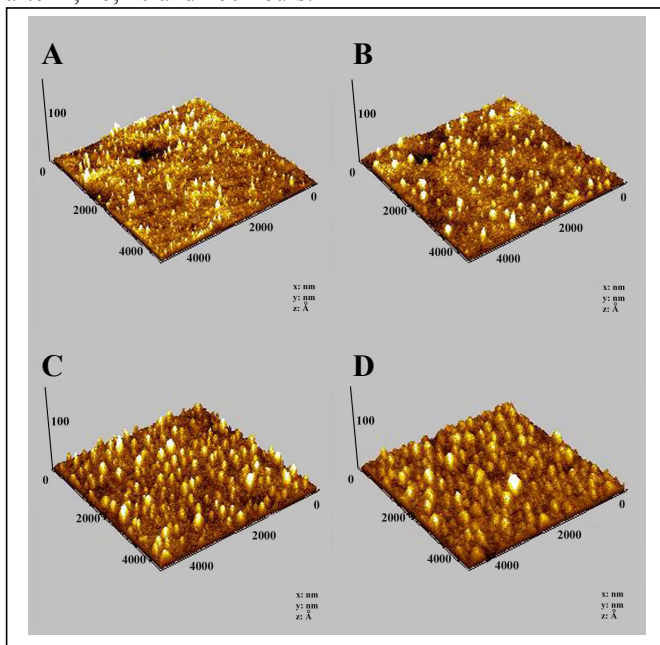


Fig. 8.

AFM $5 \mu\text{m} \times 5 \mu\text{m}$ image of a sample formed with 50 deposition cycles of PbS on Ag(111) as a function of the exposure time in air. A = 1h, B = 16h, C = 40h and D = 160h.

All images show that the surface is homogeneously covered by a film of PbS clusters of progressively increasing in diameter.

The evolution in time can be well checked through the evaluation of the root mean square roughness parameter (RMS) provided by the AFM software. RMS roughness was calculated via the standard formula:

$$\text{RMS}^2 = (1/N) \sum_{ij} [h_{ij} - \hat{h}]^2 \quad (1)$$

Here, N is the number of pixels in the image, h_{ij} is the local height at pixel ij , and \hat{h} is the mean height.

The plot of the RMS values calculated on the AFM images of Fig. 8 shows that RMS reaches a limiting value after about 40 hours (curve *a* in Fig. 9). Apart from the different limiting value, the same behavior was shown by a sample formed with 75 cycles (curve *b*). This behavior can be related to an initial process of oxidation PbS film.^{102,103}

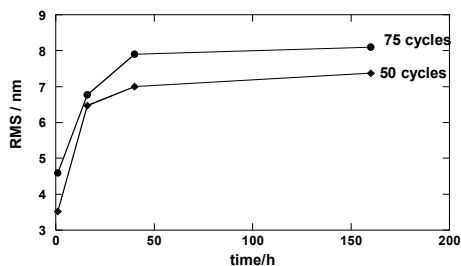


Fig. 9. Plot of RMS roughness of a sample formed with 50 and 75 deposition cycles of PbS on Ag(111) as a function of the exposure time in air.

Conclusions

PbS thin films were obtained by Electrochemical Atomic Layer Epitaxy (ECALE) method, i.e. by alternated underpotential deposition (UPD) of lead and sulfur. The analysis of the UPD processes of both S and Pb on Ag(111) suggested the deposition of Pb as the first element. The electrochemical characterization was performed on the first PbS layer by the stripping of Pb followed by the stripping of S. The charge measured in the Pb stripping was slightly smaller than expected, thus suggesting an incomplete re-dissolution. A small potential shift observed in the stripping of S suggested that the limited amount of undissolved Pb could somehow modify the silver. However, the electrochemical characterization of deposits formed

with an increasing number of deposition cycles up to 15 confirmed the layer-by-layer growth of PbS with the right 1:1 stoichiometric ratio.

The morphological analysis carried out by ex-situ AFM measurements on as prepared samples obtained with 50, 75, 100 and 125 ECALE cycle revealed that all samples consisted of homogeneous films of small PbS clusters. However, when exposed to the atmosphere, these clusters tend to enlarge. In fact, during the first few hours of exposure of the PbS film, the roughness increases rapidly, but after about 40h it reaches an almost constant value. This behavior can be related to the initial process of oxidation of PbS film. Future work will be devoted to the investigation of optical properties of these films to evaluate their potential applications in optoelectronic devices.

2.2 Electrodeposition of metal mono and multilayers on Ag(111)

The possibility of synergic effects of some metals on the catalytic activity of silver led us to study the way to perform controlled deposition of Cobalt or Iron on Silver. In fact, these metals cannot be deposited at underpotential on Silver, and any attempt to control the deposition at overpotential, even at potentials slightly negative to the Nernst value, didn't allow an effective control. To this purpose, two valid methods are presented in the present section.

The first is a novel electrochemical route to deposit monolayers of metals on Ag(111) that we called "Selective Electrodesorption Based Atomic Layer Deposition" (SEBALD). It is based on the idea of exploiting the favorable energy gain due to the formation of the corresponding metal sulfides, namely performing underpotential deposition of these metals on Sulfur covered Silver. The deposition is surface limited and the successive electrodesorption of Sulfur leaves a monolayer of the metal. The method can also be used to obtain metal layers of controlled thickness. In fact, the basic ECALE cycle can be also repeated to increase the thickness of the sulfide, so that the successive selective desorption of Sulfur leaves increasing amounts of metals. The method has been first examined using CdS, whose deposition conditions by ECALE on Ag(111) are well known. Thereafter, the method will be applied to the deposition of Cobalt and Iron.

The second way to perform controlled deposition at atomic level is constituted by the method known as Surface Limited Redox Replacement (SLRR), elaborated by Adžić et al.²⁶

According to this method an ordered metal adlayer obtained by underpotential deposition is used as a template for deposition of a more noble metal. A replacement occurs via an irreversible and spontaneous redox process in which the UPD layer is oxidatively dissolved by cations of more noble metals, which are simultaneously reduced and deposited.

Here, SLRR has been used to deposit a single layer of Cobalt on Ag(111) by replacement of a Zinc monolayer previously formed at underpotential.

Experimental section

Fluka analytical reagent grade Na_2S , Merck analytical reagent grade $3\text{CdSO}_4 \cdot 8\text{H}_2\text{O}$, $\text{CoSO}_4 \cdot 7\text{H}_2\text{O}$, $\text{FeSO}_4 \cdot 7\text{H}_2\text{O}$, HClO_4 , NH_4OH , were used without further purification. HClO_4 and NH_4OH were used to prepare the pH 9.6 ammonia buffer. The solutions

were freshly prepared just before the beginning of each series of measurements. An automated deposition apparatus consisting of Pyrex solutions reservoirs, solenoid valves, a distribution valve and a flow-cell was used under the control of a computer. The electrolytic cell was a Teflon cylinder with a 10mm inner diameter delimited by the working electrode (a disk of 12mm diameter) on one side and the counter electrode on the other side. The inlet and the outlet for the solutions were placed on the side walls of the cylinder. The counter electrode was gold foil, and the reference electrode was an Ag/AgCl (sat. KCl) placed on the outlet tubing. Both the distribution valve and the cell were designed and realized in the workshop of our Department.⁸¹ The solution is pushed into the cell by applying a pressure as low as 0.3 atm which determines a flow-rate of about 1 ml s^{-1} . When the cell is filled, the pressure is no longer applied, so that the flow is stopped during ECALE depositions. A simple homemade software allows of filling the cell with the different solutions following the sequence necessary to obtain the compound. Binary compounds are simply obtained by alternating the underpotential deposition of the metallic element with the underpotential deposition of the non-metallic element in a cycle. The silver single crystals were prepared according to the Bridgeman technique and polished by a CrO_3 based procedure preparation.^{74,75,76}

Atomic Force Microscopy (AFM). Images were taken with a commercial instrument (PicoSPM, Molecular Imaging) in contact mode with a commercial Si_3N_4 cantilever (Nanosensors, Wezlar-Blankenfeld). In conjunction with topography imaging, Lateral Force Microscopy (LFM) was used for surface morphological investigations of samples composed by areas with different chemical nature.

2.2.1 Electrodeposition of Cadmium Sulfide on Ag(111) for the obtainment of Cadmium single layers

Preparation of Cadmium Sulfide

Cadmium Sulfide (CdS) thin films of different thickness were prepared on Ag(111) by ECALE according to the known procedure.

The Sulfur UPD layer on Ag (111) was obtained from 0.5 mM Na_2S in ammonia buffer 9.6 pH, by scanning the potential from -1.1 V to -0.68 V (Figure 1). The Cadmium UPD layer on Ag (111) covered by one monolayer of Sulfur was obtained from 5mM CdSO_4 solutions in ammonia buffer 9.6 pH, by scanning the potential from -0.1 V to -0.68 V (Figure 2). The experimental sequence of the ECALE cycle is:

- Deposition of Sulfur at -0.68 V
- Washing of the cell with ammonia buffer
- Deposition of Cadmium at -0.68 V
- Washing of the cell with ammonia buffer

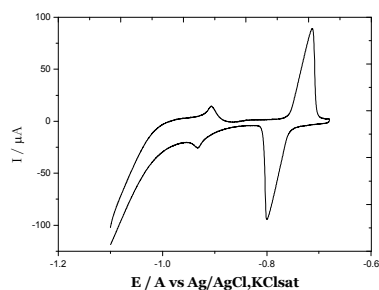


Figure 1 Cyclic voltammogram of S on Ag(111) from 0.5 mM Na_2S in ammonia buffer pH=9.6 solution. Scan rate 50mV/sec.

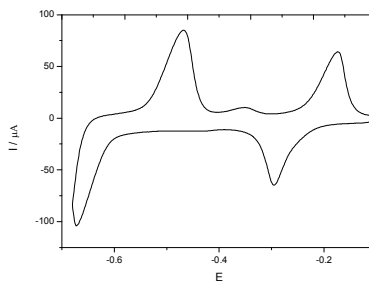


Figure 2 Cyclic voltammogram of Cd on S-covered Ag(111) from 5 mM CdSO_4 in ammonia buffer pH=9.6 solutions. Scan rate 50mV/sec.

Preparation of Cadmium deposits

After the preparation of CdS thin films of 1-2-3-5-10 cycles, Sulfur desorption was performed through the scan from -0.68V and -1.6V in ammonia buffer (Figure 3), and remaining 3 minutes at -1.6V in order to ensure a complete Sulfur dissolution. It must be noted that Sulfur stripping peak shifts towards more negative potentials as the number of deposition cycles increases, indicating an increasing stability of the compound. This behavior is analogous to the positive potential shift observed when Cadmium is desorbed as first from Cadmium Sulfide.

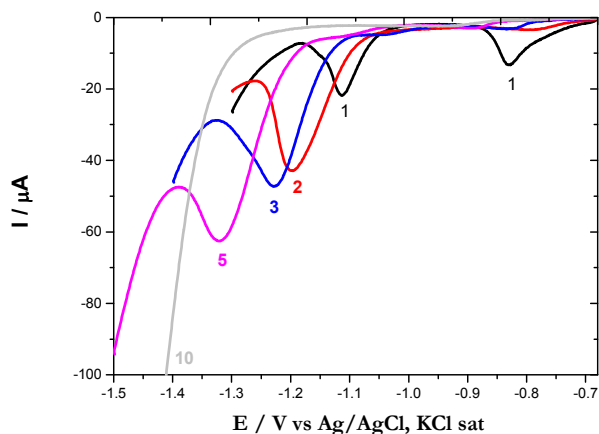


Figure 3 Linear-sweep voltammograms for the S reductive stripping of CdS films deposited with 1,2,3 5 and 10 ECALE cycles, $v = 10 \text{ mV s}^{-1}$.

Once all Sulfur has been stripped away, Cadmium stripping has been performed as well (Figure 4). After sulfur desorption, the remaining layers of Cadmium behave as a bulk deposit plus a constant contribute due to the first layer.

Cadmium stripping curves of Figure 4 presents the UPD stripping peak at -0.36V and a peak relative to the stripping of Cadmium bulk at -0.7V, whose area increases linearly with the number of cycles (Figure 5).

Figure 5 shows the plot of the charges per cm^2 for Cadmium strippings, measured from Figure4, versus the number of ECALE cycles. The slope of the line, $94 \mu\text{C cm}^{-2}$, gives the charge per cycle.

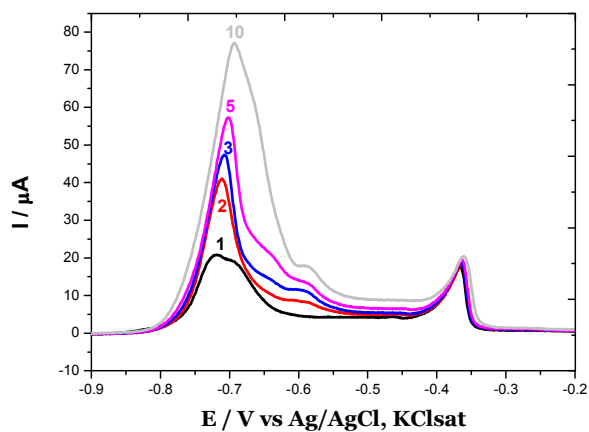


Figure 4 Linear-sweep voltammograms for the Cd oxidative stripping after S desorption (figure 4) for CdS films deposited with 1,2,3 5 and 10 ECALE cycles, $v = 10 \text{ mV s}^{-1}$.

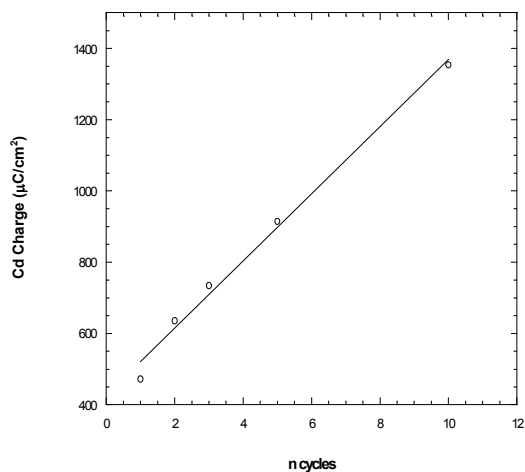


Figure 5 Plot of Cadmium charges (from stripping curves of figure4) versus the number of ECALE cycles.

AFM analysis

The AFM ex situ analysis of the morphology of the Cadmium deposits obtained evidenced that metal layers tend to rearrange themselves forming clusters

In Figure 6 the image of bare Ag(111) (Fig. 6a) is compared to an image of Ag(111) with a Cd deposit of 10 ECALE cycles after S desorption (Fig. 6b). In the latter case, the surface appears covered by clusters of various dimensions.

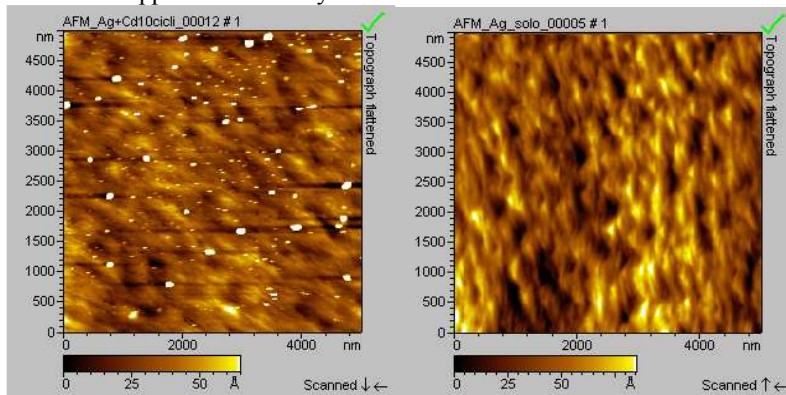


Figure 6 $5 \times 5 \mu\text{m}^2$ AFM images of bare Ag(111) (a) and Ag(111) with a Cd deposit obtained from 10 ECALE cycles CdS after S desorption (b).

2.2.2 Electrodeposition of Cobalt Sulfide and Iron sulfide on Ag(111) for the obtainment of Cobalt and Iron single layers respectively

After having checked the SEBALD method with CdS, other metals, like Cobalt and Iron, were studied due to their possible synergic catalytic effect with Silver towards Oxygen reduction. First, the possibility to deposit the metal sulfide by ECALE was analyzed, and then the metal deposits obtained by SEBALD were characterized by electrochemistry and AFM microscopy.

Preparation of Cobalt Sulfide

Cobalt underpotential deposition was studied on the first Sulfur layer deposited on Ag(111).

The S_{UPD} layer on Ag (111) was performed like for CdS, from 0.5 mM Na_2S in ammonia buffer 9.6 pH (Figure1). The Co_{UPD} layer on Ag (111) covered by one monolayer of Sulfur was performed from 0.5 mM $CoSO_4$ solutions in ammonia buffer 9.6 pH, by scanning the potential from -0.1 V to -0.65 V (Figure 7).

Cobalt Sulfide thin films of one and two ECALE cycles were prepared according to the procedure:

- Deposition of Sulfur at -0.68 V
- Washing of the cell with ammonia buffer
- Deposition of Cobalt at -0.6 V
- Washing of the cell with ammonia buffer

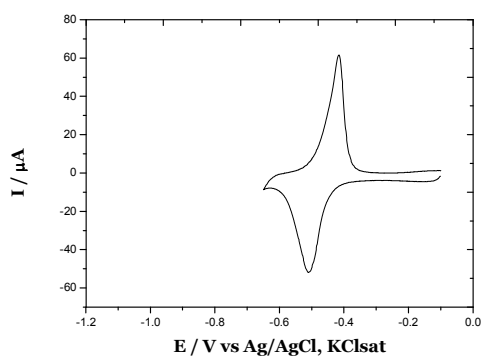


Figure 7 Cyclic voltammogram of Co on S-covered Ag(111) from 0.5 mM $CoSO_4$ in ammonia buffer pH=9.6 solutions. Scan rate 50mV/sec

Preparation of Cobalt deposits

After the preparation of 1 and 2 cycles of CoS thin films, Sulfur desorption was performed scanning the potential from -0.68V to -1.6V in ammonia buffer and keeping the potential at -1.6V for 3 minutes to ensure the complete Sulfur dissolution. Then, the amount of the deposited metal was evaluated by measuring the charge of the Cobalt stripping peak at -0.6V (Figure 8). The potential of this peak is that of bulk Cobalt, and therefore it is anticipated with respect to the stripping of Cobalt from CoS thin films (Figure 9).

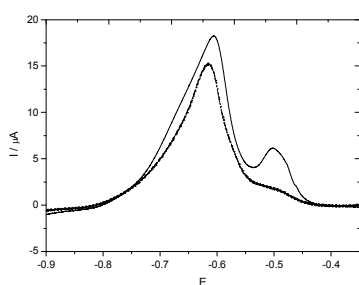


Figure 8 Linear-sweep voltammograms for the Cobalt oxidative stripping after Sulfur desorption for CoS films deposited with 1 (dash line) and 2 (solid line) ECALE cycles, $\nu = 10 \text{ mV s}^{-1}$.

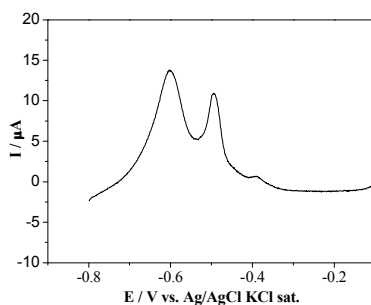


Figure 9 Linear-sweep voltammograms for the Cobalt oxidative stripping after Sulfur partial desorption (until -1.1V) from 1 ECALE cycle CoS films, $\nu = 10 \text{ mV s}^{-1}$.

AFM analysis

An AFM ex-situ investigation was performed on Cobalt deposits obtained by one CoS ECALE cycle after Sulfur desorption. As for the Cadmium deposits, also the Cobalt deposits derived from one single layer of its Sulfur compound rearranged in clusters.

AFM images in Figures 10 and 11 show Ag(111) uniformly covered by clusters of average height of 80Å.

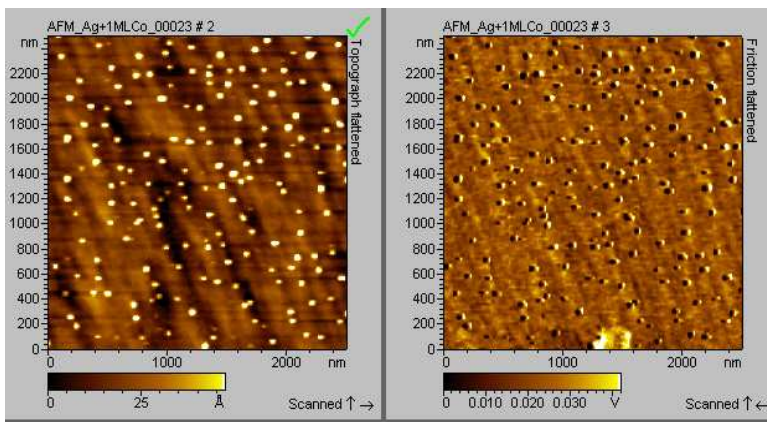


Figure 10 $2.5 \times 2.5 \mu\text{m}^2$ AFM image of Ag(111) with a Cobalt deposit obtained from one CoS ECALE cycle after Sulfur desorption. On the left the topography image and on the right the lateral force image.

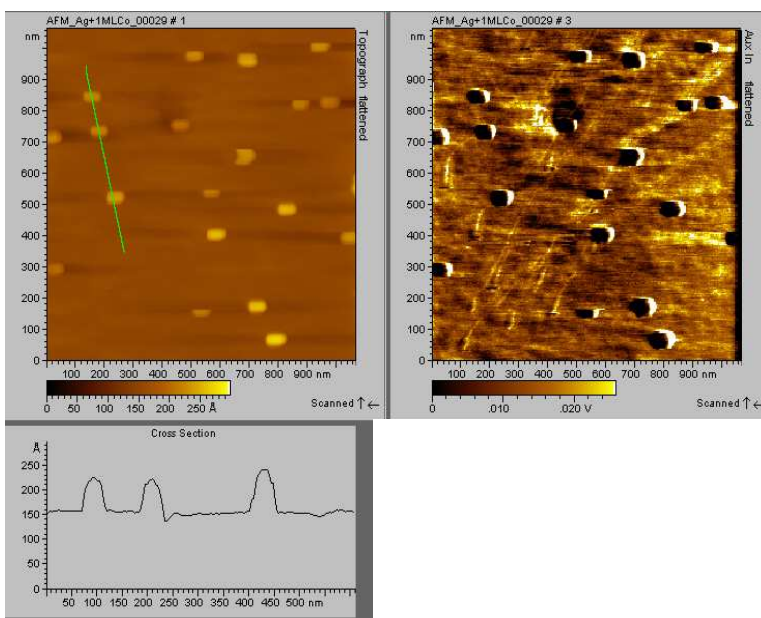


Figure 11 $1 \times 1 \mu\text{m}^2$ AFM image of Ag(111) with a Co deposit obtained from one CoS ECALE cycle after S desorption. On the left, the topography image with a profile drawn by a green line. On the right the lateral force image.

Preparation of Iron Sulfide

Iron Underpotential Deposition was studied on the first Sulfur layer deposited on Ag(111).

As usual, the Sulfur UPD layer on Ag (111) was performed from 0.5 mM Na₂S in ammonia buffer 9.6 pH (Figure 1). The Iron UPD layer on Ag (111) covered by one monolayer of Sulfur was performed from 1 mM FeSO₄ solutions in 0.1M NaClO₄, by scanning the potential from -0.4 V to -0.6 V (Figure 12). The experimental sequence of the ECALE cycle is:

- Deposition of Sulfur at -0.68V
- Washing of the cell with ammonia buffer
- Deposition of Iron at -0.6V
- Washing of the cell with 0.1M NaClO₄

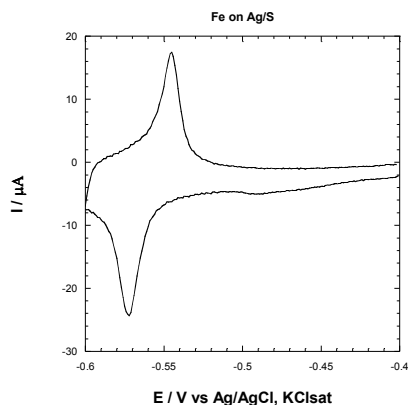


Figure 12 Cyclic voltammogram of Fe on S-covered Ag(111) from 1 mM FeSO₄ in 0.1M NaClO₄ solutions. Scan rate 10mV/sec

Preparation of Iron deposits

After the preparation of one layer of Iron Sulfide, Sulfur desorption was performed scanning the potential from -0.68V to -1.6V in ammonia buffer and keeping the potential at -1.6V for 3 minutes to ensure the complete Sulfur dissolution. Then, the amount of deposited metal is evaluated by measuring the charge of the Iron stripping peak at -0.8V (Figure 11). The potential of this peak is that of bulk Iron, anticipated with respect to the stripping of Iron from Iron Sulfide thin films at -0.4V (Figure 12).

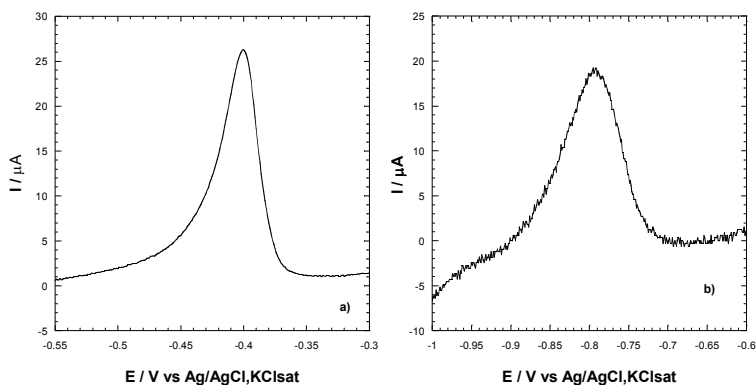


Figure 13 Linear-sweep voltammograms for the Iron oxidative stripping before (a) and after (b) S desorption for Iron Sulfide single layer thin film deposited by ECALE, $\nu = 10 \text{ mV s}^{-1}$.

Conclusion

An effective way to obtain well controlled atomic level deposition of a metal M on a foreign substrate S is here proposed for the first time. The method is mainly applicable for those metals that are not deposited at underpotential on S . Underpotential Deposition is a surface limited phenomenon that generally yields no more than one monolayer. As a consequence, the amount of deposition is well controlled at the nanometer scale. Such level of control is not achievable in overpotential deposition through the application of Faradays laws, even trying to limit the extent of deposition operating at very low overpotentials, that is at very low values of current.

A first morphological analysis of metal deposits obtained by SEBALD shows, at least in the cases under study, that they assemble in clusters.

The next investigation on SEBALD should verify the existence of a correlation between the number of ECALE cycles used to form the sulfide film and the dimensions of metal clusters remained after Sulfur desorption. If this correlation exists, SEBALD would constitute a simple method to prepare various sized bimetallic surfaces with morphological control at atomic level. Moreover, these structures could be tested as catalysts towards Oxygen reduction, giving information on the influence that different nanostructures have on this catalytic reaction.

2.2.3 Surface Limited Redox Replacement (SLRR) method for Cobalt single layer deposition

Cobalt electrodeposition on Ag(111) was studied from 0.5 mM $\text{CoSO}_4 \cdot 7\text{H}_2\text{O}$ in ammonia buffer solution of pH 9.6. Only freshly prepared solutions were used in order to avoid the presence of Co^{3+} . Since Cobalt does not present Underpotential Deposition on Silver, an alternative approach of metal deposition, named Surface Limited Redox Replacement (SLRR), recently elaborated by Adžić et al,²⁶ was used. According to this method an ordered metal adlayer obtained by Underpotential Deposition is replaced by a more noble metal monolayer. Such a replacement occurs via an irreversible and spontaneous redox process in which the UPD layer is oxidatively dissolved by cations of more noble metals, which are simultaneously reduced and deposited. The use of Silver as a substrate limits the possibility of application of the SLRR method to metals that give UPD on Silver and which are less noble than Cobalt. A good candidate is Zinc, whose UPD on Ag(111) is shown in Figure 14.

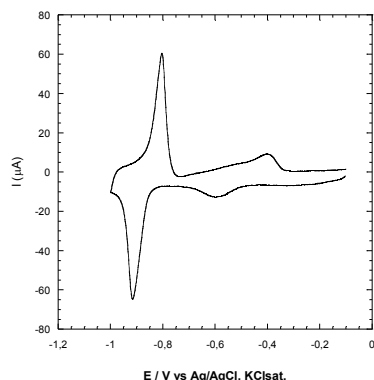


Figure 14 Cyclic voltammogram obtained from 1 mM $\text{ZnSO}_4 \cdot 7\text{H}_2\text{O}$ in pH 9.6 ammonia buffer on Ag(111) in the UPD region. Scan rate: 50 mV/s. Deposition of a complete Zinc monolayer at -1 V.

The process of spontaneous and complete substitution of Zinc with Cobalt needs a few minutes. In fact, the degree of replacement of Zinc, checked through the values of Cobalt stripping charge, is complete after 5 minutes, as shown in Figure 15 ((a) Cobalt oxidative stripping after 30s, 1 min and 5 minutes of replacement, and (b) plot of the charge of Cobalt stripping peaks versus replacement times).

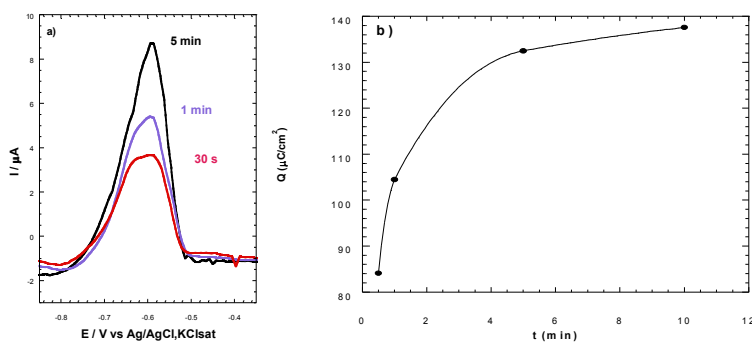


Figure 15 (a) Linear-sweep voltammograms for the Cobalt oxidative after 30s, 1 min and 5 minutes of replacement. (b) Charge from Cobalt stripping peaks as a function of the replacement time.

The charge involved in the Cobalt stripping corresponds to that involved in the dissolution of a single Zn UPD monolayer, that is $136 \mu C/cm^2$.

Conclusion

In this chapter a second method to control deposition of metals at atomic level is applied to Cobalt deposition on Silver. This method, known as Surface Limited Redox Replacement, allowed to prepare a single layer of Cobalt through spontaneous substitution of a monolayer of Zinc deposited at underpotential..

Therefore, SLRR results as a valid tool for single layer deposition of metals that do not present UPD on a substrate.

2.3 Electrodeposition Confined into nanosized patterns and Catalysis towards Oxygen Reduction

2.3.1 Electrodeposition of Cadmium Sulfide into a patterned hexadecanethiol Self Assembled Monolayer obtained by microcontact printing

Introduction

This chapter describes the growth of CdS confined between the submicrometric strips of hexadecanethiol (HDT) deposited on Ag(111) by microcontact printing μ CP.^{104,105} Since long chain thiols act as insulators, this arrangement can represent a starting point for the attainment of nanocircuits. μ CP is a widely used top-down approach to create patterns. It consists of a high-resolution technique used to transfer a pattern from an elastomeric stamp to a solid substrate by conformal contact. The method was introduced by Whitesides and co-workers.^{106,107,108} who brought a polymer inked with alkanethiols into contact with a Gold substrate to form a self assembled monolayer (SAM) in the area of contact. CdS electrodeposition was performed by ECALE. ECALE method is based on the alternate electrodeposition of the elements that form the compound at underpotential.⁴ The deposits have been characterized by electrochemical techniques and AFM measurements.

Experimental

Merck analytical reagent grade $3\text{CdSO}_4 \cdot 8\text{H}_2\text{O}$, HClO_4 , NH_4OH , Aldrich analytical reagent grade Na_2S , Fluka analytical reagent grade hexadecanethiol and EtOH 99.8% (Fluka) were used without further purification. HClO_4 and NH_4OH were mixed to prepare the pH 9.6 ammonia buffer that was used to prepare solutions of 0.5mM Na_2S and 5mM $3\text{CdSO}_4 \cdot 8\text{H}_2\text{O}$ for ECALE deposition. The solutions were freshly prepared and deaerated with nitrogen just before the beginning of each series of measurements. An automated deposition apparatus consisting of Pyrex solution reservoirs, solenoid valves, a distribution valve and a flow-cell, was used under the control of a computer. Both the distribution valve and the cell were designed and realized in the workshop of our department. The working electrodes were silver single crystals grown by the Bridgman technique and cut to form discs of about 1cm in diameter.⁷⁴ The electrodes

were first polished with emery paper (BuehlerMet SiC P1000, P2500, P4000) then with alumina slurry (Buehler micropolish II) using 0.05 mm particle size alumina for the final step. Before their use in the electrochemical cell, the working electrodes were chemically polished with solutions of 0.15M CrO₃ in 0.1M HCl.^{75,76} After polishing, the electrode was soaked first in concentrated ammonia for about 10 min, and then in concentrated sulfuric acid for about 20 min. Finally, it was rinsed thoroughly with water. The counter electrode was gold foil, and the reference electrode was an Ag/AgCl/sat. KCl placed on the outlet tubing of the cell. CdS deposition was performed as described in Chapter 2.1.2. Ag(111) substrates were patterned by μ CP using polydimethylsiloxane (PDMS) stamps. The stamps were obtained by replica molding,^{109,110} by casting the liquid prepolymer against a blank commercial digital versatile disk (DVD), while keeping the system at 60°C for 2 h. The stamp obtained by this procedure consists of parallel lines 410nm wide, 150nm deep with a periodicity of 74 nm. Before use, the stamp was kept in a solution of 0.03mM HDT in ethanol for 24 h; then it was washed with ethanol and dried with a nitrogen stream. Finally, it was brought into contact with the metal surface while applying a force of about 0.35N for 6 s. A mechanical apparatus allows one to control that the stamp is as parallel as possible to the metal, and a pneumatic system allows one to control the applied force.

The μ CP method has been tested using AFM, in order to verify the results and choose the best parameters (applied force, contact time and ink solution concentration). As will be shown later, the whole patterning procedure has been checked by selectively etching the silver surface uncovered by HDT with a solution of 30mM Thiourea (Fluka) and 20mM Fe(NO₃)₃·9H₂O (Fluka) in water.¹¹¹ AFM imaging was performed ex-situ using a Molecular Imaging AFM (PicoSPM, Molecular Imaging) operating in contact mode, with a commercial Si₃N₄ cantilever (Nanosensors, Wetzlar-Blankenfeld).

Results and Discussion

Assessment of the experimental conditions for patterning

The results of the patterning process by μ CP can be monitored by AFM. Nevertheless, there are remarkable experimental difficulties, since thiols tend to stick to the AFM tip. Moreover, AFM imaging is usually limited to surface areas (less than 25mm x 25mm) that are too small to be representative of the whole surface. On the other hand, SAMs of HDT formed on silver surface can act as physical barriers against etchants. As a consequence, the uncovered silver can be grooved by using a selective etching solution. To this end patterned silver surfaces are kept in a stirred solution of 30mM Thiourea (Fluka) and 20mM Fe(NO₃)₃·9H₂O for 30 s, which, according to Ref.111, produces the selective etching of silver. These etching conditions produce grooves about 150nm deep, 500nm wide with a periodicity of

740nm (Fig. 1), in good agreement with the morphological characteristics of the starting DVD master (Fig. 2). However, since the electrochemical processes take place on the whole surface uncovered by HDT, significant electrochemical data can be obtained only from uniformly patterned surfaces with a low number of defects.

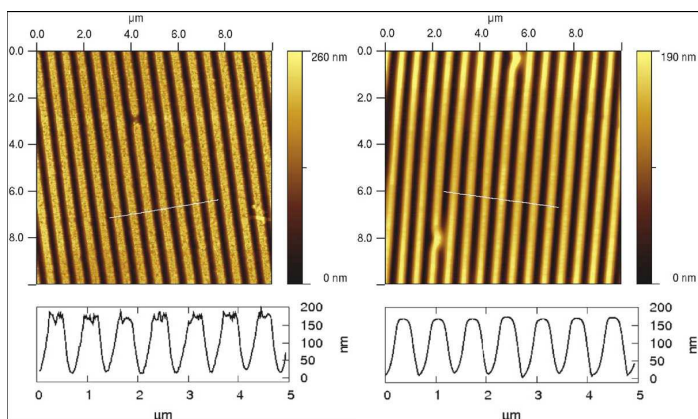


Fig. 1. AFM image (tapping mode) of a Ag(111) surface covered with patterns of HDT and etched as described in the text.

Fig. 2. AFM image (tapping mode) of a PDMS stamp used for μ CP.

Electrochemical characterization

The quality of silver electrodes was checked by cyclic voltammetry before and after μ CP. The patterned Ag(111) electrodes were then used to deposit CdS by ECALE, and each sample was electrochemically characterized by measuring the charge involved in the stripping of Cd followed by the stripping of S. These charges are proportional to the amount of CdS, and, therefore, to the uncovered silver areas that are the only ones where CdS is deposited; therefore the comparison between the stripping charges obtained from CdS deposited on patterned Ag(111) and on bare Ag(111) allows for the determination of the percentage of silver areas that are actually covered by HDT. As an example, Fig. 3 shows the stripping curves of the first Cd monolayer deposited at under-potential on Ag(111) (solid line) and on Ag(111) patterned by hexadecanethiol (dashed line). Integration of the voltammetric peaks gives the charges involved in the strippings and the ratio between the value of the two charges indicates that the percentage of surface free from HDT corresponds to $70 \pm 5\%$ of the total area, thus confirming the AFM data suggested by Fig. 1. If we consider a hypothetical surface of Ag quite smooth and assume that the patterns have the periodicity of 740 nm, the HDT strips turn out to be 220 ± 35 nm wide.

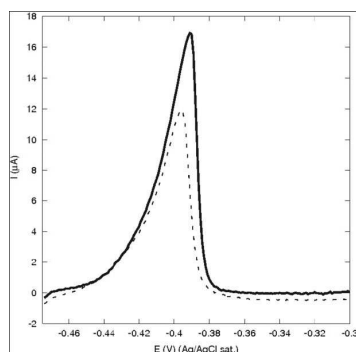


Fig. 4. Stripping curve of the first Cd layer deposited at underpotential on Ag(111) (solid line) and on Ag(111) patterned by hexadecanethiol, (dashed line). Both curves are recorded in pH 9.6 ammonia buffer, at a scan rate of 10 mV/s.

Conclusions

Electrodeposition of CdS on Ag(111) patterned with HDT was performed by ECALE. It must be noted that the electrodeposition of a compound, for which the right stoichiometry must be fulfilled, is completely different from the electrodeposition of one element. The key aspects of the procedure are that the presence of patterns does not affect the surface phenomena on which the ECALE method is based, and that repeated cycles do not affect the shape of the previously deposited patterns. In fact, the underpotential deposition processes take place on patterned surfaces at the same potentials as on bare surfaces, with the only obvious result being of a decreased electrode area. The stripping of Cadmium deposits from patterned surfaces always indicates an excellent agreement between electrochemical and morphological data. In fact, the effective silver substrate area, as determined from the experimental charges, coincides with the silver surface free from the thiol pattern, as determined by AFM measurements. The described results are an example of the combined use of top-down (microcontact printing) and bottom-up (ECALE method) techniques to fabricate nanoscale surface patterns with controlled properties. The structural investigation of the confined CdS deposits is now in progress.

2.3.2 Confined Electrodeposition of CdS in the Holes Left by the Selective Desorption of 3-Mercapto-1-propionic Acid from a Binary Self-Assembled Monolayer Formed with 1-Octanethiol

Introduction

After the obtainment of patterned CdS, combining ECALE with microcontact printing, with the aim of further reducing the size of the electrodeposited material, we examined the possibility of electrodeposition in the holes left in a binary SAM of thiols having different lengths after desorption of the shorter chain thiol. From this, two chapters are dedicated to this topic.

This chapter reports the electrodeposition of CdS by ECALE in the free areas of Ag(111) as obtained by the selective desorption of 3-mercapto-1-propionic acid (MPA) from mixtures with 1-octanethiol (OT). The above mixed binary SAMs on Ag(111) were investigated by cyclic voltammetry and compared with the behavior of similar mixtures on gold.¹¹² The electrodeposition of a compound is quite demanding, since it requires the right stoichiometry. In addition, the surface Underpotential Deposition phenomena exploited by ECALE technique ensures that the surface available for electrodeposition after the selective desorption is still Ag(111). Parallel electrochemical experiments show that the amount of compound electrodeposited is consistent with this free Ag(111) surface, and the morphological analysis performed both by atomic force microscopy (AFM) and by lateral force microscopy (LFM) confirm the electrochemical data.

Experimental Section

Materials. Merck analytical reagent grade $3\text{CdSO}_4 \cdot 8\text{H}_2\text{O}$ and absolute ethanol, Aldrich analytical reagent grade Na_2S , KCl , NaOH , and $\text{Ru}(\text{NH}_3)_6\text{Cl}_3$, and purity grade Fluka 95% 3-mercaptopropionic acid (MPA) and 1-octanethiol (OT) were used without further purification. Merck analytical reagent grade HClO_4 and NH_3 were used to prepare the pH 9.2 ammonia buffer. The water used was obtained from mineral water by distilling it once and then redistilling it again in alkaline permanganate medium while constantly discarding the heads. The solutions were freshly prepared just before the beginning of each series of measurements. The silver single crystals were prepared according to the Bridgman technique and polished by a CrO_3 based procedure.^{74,75,76} An automated deposition apparatus consisting of Pyrex solution reservoirs, solenoid valves, a distribution valve, and a flow-cell was used under the control of a computer. The electrolytic cell was a Teflon cylinder with

about 5 mm inner diameter and 30 mm outer diameter, whose inner volume, 0.5mL, was delimited by the working electrode on one side and the counter electrode on the other side. The inlet and the outlet for the solutions were placed on the side walls of the cylinder. The counter electrode was gold foil, and the reference electrode was Ag/AgCl/sat.KCl placed on the outlet tubing. Both the distribution valve and the cell were designed and realized in the workshop of our department. The distance between the reference and the working electrodes introduces resistive contributions that cannot be compensated. Therefore, the potential values reported hereafter may be slightly different with respect to analogous measurements performed under rigorous resistance compensation. However, this flow-cell was especially designed for layer-by-layer electrodeposition. In fact, the counter electrode facing the working electrode ensures a high homogeneity of the deposits. ECALE Cycles for CdS Deposition. The procedure for CdS deposition is thoroughly described in the chapter 2.1.2. In this chapter, experiments on CdS deposited with a number of ECALE cycles ranging from 1 to 20 are described. Considering that the thickness of CdS deposits obtained with 100 deposition cycles is about 20 nm,⁶ the thickness of these deposits is no more than 4 nm. Self-Assembly of Alkanethiols on Ag(111). For the attainment of a full layer formation, the substrate was immersed in solutions of alkanethiol in pure ethanol for at least 2 h. The single SAMs were obtained from 0.3mM alkanethiol solutions, whereas the mixed SAMS were prepared from solutions of different compositions to realize different monolayer compositions. Simultaneous adsorption of the mixed SAM was performed by immersing the silver substrate in a 99.8% ethanol solution containing the thiols. The systematic investigation was carried out using solutions containing different thiol concentrations.

Atomic Force Microscopy (AFM). AFM images were taken with a commercial instrument (PicoSPM, Molecular Imaging) in contact mode with commercial Si₃N₄ cantilever (Nanosensors, Wezlar-Blankenfeld). During AFM imaging in contact mode, it is possible to record both the vertical deflection of cantilever, which creates the topographic image, and its lateral deflection. Collecting the images of the cantilever lateral deflection, usually called lateral force microscopy (LFM), allows one to distinguish areas having different friction between the scanning tip and the sample and to obtain edge-enhanced images of any surface. We used LFM in conjunction with topography imaging to characterize our samples better. Because of the ultrathin deposited films (few atomic layers), the lateral contrast provided by LFM images was usually much better than that obtained from the topographic images.

Results and Discussion

Electrochemical Characterization of the Binary OTMPA SAMs.

The characterization of the binary SAM is performed by stripping the monolayer in 0.5 M KOH solutions. The first SAM investigated was that obtained from mixtures of

0.3 mM OT and 1 mM MPA in 99.8% ethanol. On Gold, this solution composition gives rise to a homogeneous distribution that, after desorption of the shorter thiol, forms round holes. The stripping voltammetry of this binary SAM is that reported in Figure 1. The figure shows well-defined and distinct peaks with only a slight positive shift (10 mV) in the potential value of MPA with respect to the single MPA deposited on Ag(111).

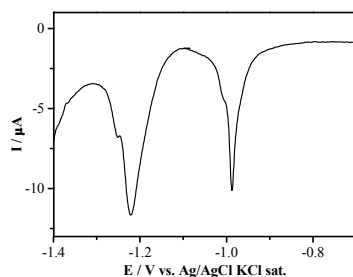


Figure 1. Stripping curves of the binary SAM obtained on Ag(111) from a solution of 0.3mM OT and 1mMMPA. The scan rate was 10 mV s^{-1} .

Integration of the area under the peaks yields the molar ratio of 40% in MPA and 60% in OT. These values are different from those reported for the binary SAM formed on Gold from the same solution composition.¹¹⁰ In fact, as already reported in the literature, the composition of the monolayers rarely equals the solution composition, since longer thiols tend to occupy larger areas; yet, less pronounced differences are observed between composition in solution and on the surface on silver.¹¹³ More particularly, Table 1 reports the direct comparison between our results on silver and those reported in ref 110 for Gold.

	MPA	OT
c/mM	1	0.3
% in solution	77	23
% on Silver surface	40	60
% on Gold surface	25	75

Table I Comparison between our results on silver and those reported in Ref. 13 for gold.

It must be noted that on Ag(111) equimolar solutions (either 0.3 mM MPA+0.3 mM OT or 1 mMMPA+1 mM OT) give the same surface molar ratios of 26% in MPA and 74% in OT. Then to perform a systematic investigation, we kept constant the solution concentration of one alkanethiol, that is, MPA, while varying the concentration of the other, that is, OT. As reported in Table 2, the surface molar ratio of OT increases with the increase in the bulk concentration of OT.

	c/mM	% in solution	% on Silver surface
MPA	1	50	26
OT	1	50	74
MPA	0.3	50	26
OT	0.3	50	74
MPA	0.3	33	18
OT	0.6	67	82
MPA	0.3	25	8
OT	0.9	75	92

Table II Bulk and surface compositions of MPA and OT

Selective desorption of MPA for the Attainment of the Template. The selective desorption has been performed from SAM 26% in MPA obtained from a solution 0.3 mM MPA + 0.3mM OT applying a potential equal to -1.05V for 10 s in 0.5M KOH. Figure 2 shows the stripping peak of the SAM remained after desorption. Both the potential and the area of the peak in Figure 2 coincide with those of the OT before desorption, with only a slight difference in the shape, probably due to a loss in the structure definition. This finding allows us to hypothesize that the silver area at disposal for the electrodeposition coincides with that of desorbed MPA.

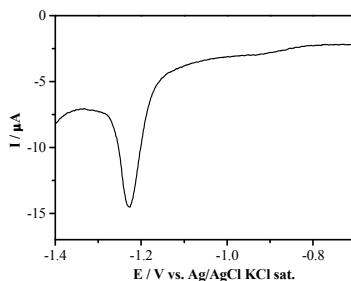


Figure 2 Stripping curves of OT remained after desorption of MPA at -1.05 V from the binary SAM of Fig. 4a. The scan rate was 10 mV s^{-1} .

Figure 3 shows the stripping curve of Sulfur deposited at underpotential on bare Ag(111) (dashed curve) and on patterned Ag(111) (solid curve). From the figure, it is evident that even if the free area of silver is that which remains after selective desorption, the presence of the remaining OT SAM does not change the potential

range of Sulfur UPD, whereas the decrease of the stripping peak indicates a reduction of the silver surface. Similar behavior is observed for Cadmium UPD. However, the charge associated with the UPD peaks in the presence of OT is about 40% and, therefore, higher than the 25% left by MPA. The discrepancy can be explained by the presence of defects in the OT SAM as shown by the stripping voltammetry of Cadmium deposited at underpotential on Ag(111) fully covered by OT (solid curve in Figure 4). The area of the small peak is about 16% of that obtained on the bare Ag(111) (dashed curve in Figure 4).

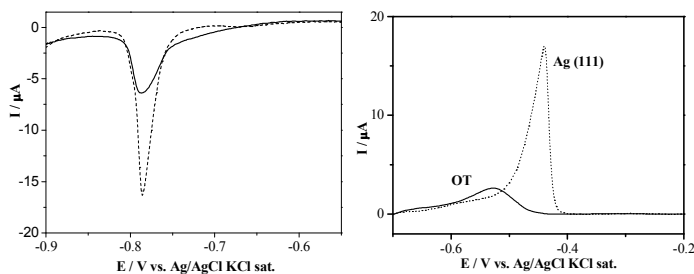


Figure 3 Stripping curves of S_{UPD} deposited on bare (dashed curve) and patterned (solid curve) Ag(111). The scan rate was 10 mV s⁻¹.

Figure 4 Stripping peaks of Cd deposited at underpotential on Ag(111) fully covered by OT (solid curve) and on bare Ag(111) (dashed curve). The scan rate was 50 mV s⁻¹.

Estimate of the Film Quality. An exhaustive discussion on the criteria used for assessment of the defects level in the monolayer is given by Miller et al. in ref ¹¹⁴. Here, electron tunnelling through the full thickness of self-assembled organic monolayers of ω -hydroxy thiols is demonstrated. Briefly, the possibility of either small pinholes exposing the electrode surface, or collapse sites¹¹⁵ causing the monolayer to be significantly thinner than the bulk monolayer film are taken into account. Because of the strong dependence of the electron-transfer kinetic on the thickness of the insulating film, even a small area containing such defects could be entirely responsible for the current measured. In order to assess the effect of such defects, Miller et al. used the theoretical model of Amatore et al. for the redox kinetics at partially blocked electrodes.¹¹⁶ According to this model, the presence of pinholes or collapse sites separated by distances greater than the characteristic diffusion length of the experiment (which, in our experiments, is of the order of tens of micrometers) should give rise to sigmoidal voltammetric waves. On the other hand, no blocking effect should be seen in the presence of defects separated by distances smaller than the characteristic diffusion length. Therefore, the use of suitable electrochemical redox probes such as $[\text{Ru}(\text{NH}_3)_6]^{2+/3+}$ allows us to evaluate the film quality. Figure 5 shows the cyclic voltammograms of 1 mM $\text{Ru}(\text{NH}_3)_6^{3+}$ as performed on bare Ag(111) (curve a) and on fully covered by OT Ag(111) substrates (curve b). On the basis of the above considerations, the monolayer of OT produces only a limited effect on the voltammetric peak, indicating either the presence of pinholes which act as an array of microelectrodes or an insufficient blocking effect of $[\text{Ru}(\text{NH}_3)_6]^{2+/3+}$ as observed in some cases with respect to other electrochemical redox probes such as $[\text{Fe}(\text{CN})_6]^{3-/4-}$.¹¹⁷

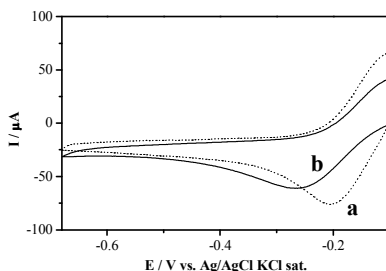


Figure 5 Cyclic voltammograms obtained from 1mM $\text{Ru}(\text{NH}_3)_6^{3+}$ in 0.1M KCl on Ag(111) fully covered by OT (solid curve) and on bare Ag(111) (dashed curve). The scan rate was 50 mV s^{-1} .

However, the limited double layer region of silver does not allow us to reach the positive potential values of ferro/ferricyanide redox couple or observe the oxidation wave of $[\text{Ru}(\text{NH}_3)_6]^{2+}$. On the other hand, the presence of defects is consistent with the possibility of depositing a small fraction of Cadmium UPD on a single OT SAM.

It must also be noted that the Underpotential Deposition is a surface sensitive phenomenon and, therefore, requires that free areas of Ag(111) are exposed to the solution. However, it is important to stress that the defects in the OT SAM are not caused by ECALE electrodeposition, since they are already highlighted by the electrochemical probe.

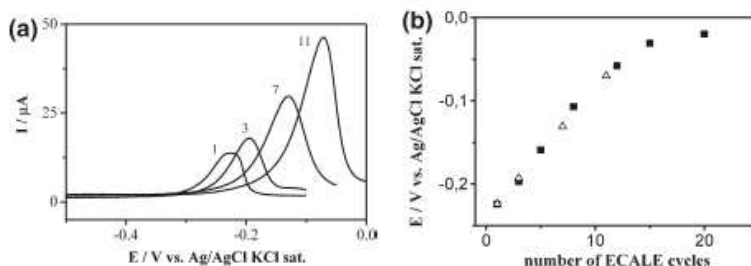


Figure 6. (a) Linear-sweep voltammograms for the Cadmium oxidative stripping from patterned CdS films deposited with 1, 3, 7, and 11 ECALE cycles (scan rate equal to 10 mV s⁻¹); (b) potentials of the stripping peaks as a function of the number of ECALE cycles for patterned CdS (Δ) and for CdS grown on bare Ag(111) (\blacksquare).

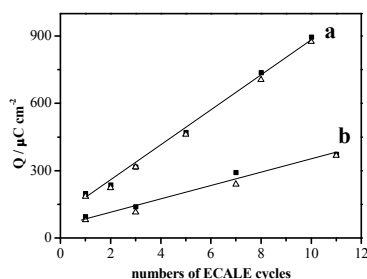


Figure 7 Plots of the charge involved in the oxidative stripping of Cadmium (\blacksquare) and the reductive stripping of Sulfur (Δ) as a function of the number of ECALE cycles as obtained on bare (line a), and on patterned (curve b) Ag(111).

ECALE Growth of CdS in the Holes Left by MPA

Desorption.

The template deposition of CdS was performed according to the procedure described in the Experimental Section. Deposits obtained by progressively increasing the number of cycles were then electrochemically redissolved to measure the charge, stripping first the Cadmium and then the Sulfur. Figure 6a shows the stripping peaks of Cadmium while increasing the number of ECALE cycles. Apart from the current values, these curves exactly reproduce the stripping curves of CdS deposits grown on

bare Ag(111) substrates.⁷⁷ As usual, the stripping process of the first element (in our case Cadmium) becomes progressively more difficult as the number of deposition cycles increases. As it has been shown previously,⁷⁷ the observed potential shift is much greater than that ascribable to the slow kinetics of the dissolution process and it is mostly due to an increasing stability of the compound up to the attainment of a limiting value. Figure 6b shows that the potentials of the stripping peaks of Figure 6a are in excellent agreement with those previously reported for CdS grown on bare Ag(111).⁷⁷ It must also be noted that the well-defined shape of the stripping peaks of Figure 6a suggests that all Cadmium is present as CdS. Another important conclusion suggested by Figure 6 is that in both cases the thickness of the CdS film was proportional to the number of ECALE cycles used. Integration of the stripping curves gives the amount of the elements deposited in a given number of ECALE cycles. Line a in Figure 7 shows plots of the charges per cm² for Cadmium and Sulfur strippings obtained from CdS deposited on a bare Ag(111) substrate,⁷⁷ whereas line b shows the plots obtained from CdS deposited on our template substrates. Of course, in the latter case, this quantity is not to be considered as a true charge density, since the area is the geometrical area of the electrode and not that which is electrochemically active. As showed above, the electrochemical characterization of the deposits of Cadmium Sulfide on the patterned Ag(111) showed that the deposition process is similar to the one performed on the bare Ag(111), apart from a decrease in the amount of material, due to the reduced electrode surface. In particular, the coinciding charges associated with Cadmium and Sulfur strippings gives a 1:1 stoichiometric ratio between the elements as expected for the compound, and the linear increase of the deposit with the number of deposition cycles suggests a layer-by-layer growth mechanism that is the aim of ECALE method.⁷⁷ The slope of each line gives the charge per cycle. The slope of 28 $\mu\text{C cm}^{-2}$ relative to the patterned Ag(111) amounts to 40% of the slope, 70 $\mu\text{C cm}^{-2}$,⁷⁷ relative to the bare Ag(111). It must be noted that this value confirms the previous observations.

AFM Characterization of Template CdS.

The electrochemical characterization was completed with a morphological analysis performed on a CdS sample formed by 20 ECALE cycles. According to the estimate of our CdS sample thickness made previously,⁷⁷ this number of cycles should result in a CdS film thickness of about 4 nm. Figure 8 reports both the topography (a) and the left-scanned (b) and right-scanned (c) LFM images. The topographic image shows the formation of clusters with an average value of 50 nm and not greater than 200 nm. The LFM images show that well defined areas (dark in the left scan and bright in the right scan) are of a different nature with respect to the homogeneous background, thus suggesting that they can be identified as clusters of CdS. An approximate evaluation obtained by summing the areas occupied by the clusters yields a CdS coverage equal to 35-40%, in good agreement with the electrochemical results.

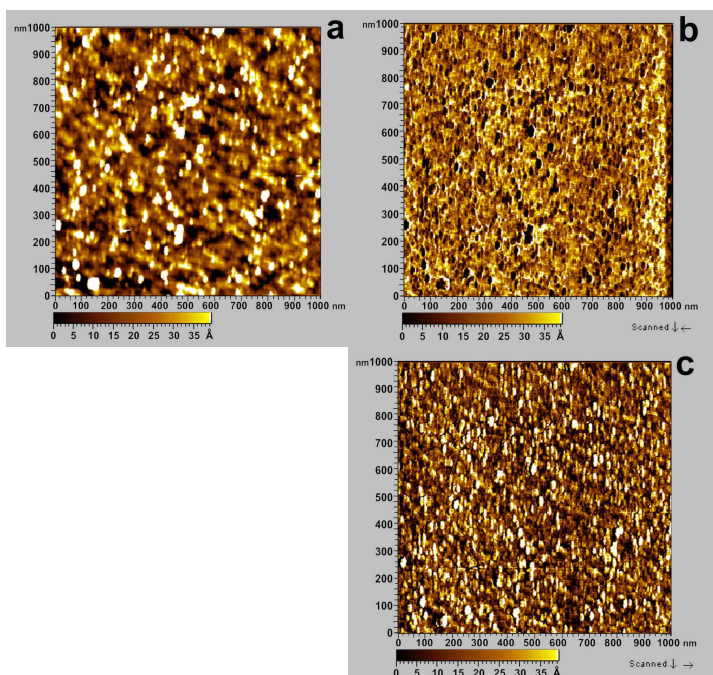


Figure 8 CdS deposited on patterned Ag(111): (a) AFM topographic image, (b) left-scanned LFM image, and (c) right-scanned LFM image.

Conclusions

The described results are an example of confined electrodeposition of CdS through the use of templates obtained by the selective desorption of a “short-chain” thiol from a binary SAM formed on Ag(111). The electrodeposition of a compound is quite demanding, since it requires the right stoichiometry. In addition, the surface underpotential deposition phenomena exploited by ECALE ensure that the surface available for electrodeposition after the selective desorption is still Ag(111).

The comparison between the amount of compound deposited on a bare Ag(111) and that deposited after MPA desorption shows that the free surface available for electrodeposition amounts to 40% of the whole surface. This value is equal to the sum of the area left after MPA desorption, 25%, and that, 16%, due to the presence of defects in the remaining OT SAM. While the presence of defects could be reasonably avoided using a “long chain” thiol that forms more compact SAMs on Ag(111), it is worthwhile to note that the defects are not due to the deposition process since they are

suggested by the limited blocking effect of $[\text{Ru}(\text{NH}_3)_6]^{2+/3+}$ on a single OT SAM formed on Ag(111). Moreover, the presence of defects is consistent with the possibility of depositing a small fraction of Cadmium UPD on the single OT SAM. It must also be noted that the underpotential deposition is a surface sensitive phenomenon and, therefore, requires that free areas of Ag(111) are exposed to the solution. It must be stressed that the presence of the templating thiol on Ag(111) does not affect the surface phenomena on which the ECAL procedure is based and that, in turn, the ECAL procedure seems not to modify the amount of thiol used as a template. The combined AFM and LFM analysis shows that the holes left by MPA desorption are homogeneously distributed over the whole surface and that the approximate evaluation obtained by summing the areas occupied by the clusters yields a CdS coverage equal to 35-40%, in good agreement with the electrochemical results. Future work will be directed to the selection of "long-chain" thiols able to form more compact SAMs. Then a systematic morphological analysis will be performed on binary SAMs of different compositions in the attempt to control the shape of the holes.

2.3.3 Confined Electrodeposition of Cadmium Sulfide in the Holes Left by the Selective Desorption of 3-Mercapto-1-propionic Acid from a Binary Self-Assembled Monolayer Formed with 1-Dodecanthiol

Introduction

In this second chapter dedicated to mixed SAMs, we present a procedure based on the selective desorption of 3-Mercaptopropionic acid (MPA) from a mixture with 1-Dodecanethiols (DDT) that forms a compact SAM on Ag(111). The compound grown is Cadmium Sulfide (CdS), whose experimental growth conditions are simple and reproducible and make it a good “electrodeposition probe”.

It must be stressed that the electrodeposition of a compound presents more difficulties than the electrodeposition of a single element or metal, since a compound requires the right stoichiometry. Then, the analysis carried out on CdS electrodeposition is quite demanding.

Experimental

Materials Merck analytical reagent grade $3\text{CdSO}_4 \cdot 8\text{H}_2\text{O}$ and absolute ethanol, Aldrich analytical reagent grade Na_2S , KCl , NaOH , $\text{Ru}(\text{NH}_3)_6\text{Cl}_3$ and purity grade Fluka 90% 3-mercapto-1-propionic acid (MPA), 1-octanethiol (OT), 1-decanethiol (DT), and 1-dodecanethiol (DDT), were used without further purification. Merck analytical reagent grade HClO_4 and NH_3 were used to prepare the pH 9.2 ammonia buffer.

ECALE cycles for CdS deposition CdS growth was obtained by alternating the underpotential deposition of Sulfur with that of Cadmium and repeating this basic cycle as many times as desired to attain the wanted thickness (chapter 2.1.2). The silver single crystals were prepared according to the Bridgman technique and polished by a CrO_3 based procedure.⁷⁴⁻⁷⁶

Self assembly of alkanethiols on Ag(111) To obtain full layer formation, the substrate was immersed in solutions of alkanethiol in pure ethanol for at least 2 h. To avoid the formation of thiol multilayers the substrates were later kept in pure ethanol for 1 h. The single SAMs were obtained from 0.3mM alkanethiol solutions whereas the mixed SAMs were prepared from solutions of different compositions to achieve different monolayer compositions.

Atomic force microscopy (AFM) AFM topographic images were taken with a commercial instrument (PicoSPM, Molecular Imaging) in contact mode with a commercial Si_3N_4 cantilever (Nanosensors, Wezlar- Blankenfeld).

Lateral force microscopy (LFM) Together with the vertical deflection of cantilever, which creates the topography image, images of the cantilever lateral deflection allow areas with different frictions to be distinguished, and therefore of different chemical natures, between the scanning tip and the sample. LFM used in conjunction with topography imaging is a sensitive tool for surface morphological investigations.

Results and discussion

Estimate of film quality

Electrodeposition requires that free metal areas acting as cathode face the solution. However, free silver areas can either be due to the selective desorption or to the presence of defects. As reported in the literature, the compactness of a self-assembled monolayer can be estimated on the basis of the electron transfer kinetic.¹¹³⁻¹¹⁵ Cyclic voltammograms of $[\text{Ru}(\text{NH}_3)_6]^{2+/3+}$ performed on Ag(111) fully covered by OT, DT or DDT show an increasing compactness of the SAM (Fig. 1). At the same time, Fig. 2 shows that the amount of defects decreases, as shown by the decreasing stripping peaks of Cadmium deposited at underpotential on OT, DT and DDT, respectively. In fact, the stripping peak of Cadmium from OT/Ag(111) is about 16% of that on the bare Ag(111) and that of Cadmium from DT/Ag(111) is only 5%, whereas no deposits are formed on DDT/Ag(111). Also note the negative potential shift of the peaks in Fig. 2, maybe explained by the fact that diminished lateral interactions between the deposited CdS clusters make the re-dissolution process easier. The above analysis supports well the use of DDT as a “long chain” thiol to combine with MPA.

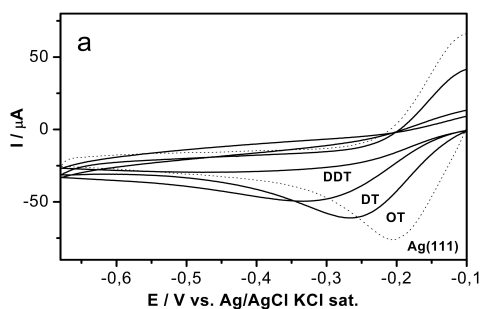


Fig. 1. Cyclic voltammograms obtained from 1mM $\text{Ru}(\text{NH}_3)_6^{3+}$ in 0.1M KCl on the bare Ag(111) and on Ag(111) fully covered by OT, DT, DDT. The scan rate was 50mVs^{-1} .

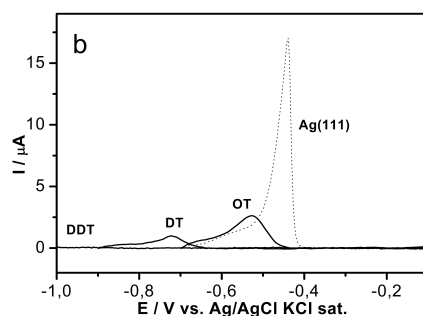


Fig. 2. Stripping peaks of Cd deposited at underpotential on the bare Ag(111) and on Ag(1 1 1) fully covered by OT, DT, DDT. The scan rate was 50mVs⁻¹.

Electrochemical characterization of the binary DDT-MPA SAMs

The surface molar ratio of the single thiols in a multi component SAM can be estimated by the charge involved in the desorption of each single component¹¹⁵. As already reported in the literature, the composition of the monolayers never equals the solution composition, since longer thiols tend to occupy larger areas; yet, less pronounced differences are observed between composition in solution and on the surface on silver.¹¹¹ Fig. 3 shows the systematic voltammetric analysis performed by stripping binary SAMs obtained on Ag(111) by keeping the DDT bulk concentration equal to 0.3mM (Fig. 3a) and varying that of MPA from 0.3 to 0.9mM (Fig. 3b). More precisely, curves 1 are given by a solution 0.3mM DDT+ 0.3mM MPA, curves 2 by 0.3mM DDT+ 0.6mM MPA, and curves 3 by 0.3mM DDT+ 0.9mM MPA. The corresponding surface molar ratios are reported in Table I. As expected, the surface molar ratio of MPA increases while increasing its bulk concentration. Note that while MPA stripping is performed in an aqueous KOH solution, DDT stripping is performed in an alcoholic KOH solution where it is shifted towards less negative potential (Fig. 4b). In fact, in aqueous KOH solutions the DDT stripping peak is hidden by hydrogen evolution even working at KOH concentrations as high as 0.5M (Fig. 4a).

	c/mM	% in solution	% on Silver surface
MPA	0.3	50	12
DDT	0.3	50	88
MPA	0.6	67	22
DDT	0.3	33	78
MPA	0.9	75	30
DDT	0.3	25	70

Table I Bulk and surface compositions of MPA and DDT.

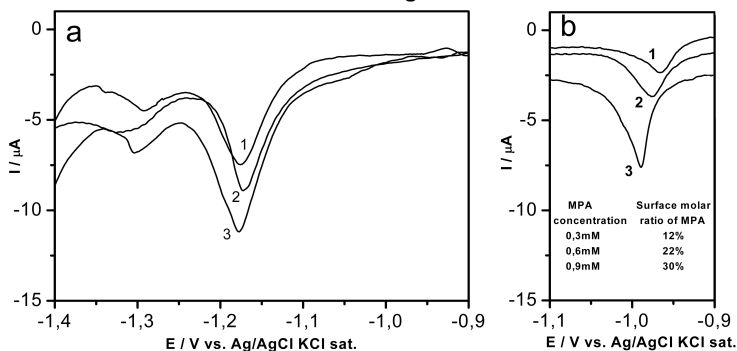


Fig. 3. Stripping curves of DDT in 0.5M KOH in ethanol 90% (a) and of MPA in 0.5M KOH (b) from the binary SAMs obtained on Ag(1 1 1) in solutions: 0.3mM DDT+ 0.3mM MPA (curves 1); 0.3mM DDT+ 0.6mM MPA (curves 2); 0.3mM DDT+ 0.9mM MPA (curves 3). The scan rate was 10mV s⁻¹.

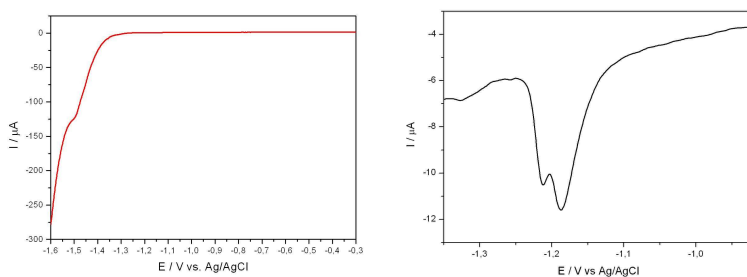


Fig. 4. Stripping curves of the DDT SAM formed on Ag(1 1 1) in 0.5M KOH (a) and in 0.5M KOH in ethanol 90% (b). The scan rate was 10mVs⁻¹

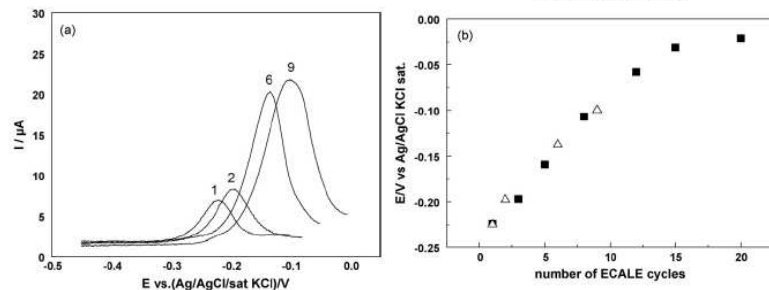


Fig. 5. (a) Linear-sweep voltammograms for the Cd oxidative stripping from patterned CdS films deposited with 1, 2, 6 and 9 ECALE cycles (scan rate equal 10mVs⁻¹); (b) potentials of the stripping peaks as a function of the number ECALE cycles for patterned CdS (■) and for CdS grown on bare Ag(111) (Δ).

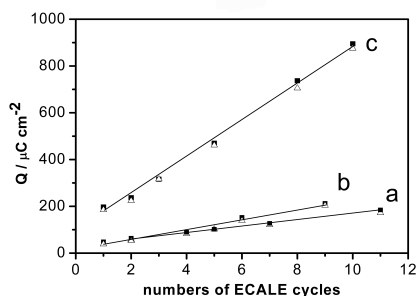


Fig. 6. Plots of the charge involved in the oxidative stripping of Cd (■) and the reductive stripping of S (Δ) as a function of the number of ECALE cycles as obtained on template A (curve a), on template B (curve b) and that previously obtained on a bare Ag(1 1 1) substrate (curve c).

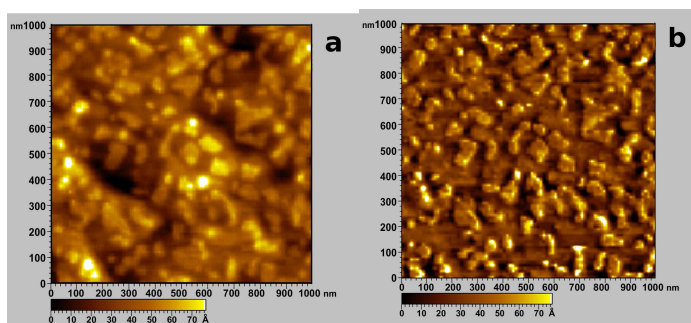
ECALE growth of CdS on the holes left by MPA desorption

Fig. 3 suggests that suitable templates can be obtained by applying a potential equal to -1.1V to the substrate covered by the binary SAM. It must be noted that in KOH this potential is not able to cause DDT stripping since, as shown in Fig. 4a, its stripping peak is negatively shifted. Two different templates were obtained: template A corresponding to a SAM 22% in MPA was obtained from a solution of $0.6\text{mM MPA} + 0.3\text{mM DDT}$, and template B corresponding to a SAM 30% in MPA was obtained from a solution of $0.9\text{mM MPA} + 0.3\text{mM DDT}$. The deposition of CdS and the electrochemical characterization of the compound obtained was performed like in chapter 2.1.2. Accordingly, deposits obtained with an increasing number of cycles are electrochemically re-dissolved by measuring the charge involved in the stripping of Cadmium followed by the stripping of Sulfur. This procedure is usually employed to determine the amount of elements deposited in a given number of ECALE cycles. Fig. 5a shows the stripping peaks of Cadmium while increasing the number of ECALE cycles. Apart from the current values, these curves exactly reproduce the stripping curves of CdS deposits grown on bare Ag(111) substrates.⁷⁷ As usual, the stripping process of the first element (in our case Cadmium) becomes progressively more difficult as the number of deposition cycles increases. As it has been shown previously⁷⁷ the observed potential shift is much greater than that ascribable to the slow kinetics of the dissolution process and it is mostly due to an increasing stability of the compound up to the attainment of a limiting value. Fig. 5b shows that the potentials of the stripping peaks of Fig. 5a are in excellent agreement with those previously reported for CdS grown on bare Ag(111). It must also be noted that the well-defined shape of the stripping peaks of Fig. 5a suggests that all Cadmium is present as CdS. Another important conclusion suggested by Fig. 5 is that in both cases the thickness of the CdS film was proportional to the number of ECALE cycles used. Fig. 6 shows plots of the charges per cm^2 for Cadmium and Sulfur strippings

obtained from CdS deposited on template A (curve a), on template B (curve b) and that previously obtained⁷⁷ on a bare Ag(111) substrate (curve c). Figs. 5 and 6 show that the deposition process performed on the patterned Ag(111) is similar to the one performed on the bare Ag(111), with the obvious decrease in the amount of material, due to the reduced electrode surface. In particular, the coincidence of the charges associated with Cadmium and Sulfur strippings gives a 1:1 stoichiometric ratio between the elements as expected for the compound, and the linear increase of the deposit with the number of deposition cycles suggests the layer-by-layer growth mechanism that is the aim of ECALE method. The slope of each plot gives the charge per cycle. The slope of $13 \mu\text{Ccm}^{-2}$ obtained on the template A and that, $21 \mu\text{Ccm}^{-2}$, obtained on the template amount to 19% and 30% respectively of the slope, $70\mu\text{Ccm}^{-2}$,⁷⁷ observed on the bare Ag(111). This result allows us to hypothesize that the silver area at disposal for the electrodeposition coincides with that of desorbed MPA.

AFM characterization of template CdS

The electrochemical characterization was completed with a morphological analysis performed on samples formed with 20 ECALE cycles on template A. According to the estimate of our CdS sample thickness made previously,⁷⁷ this number of cycles should result in a CdS film thickness of about 4 nm. The AFM topographic image shows that CdS clusters are distributed over the whole surface (Fig. 7a). These clusters are better evidenced by the bright areas in the left-scanned LFM image (Fig. 7b) and by the dark areas in the right-scanned LFM image (Fig. 7c). The clusters have an average equivalent radius lower than 60 nm. More precisely, the distribution analysis performed on different regions of the samples shows that most of them (95–98%) occupy an area lower than 5000 nm^2 corresponding to an equivalent radius of about 40 nm. The total area occupied by CdS, i.e. the sum of the single clusters, always yields the value of $20\pm 2\%$ of the whole surface.



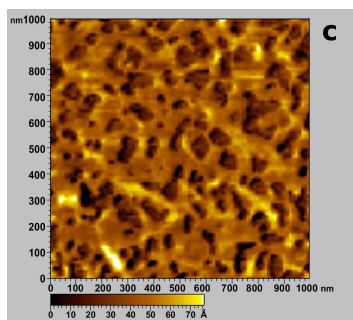


Fig. 7. CdS deposited on template A: (a) AFM topographic image, (b) left-scanned LFM image, and (c) right-scanned LFM image.

Conclusions

Templates suitable for electrodeposition are simply obtained with a procedure based on the selective desorption MPA from a MPA+DDT SAM formed on Ag(111). Two templates corresponding to different surface molar ratios of MPA and DDT were used to grow CdS, whose experimental growth conditions by ECALE are simple and reproducible and make it a good “electrodeposition probe”. The electrochemical characterization confirms that the silver area at disposal for the electrodeposition coincides with that of desorbed MPA and shows that the deposition process performed on the patterned Ag(111) is similar to the one performed on the bare Ag(111), with the obvious decrease in the amount of material, due to the reduced electrode surface. The present work aims to point out that the presence of the templating thiol on Ag(111) does not affect the surface phenomena on which the ECALE procedure is based, and that, in turn, the ECALE procedure seems not to modify the amount of the thiol used as a template. It must also be noted that the underpotential deposition is a surface sensitive phenomenon, and, therefore, requires that free areas of Ag(111) are exposed to the solution, therefore we can assume that the desorption of MPA does not affect the silver surface. The combined AFM and LFM analysis performed on template A shows the formation of clusters, whose nature is surely different from that of its background, confirming that the electrodeposition of CdS successfully occurred. As shown by the distribution analysis, the clusters have an average equivalent radius lower than 60 nm, and the total area occupied by CdS, i.e. the sum of the single clusters is $20\pm 2\%$ of the whole surface, in good agreement with the electrochemical data for both MPA desorption and CdS deposition.

These results have been obtained by analysis performed in different regions of the sample and, therefore, indicate a homogeneous CdS deposition. A systematic analysis

of binary mixtures of MPA and longer chain thiols such as OT, DT, DDT and hexadecanethiol (HDT) on gold was carried out in Ref. 11210 by measuring the areas (A) and the circumferences (L) of the holes. The ratio L^2/A equals 4π for a perfect round hole and becomes larger with an increasing deviation from linearity. This semi-quantitative evaluation shows that for OT the shape of the holes can be controlled to some degree, and less for the other thiols. This is ascribed to the fact that the difference between the molecular interaction of OT in its SAM is larger than that of MPA, so that MPA tends to form round domains for relatively low values of its surface molar ratio. However, when the difference between the molecular interaction is large as, for example, in the case of HDT and MPA, the molecular interactions of MPA become negligible so that MPA distributes around the long thiol domain. In this case, the use of thiols having specific terminal groups can be used to change the interactions of the adsorbed thiols. Future systematic morphological analysis will be directed to the attempt of controlling the shape of the holes, both by changing the relative compositions of MPA and DDT and by exploring other thiol combinations.

2.3.4 Cobalt deposition into the pattern obtained by selective desorption of the short chain-thiol from a binary alkanethiol SAM and catalysis towards oxygen reaction reaction

Introduction

This chapter focused on the Oxygen Reduction Reaction (ORR), which is one of the most important electrocatalytic reaction, using silver substrates as cathodes. Following the most recent guidelines of theoretical studies on this topic, we tried to study the catalytic effect of silver substrates electrochemically modified at nanometer scale. Aim of this work was the achievement of the synergic effect of two different metals, each of them acting on different steps of ORR, and to stress the role of the surface morphology and structure.

The catalytic activity of Silver, already known and characterized, can be enhanced by the presence of a monolayer of Cobalt rearranged in nanosized islands. In order to obtain such a controlled nanostructure, a novel method using self-assembled monolayer (SAMs) based templates was used. According to a recent work of ours, the confined electrodeposition of Cobalt on Ag(111) was performed into a template formed by the selective desorption of a short chain thiol (3-Mercaptopropionic acid, MPA) from the binary SAMs with 1-Dodecanethiols (DDT). This method allows a deep control of the morphology of the deposit, by varying the molecular ratio of thiols.

Well-ordered layers of metals able to exert a synergic effect on the catalytic properties of silver can be obtained by exploiting surface phenomena such as Underpotential Deposition (UPD).²⁵ However, Cobalt is not deposited at underpotential on Silver and, therefore, the alternative approach of Surface Limited Redox Replacement (SLRR) was used to limit Co deposition to a monolayer. This method, recently elaborated by Adžić et al., consists in the use of a single layer of a third metal, deposited at underpotential, as template for spontaneous deposition of a more noble meta.²⁶ Here, we choose Zinc as template for Cobalt deposition. The first step of this technique involves the formation of the UPD layer of a metal M on a substrate S . In the second step, the adlayer of metal M is replaced by a more noble metal P in an electroless deposition process. The replacement of metal M occurs via an irreversible and spontaneous redox process in which the UPD adlayer is oxidatively dissolved by cations of more noble metals, which are simultaneously reduced and deposited. The method is used when the direct UPD layer of P on S

cannot be formed. Here, the electrodeposition of Cobalt through SLRR method, will replace a layer of Zinc deposited at underpotential on Silver.

In the present work, Ag(111) crystals were covered by islands of Cobalt with surface atomic ratios Co:Ag ranging between 12% and 39%. The catalytic activity of such samples towards the Oxygen Reduction Reaction (ORR) was valued and the best improvement, with respect to bare silver, was found for a percentage of Cobalt around 30%, in good agreement with the theoretical hypothesis.

The scope of this chapter is to present a method to study the influence of the ratio Ag/Co on the catalytic activity in the oxygen reduction reaction with the minor possible contribute of the surface roughness. In order to reduce the “crystallite size effect”,¹¹⁸ and others variable in the “building” the catalyst Ag-Co we start from a single crystals of Ag(111), prepared in our laboratory¹¹⁹ under roughness control.

Experimental section

Materials. Merck analytical reagent grade $\text{ZnSO}_4 \cdot 7\text{H}_2\text{O}$, $\text{CoSO}_4 \cdot 7\text{H}_2\text{O}$ and absolute ethanol, Aldrich analytical reagent grade Na_2S , KOH and purity grade Fluka 90% 3-mercaptopropionic acid (MPA) and 1-dodecanethiol (DDT) were used without further purification. Merck analytical reagent grade HClO_4 and NH_3 were used to prepare the ammonia buffer at pH 9.6.

The silver single crystals Ag(111) (0.785 cm^2) were prepared according to the Bridgman technique and mechanical polished first with progressively finer papers (BuehlerMet SiC) and then with alumina powder of different grades (Buehler micropolish), down to $0.05 \mu\text{m}$. Before each measurements, a chemical polishing with a CrO_3 based procedure⁷⁴⁻⁷⁶ was performed. It consists in the surface oxidation of silver by means of a solution 0.15M CrO_3 and 0.1M HCl . After polishing, the electrode was soaked first in a concentrated ammonia solution for about 5 minutes, and then in concentrated sulfuric acid for about 20 minutes. Finally, it was thoroughly rinsed with water.

Self-Assembly of Alkanethiols on Ag(111). To obtain full layer formation, the substrate was immersed in solutions of alkanethiol in pure ethanol for 2 hours.

Preparation of SAM based template and Cobalt electrodeposition. All the electrochemical experiments, for selective desorption of MPA followed by electrodeposition of Co within the pattern, were performed in a flow-electrochemical cell. An automated apparatus containing Pyrex solution reservoirs, solenoid valves and distribution valves, connected to a computer, permitted to send the desired deaerated solutions through the cell.

Atomic Force Microscopy (AFM). Images were taken with a commercial instrument (PicoSPM, Molecular Imaging) in contact mode with a commercial Si_3N_4 cantilever (Nanosensors, Wezlar-Blankenfeld). In conjunction with topography imaging, Lateral Force Microscopy (LFM) was used for surface morphological investigations of samples composed by areas with different chemical nature, like thiol

and metal.

Oxygen Reduction Measurements. Experiments were carried out in a conventional one-compartment glass cell containing O₂ saturated 0.1M KOH. KOH solutions were freshly prepared, since silver catalytic activity is reduced in aged hydroxide solutions.¹²⁰ The cell is equipped with a rotating-disk working electrode (Autolab RDE-2) with a Teflon attachment to enclose the silver crystal, a large area Pt wire as a counter electrode and a Ag/AgCl, KCl_{sat} reference electrode. All the potentials are referred to this electrode. All experiments were performed at room temperature using an AUTOLAB potenziostat (μ Autolab Type II).

Result and Discussion

Preparation templates with different sized holes from binary DDT-MPA SAMs on Ag(111). A detailed electrochemical and morphological characterization of the binary DDT-MPA SAMs on Ag(111) was recently done in our laboratory using CdS as “electrodeposition probe”.¹¹⁹ More precisely, we prepared different surface compositions of the SAMs (12%, 22% and 30% surface percentage of MPA). Then, the selective desorption of the shortest chain thiol MPA left different sized holes in the SAMs in which CdS was later deposited. The total area available for CdS electrodeposition was determined by the integration of the desorption peak of MPA. In the present work, we prepared the same templates 12%, 22% and 30% plus a new one of 39% (all experimental conditions are summarized in Table 1) for the confined underpotential electrodeposition of Cobalt.

		<i>C/mM</i>	<i>% in solution</i>	<i>% on Silver surface</i>
Sample 1	MPA	0.3	50	12
	DDT	0.3	50	88
Sample 2	MPA	0.6	67	22
	DDT	0.3	33	78
Sample 3	MPA	0.9	75	30
	DDT	0.3	25	70
Sample 4	MPA	0.9	82	39
	DDT	0.2	18	61

Table 1. Bulk and surface compositions of MPA and DDT

Cobalt underpotential deposition using the Surface Limited Redox Replacement (SLRR) method. Cobalt electrodeposition on Ag(111) was performed from 0.5 mM CoSO₄·7H₂O in ammonia buffer solution of pH 9.6. To avoid the presence of Co³⁺ only freshly prepared solutions were used. Since Cobalt does not present underpotential deposition on Silver, we tried to limit its deposition maintaining the current at a constant value of 10 μ A for a time of a few seconds. In

that way, the extent of deposition can be controlled by controlling the time. However, this procedure couldn't be applied to the deposition of Cobalt on patterned silver since the deposit was not confined into the SAM template. In fact, electrochemical and AFM measurements showed that Cobalt deposition was not limited to the free silver areas, but partly extended under the patterning thiol SAM. To overcome this problem, an alternative approach of metal deposition, named Surface Limited Redox Replacement (SLRR), recently elaborated by Adžić et al.,²⁶ was used. According to this method, an ordered metal adlayer obtained by underpotential deposition is replaced by a more noble metal monolayer. Such a replacement occurs via an irreversible and spontaneous redox process in which the UPD layer is oxidatively dissolved by cations of more noble metals, which are simultaneously reduced and deposited. The use of Silver as a substrate limits the possibility of application of SLRR method to metals which give UPD on Ag and which are less noble than Cobalt. A good candidate is Zinc, whose UPD on Ag(111) is shown in Figure 1.

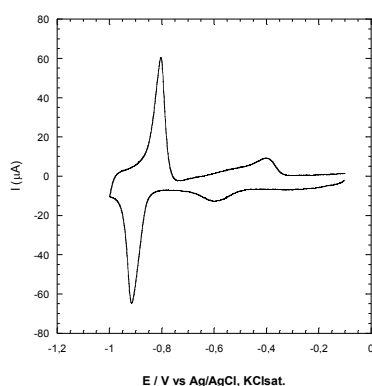


Figure 1 Cyclic voltammogram obtained from 1 mM $\text{ZnSO}_4 \cdot 7\text{H}_2\text{O}$ in pH 9.6 ammonia buffer on Ag(111) in the UPD region. Scan rate: 50 mV/s. Deposition of a complete Zn monolayer at -1 V.

The process of spontaneous and complete substitution of Zinc with Cobalt requires a few minutes. In fact, the replacement of Cobalt, checked through the values of Cobalt stripping charge, is complete after 5 minutes, as shown in Figure 2 (plot of the charge of Cobalt stripping peaks versus replacement times).

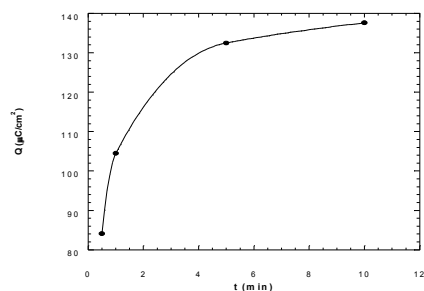


Figure 2 Charge from Cobalt stripping peaks as a function of the replacement time.

The charge involved in the Cobalt stripping corresponds to that involved in the dissolution of a single Zinc UPD monolayer ($136 \mu\text{C}/\text{cm}^2$).

The procedure for the deposition of a single layer of Cobalt was repeated on each of the four patterned samples described in Table 1. The amounts of deposited Cobalt within the different templates were determined by the charge of stripping (see inset in Fig. 3). These charges are obviously related to the silver surface area available for deposition and allow to understand if Cobalt is really deposited only within the holes of the templates. In fact, Cobalt stripping charges obtained from the different templates and from the whole electrode are in good agreement with MPA stripping charges that give a direct measure of the area (see inset in Fig. 3).

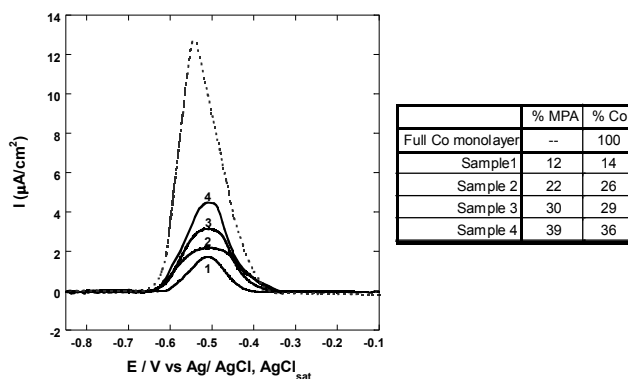


Figure 3 On the left Cobalt stripping in ammonia buffer solution of Ag(111) covered by a full monolayer of Cobalt (dashed line) and by fractional Cobalt monolayers according to the procedure described (solid lines relative to samples 1-4). Scan rate: 10 mV/s. The table on the right shows percentages of MPA on the surface determined by electrochemistry and percentages of Cobalt deposited for samples 1-4.

AFM analysis. After Cobalt electrodeposition, and still in presence of the long chain thiol, a morphological analysis with AFM was performed on each sample. Together with the vertical deflection of cantilever, which creates the topography AFM image, images of the cantilever lateral deflection allow to distinguish areas with different friction, and therefore areas of different chemical nature. For this reason, LFM, in conjunction with topography imaging, was used for the morphological investigations of the samples.

LFM images of the samples 1-4, in Figure 4, show $5 \times 5 \mu\text{m}^2$ areas in which Cobalt islands (dark areas) are uniformly distributed. Shape and dimension of the islands vary from Fig4a to Fig 4d: small islands in Figure a become bigger in b and still bigger in c until they partially coalesce in a continuous network in d. Table 2 shows that the percentages of area occupied by Cobalt islands estimated by the AFM analysis are in good agreement with the values obtained by MPA and Cobalt stripping charges.

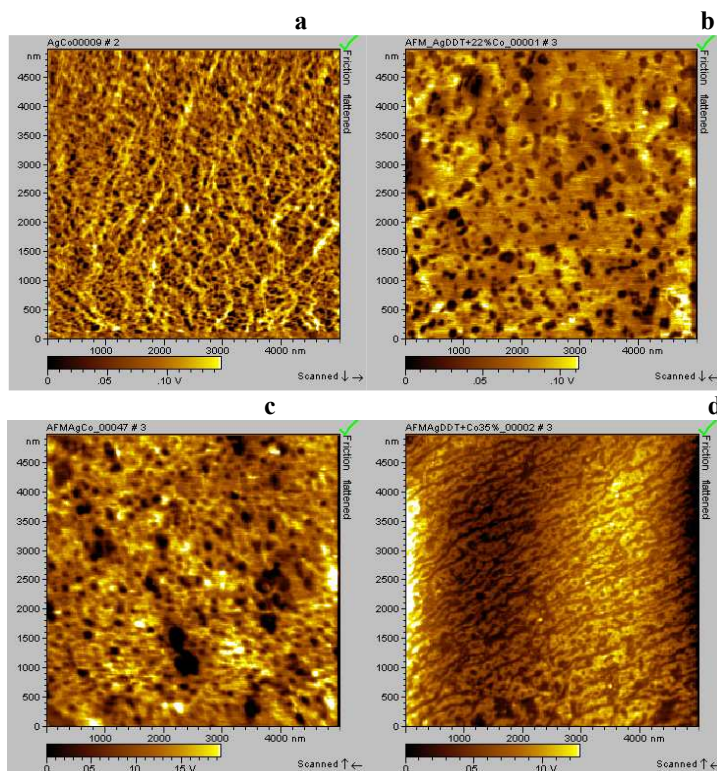


Figure 4. $5 \times 5 \mu\text{m}$ LFM images of Ag(111) covered by 12% (a), 22% (b), 30% (c) and 39% (d) of Co and the remaining covered by DDT.

	<i>% Co from AFM analysis</i>
Sample 1, 12% MPA	14% (Image a)
Sample 2, 22% MPA	23% (Image b)
Sample 3, 30% MPA	32% (Image c)
Sample 4, 39% MPA	43% (Image d)

Table 2. 5x5 μm LFM images of Co deposited on template 1 (image a), 2 (image b), 3 (image c), 4 (image d). Dark areas represent Co islands.

Oxygen Reduction Measurements. To verify the synergic effect of Cobalt and Silver, the DDT SAM still covering and protecting Silver has to be removed. This was directly done in the electrochemical cell applying a potential $E = -1.6\text{ V}$, which is negative enough to desorb DDT, for 3 minutes. Polarization curves for the ORR on Ag(111) and on Ag(111) covered by different percentages of Cobalt were recorded in O_2 saturated 0.1M KOH electrolyte, at different rotation rates and with a scan rate of 50 mV/s. The potential was linearly scanned from -1.1V to -0.1V and reversed. No significant hysteresis between polarization curves recorded in positive and negative going sweep directions was found, as for different silver single crystals surfaces.¹²¹ Figure 5 shows the polarization curves for the ORR on Ag(111) and on Ag(111) covered by different percentages of Cobalt (positive sweep direction at 500 rpm).

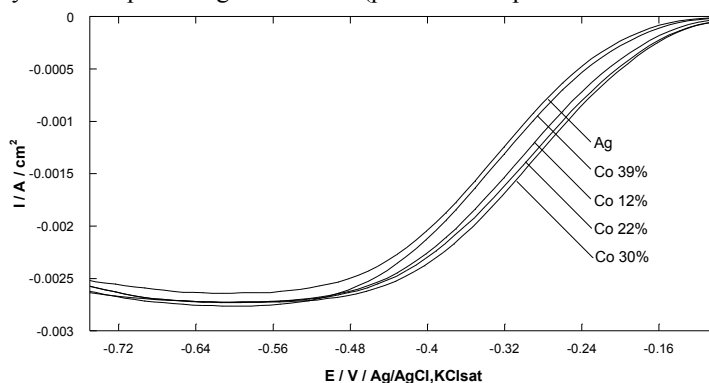


Figure 5. Current-potential curves for Oxygen Reduction Reaction in KOH 0.1M at 500 n/min for different samples.

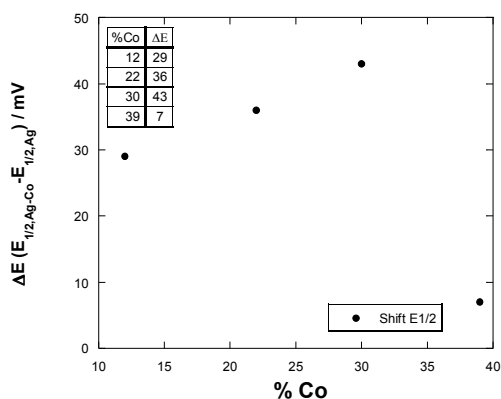


Figure 6. Difference between $E_{1/2}$ of the curves of Ag-Co and $E_{1/2}$ of the curve of Ag respect to the percentage of Co

The curves in Figure 5 show that the catalytic effect of Ag-Co is greater than that of Ag. It increases with the percentage of Co in the order 12<22<30 and then decreases for the sample with 39% of Cobalt. In fact, plotting the difference between $E_{1/2}$ of the curves of Ag-Co and $E_{1/2}$ of the curve of Ag respect to the percentage of Cobalt, a nearly linear increasing trend is shown in the range 12-30%, whereas an abrupt decrease is shown for the sample with 39% Co (Figure 6).

The number of electrons transferred per O_2 molecule in the ORR on the different catalysts can be estimated by Levich plots. Plotting ORR limiting current densities versus the corresponding rotation rates, straight lines (Levich plots) with different slopes are obtained for the different samples (Fig. 7).

Values of the exchanged electrons are calculated from the slopes of the Levich lines using Eq(1):

$$i_d = 0.620 n F A D_0^{2/3} \omega^{1/2} \nu^{-1/6} C_0 \quad (1)$$

in which i_d is the current density, n is the number of exchanged electrons, F is the Faraday constant, A is the area of the electrode (0.785 cm^2), D_0 is the oxygen diffusion coefficient ($1.95 \cdot 10^{-5} \text{ cm}^2/\text{s}$), ω is the angular rotation rate of the electrode (in rad/s), ν is the kinematic viscosity of the solution ($0.008977 \text{ cm}^2/\text{s}$), C_0 is the O_2 solubility in solution ($1.15 \cdot 10^{-3} \text{ mol}/\text{dm}^3$).

Interestingly, the number of exchanged electrons, calculated by the slopes of the plots, increases towards the best value of $4 e^-$ with the same order in which the catalytic activity increases. In fact, the sample with 30% Co, besides having the best catalytic activity, is also the one that follows a pathway with the number of electrons closest to the optimal number of 4.

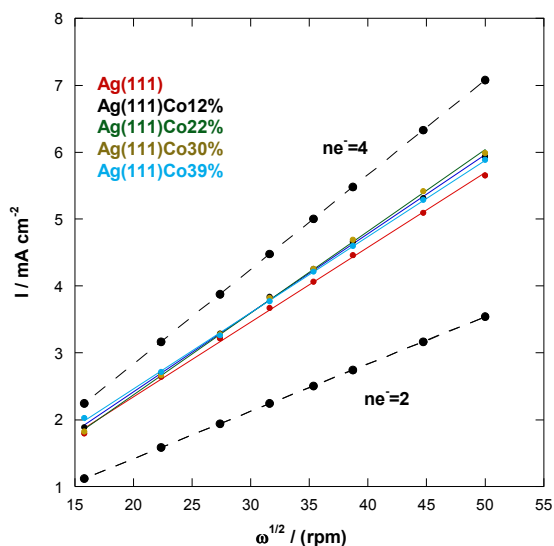


Figure 7. Levich plots for ORR on bare Ag(111) (red line), and Ag(111) covered by 12% Co (black), 22% (green), 30% (brown), 39% (blue). i_d collected at -0.7V (vs Ag/AgCl, KCl sat). The dotted lines correspond to the theoretical slope calculated for 2 and 4 electrons processes.

Conclusion

The aim to achieve the synergic effect of two different metals, both of which acting on different steps of ORR, drove the design of bimetallic catalysts of Cobalt and Silver in this chapter. The catalytic activity of Silver, already known and characterized, was enhanced by the presence of a layer of Cobalt subdivided in nanostructured islands. In order to obtain such a controlled nanostructure, a novel method using self-assembled monolayer (SAMs) based templates was used. The confined electrodeposition of Cobalt on Ag(111) was performed into a template formed by the selective desorption of a short chain thiol (3-mercaptopropionic acid, MPA) from the binary SAMs with 1-Dodecanthiols (DDT). This method allows a deep control of the morphology of the deposit, by varying the molecular ratio of thiols. Since Cobalt is not deposited at underpotential deposition on Silver, the alternative approach of Surface Limited Redox Replacement was used. This method, recently elaborated by Adžić et al., consists in the use of a single layer of a third metal, deposited in underpotential, as a template for spontaneous deposition of a more noble metal. Here, we choose Zinc as a template for Cobalt deposition. Ag(111) crystals were covered by islands of Cobalt achieving superficial atomic ratios ranging between 12% and 39% for Cobalt. The catalytic activity of such samples towards the

Oxygen Reduction Reaction (ORR) was valuated and the best improvement, with respect to bare Silver, was found for a percentage of Cobalt around 30%, in good agreement with the theoretical hypothesis.

Electrodeposition on Gold single crystals:

The last two sections of the thesis contain the results obtained during a period of six months of research carried out at the University of Ulm, under the supervision of Professor Kolb. The same concepts of Underpotential Deposition (UPD) and thiol based SAM formation studied on Silver have been applied on Au(111). More precisely, the Underpotential Deposition of Palladium on Au(111) was followed by Electrochemical STM (EC-STM), with the observation of the structures of the first two layers of Palladium. After that one layer of Palladium was formed on Au(111), the morphology of a SAM of 4-Mercaptopyridine prepared on it was studied by EC-STM.

2.4 Electrodeposition of Palladium on Au(111)

Introduction

The initial stages of Palladium deposition on Au(111) from PdSO₄ 0.2 mM, H₂SO₄ 0,1M were studied by cyclic voltammetry and EC-STM. Underpotential Deposition of the first layer of Palladium was performed and a second layer was prepared at slight overpotentials, as is reported in literature.¹²² Structures of sulfate adsorbed on the first and the second Palladium layers were evaluated. Electrochemical behavior of Au(111) covered by a single layer of Palladium was studied in H₂SO₄ 0,1M, as a starting point for its use as a substrate for thiol based SAM, studied in the next section.

Experimental section

Gold single crystal electrodes used in electrochemical and STM measurements were cylinders with the polished surface oriented along the (111) plane to better than 1°. Prior to each experiment, the Gold crystal was annealed for 5 min in a propane or hydrogen flame, allowed to cool in air, and then immersed into water, before contacting with the electrolyte in the electrochemical cell, or into thiol solution for modification. Analytical suprapure H₂SO₄ and PdSO₄ were used without further purification. For the electrochemical experiments, the electrolyte was deaerated by purging N₂. For both electrochemical and STM measurements, rapid potential control

was achieved by setting the potentiostat in the operating mode at the desired value prior to contacting the electrode with the solution. Cyclic voltammograms were obtained with standard electrochemical equipment.

In situ STM measurements were performed with a Topometrix TMX 2010 Discoverer, using an all Kel-F custom-made cell and Pt/Ir (80:20) tips electrochemically etched in 3.4 M NaCN. Tips were coated with an electrophoretic paint to minimize faradic currents. Tunneling currents for image acquisition were in the range of 0.5-1.0 nA. Two Pt wires, cleaned by annealing in a hydrogen flame, were used as counter and pseudo-reference electrodes ($E_{\text{Pt}} = +0.55 \pm 0.05$ V vs Saturated Calomel Electrode, SCE, in 0.1 M H_2SO_4). However, all electrode potentials are quoted with respect to SCE.

Results and Discussion

Cyclic Voltammetry

Au(111) in 0.1M H_2SO_4

A voltammetric study was performed with the electrochemical cell and the crystals described above. As first, a cyclic voltammogram of bare Gold in 0.1 M H_2SO_4 was performed in order to check the good state of the surface (Fig. 1). The attribution of the significance of the peaks in Figure 1, as shown in literature, will be confirmed in the STM analysis. The peak at 0.3V is connected with the lifting of reconstruction of Gold and the sharp peak at 0.75V marks the disorder-order transition phase of Sulfate.

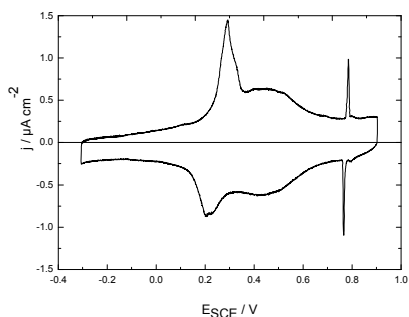


Figure 1. Cyclic voltammogram of Au(111) in 0.1M H_2SO_4 solution. Scan rate: 5 mV/s.

Palladium deposition on Au(111)

Palladium deposition was performed in PdSO_4 0.2 mM, H_2SO_4 0,1M solution. While the equilibrium potential for Pd/Pd^{2+} in the solution is 0.53V, Palladium deposition starts at slightly more positive potential. For this reason, a very low cathodic scan was performed in order to yield the peak of Underpotential Deposition. This is done in Figure 2, where a current-potential curve relative to the cathodic scan from the initial value of 0.8 V at a scan rate of 1mV/s is shown. An UPD peak is observed at 0,55V.

With the purpose to limit the deposition at the first layer, the scan is interrupted just after the maximum and the deposition current is allowed to flow until zero. The charge density over this peak is about $440 \mu\text{C}/\text{cm}^2$, in good agreement with a pseudomorphic layer on Au(111).

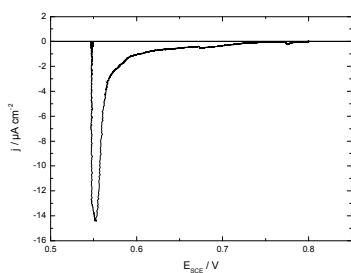


Figure 2. Current-potential curve, starting at 0.8V for Au(111) in PdSO_4 0.2 mM and H_2SO_4 0,1M. Scan rate: 1 mV/s

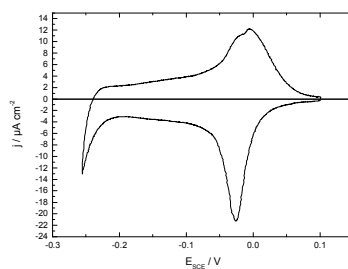


Figure 3. Cyclic voltammogram in the Hydrogen adsorption region for 1Pd ML on Au(111) in H_2SO_4 0,1M. Scan rate: 5 mV/s.

The electrochemical behavior and the range of stability of the Palladium layer on Au(111) in H_2SO_4 0,1M is shown in the cyclic voltammograms in Figures 3 and 4. Figure 3 shows peaks related to Hydrogen adsorption/desorption. This behavior is typical of Au(111) covered by one monolayer of Pd, because 2 ML already shows a more intense peak of H adsorption (not shown). Figure 4 shows repeated cyclic voltammograms extended to more positive potential, beyond Palladium oxidation. Repeated scans have shown a gradual dissolution of Palladium, that is proven by the decreasing of Hydrogen adsorption and oxide formation (at 0.73V) peaks, while an emerging peak at 0.6V could be related to oxide formation at the defects.

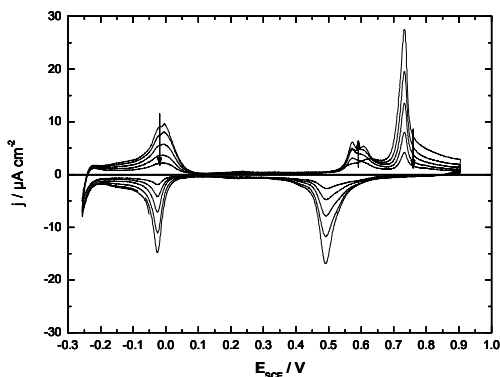


Figure 4. Repeated cyclic voltammograms of Au(111) with 1 ML Pd in H_2SO_4 0,1M; the arrows are drawn from the first scan towards the last scan. Scan rate: 5 mV/s

STM analysis

Au(111) in H₂SO₄ 0,1M

A first characterization of the Gold surface was done in H₂SO₄ 0,1M at different potentials. Relative to the peaks of the cyclic voltammogram in Figure 1, three different potential regions were investigated:

- The potential region negative of peak 0.3 V, where the reconstructed surface shows the characteristic herring-bone structures (Fig 5a).
- After the sharp peak at 0.3V, the surface becomes unreconstructed, the herring-bone structures disappears and islands are generated from the lower atomic density of (1x1) surface structure (Fig 5b).
- After the sharp peak at 0.75V, where specifically adsorbed Hydrogensulfate species order into a densely packed structure (Fig. 5c).

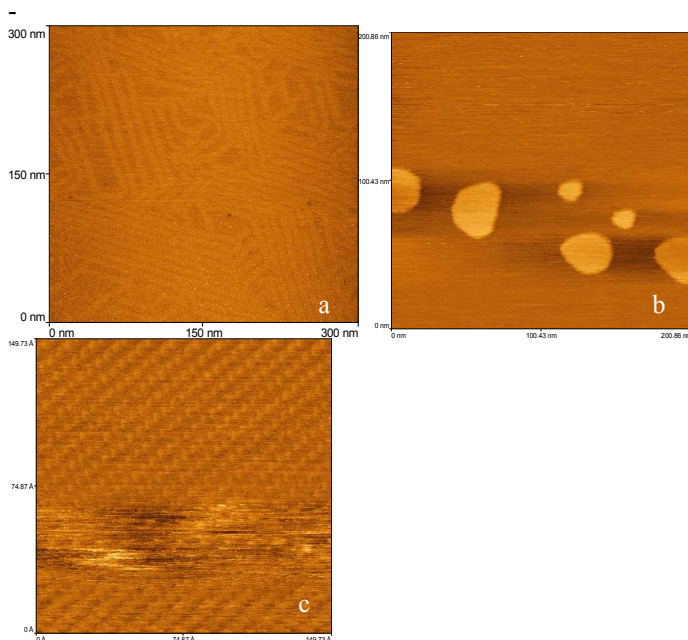
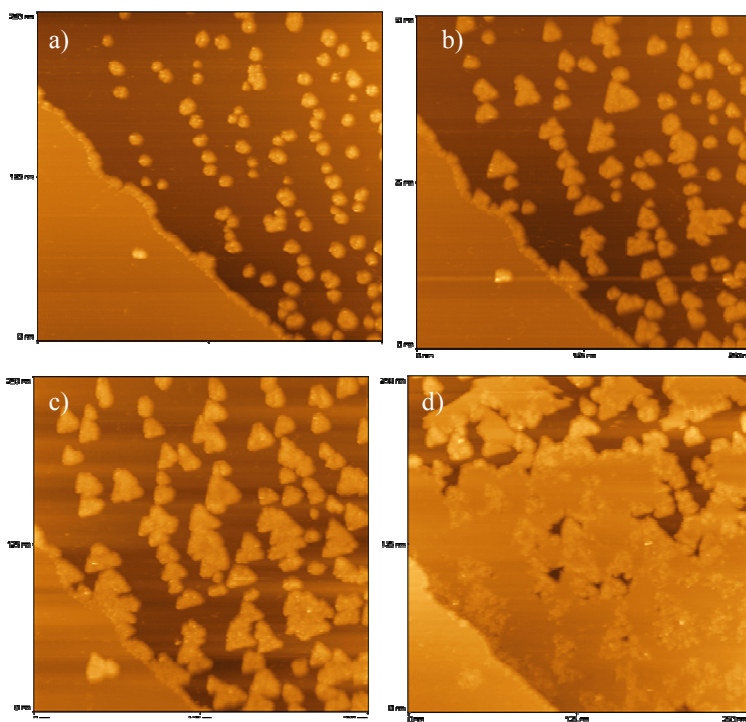


Figure 5. *in-situ* STM images of Au(111) in 0.1M H₂SO₄ (a) at E_{SCE}=200 mV, 300x300 nm², corresponding to the reconstructed surface, (b) at E_{SCE}=400 mV, 200x200 nm², corresponding to the unreconstructed surface, (c) at E_{SCE}=750 mV, 15x15 nm², corresponding to the compact sulfate structure.

Palladium deposition on Au(111)

For the structural investigation, Palladium deposition on Au(111) from PdSO_4 0.2 mM and H_2SO_4 0,1M was performed in the STM cell, using crystals 12 mm large. The cell was connected at an initial potential of 750 mV vs SCE and the potential was gradually decreased following the morphological changes of an area of $250 \times 250 \text{ nm}^2$. When the deposition started, the potential was left constant until the first Palladium monolayer was complete.

At the starting potential, as well as at the deposition potential, the surface reconstruction is known to be lifted, as shown by the presence of Gold islands. Figure 6 represents the evolution of a $250 \times 250 \text{ nm}^2$ area of Au(111) at the beginning of Palladium deposition (Fig 6a) and every 10 minutes (Fig 6b-d) until, after 40 minutes, the UPD monolayer is completed (Fig 6e). The images show that deposition starts at the step edges and at the rims of islands. Moreover, the growth of the deposit gives rise to triangular shape islands, giving evidence to follow the (111) texture of the substrate. When the UPD deposition is complete, gold islands remain uncovered by Palladium.



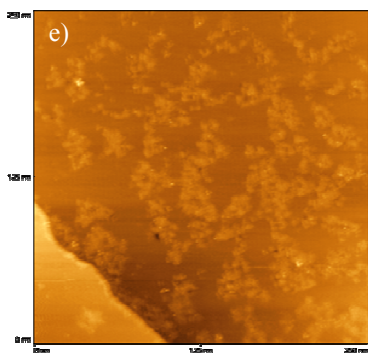
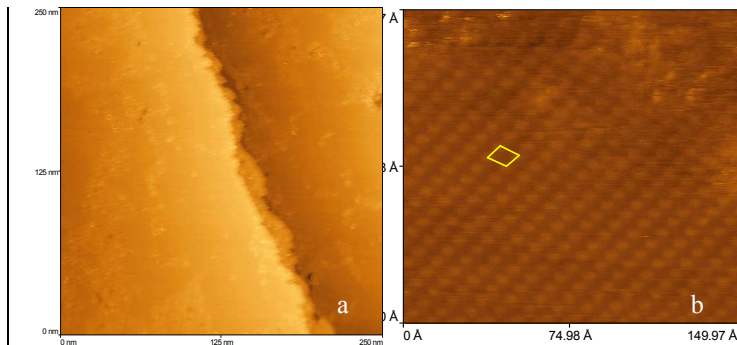


Figure 7. 250 x 250 nm *in-situ* STM images of the same area of a Au(111) electrode during Palladium deposition. Images are registered at constant potential $E_{SCE}=470$ mV at increasing time intervals from the start, until the monolayer is complete: (a) $t=0$, (b) 10min, (c) 20min, (d) 30min, (e) 40min. Tip potential $E_{tip}=0.85$ V

The deposition of the second layer of Palladium was possible at about 50mV more negative potential. An attempt to determine the atomic structures of the first and the second complete Palladium layers was done in the same deposition solution. Figure 8a shows the morphology of the Palladium UPD layer, where borders of different Sulfate domains are visible, and Figure 8b shows the molecular structure of such adsorbate. Figure 8c shows the Sulfate structure on the second Palladium layer. Sulfate structure of Figures 8b and c are both very similar with the one on Au(111) ($(\sqrt{3}\times\sqrt{7})R19.1^\circ$), giving further prove of the pseudomorphic geometry of such layers with the substrate.



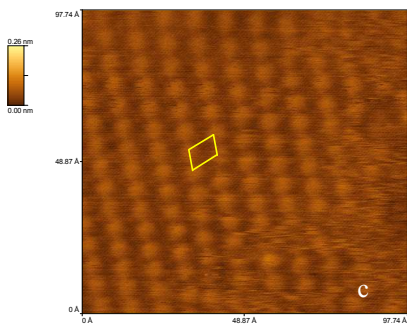


Figure 8. $250 \times 250 \text{ nm}^2$ (a) and $15 \times 15 \text{ nm}^2$ (b) *in-situ* STM images of Au(111) covered by one layer of Palladium at $E_{\text{SCE}}=470 \text{ mV}$ and $E_{\text{SCE}}=520 \text{ mV}$. $10 \times 10 \text{ nm}^2$ STM image (c) of Au(111) covered by two layers of Pd at $E_{\text{SCE}}=430 \text{ mV}$. Images (b) and (c) show the ordered structures of Sulfate on the first and the second layer of Pd on Au(111)

2.5 Structural analysis of a SAM of 4-Mercaptopyridine on Au(111) covered by one monolayer of Palladium.

Introduction

SAMs of 4-Mercaptopyridine attract much attention, as other thiols containing aromatic or heterocyclic groups, thanks to their capacity to immobilize biological molecules or protein on surfaces.^{123,124,125} Moreover the nitrogen end groups exposed to the solution make it interesting for bonding of molecules or coordination of metals. Recently, a new approach of electrochemical metallization of an organic monolayer was performed on this SAM, just exploiting the end-group coordination of metals.^{37,38} The SAM of 4-Mercaptopyridine was already studied on Au(111),³⁸ providing the formation of a well ordered structure of the SAM within a range of potential delimited by reductive desorption and competition of Sulfate adsorption. It was proven that the disulfide adsorbs on Gold via the S endgroup and the S-S bond breaks during adsorption, giving the thiolate species adsorbed.

The study of thiol based SAMs on Palladium surfaces is still a relative unexplored area of research, although the first studies attribute interesting features to the system, like high stability and a particular resistance at etching agents.³⁷ Moreover, the early experimental and theoretical studies^{37,38,126} attribute to the Palladium-thiol interface a complex nature because of its mixed composition of both sulfides and thiols, that is not yet completely understood.

Given the stability of thiol based SAMs on Palladium and given the ordered structures of 4,4'-Mercaptopyridine SAMs on Au(111), a (111) layer of Palladium is supposed to be a good substrate for ordered SAMs of the same thiol.

For this reason, the simple method of Pd(111) layers preparation presented in the previous section is used as a starting point for an attempt to study the interface Palladium-SAM with electrochemical and STM techniques. More precisely, the SAM of 4-Mercaptopyridine formed on a single layer of Palladium deposited at underpotential on Au(111) was studied in sulfuric acid solution with cyclic voltammetry and EC-STM.

Experimental section

Gold single crystal electrodes used in electrochemical and STM measurements were cylinders with the polished surface oriented along the (111) plane to better than 1°. Prior to each experiment, the Gold crystal was annealed for 5 min in a propane or hydrogen flame, allowed to cool in air, and then immersed into water, before

contacting with the electrolyte in the electrochemical cell, or into thiol solution for modification. For the electrochemical experiments, the electrolyte was deaerated by purging with N_2 . For both electrochemical and STM measurements, rapid potential control was achieved by setting the potentiostat in the operating mode at the desired value prior to contacting the modified electrode with the solution.

SAMs of 4-Mercaptopyridine (Aldrich) were prepared by immersing without potential control the freshly annealed Au(111) electrode into a 4,4'-Dithiodipyridine solution prepared with deaerated water to prevent thiol oxidation, according to the procedure described in the text. Immediately thereafter, the electrode was removed from the solution, rinsed thoroughly with ultrapure water, and then introduced to either a conventional electrochemical cell or a STM cell filled with 0.1 M H_2SO_4 or NaOH 0.1M.

Cyclic voltammograms were obtained with standard electrochemical equipment. In situ STM measurements were performed with a Topometrix TMX 2010 Discoverer, using an all Kel-F custom-made cell and Pt/Ir (80:20) tips electrochemically etched in 3.4 M NaCN. Tips were coated with an electrophoretic paint to minimize faradaic currents. Tunneling currents for image acquisition were in the range of 0.5-1.0 nA. Two Pt wires, cleaned by annealing in a hydrogen flame, were used as counter and pseudo-reference electrodes ($E_{Pt} = +0.55 \pm 0.05$ V vs saturated calomel electrode, SCE, in 0.1 M H_2SO_4). However, all electrode potentials are quoted with respect to SCE.

Results

Electrochemical Analysis

4-Mercaptopyridine SAM on Au(111)

For the preparation of the SAM, the Gold crystal was immersed into a 20 μ M 4,4'-Dithiodipyridine (PySSPy) ethanol solution for 6 minutes, then rinsed with ethanol and with water.¹²⁷ Afterwards, the crystal was dipped into the electrolyte for the cyclic voltammetry. Figure 9 shows the cyclic voltammogram in H_2SO_4 0,1M with a couple of sharp peaks at about 0.4V, that mark a phase transition between two compact structures of the SAM.¹²⁷ Figure 10 shows two cyclic voltammograms in NaOH 0,1M: the first scan shows a cathodic peak relative to the reductive desorption of the thiol while the third scan has no trace of such peak. The charge under the reduction peak is 51 μ C cm^{-2} . Assuming a single electron process and an adsorption of the thiolate, it corresponds to a coverage of 0.25, in good agreement with the precedent data of Ref 127.

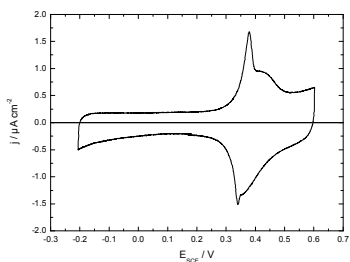


Figure 9. Cyclic voltammogram for 4-Mercaptopyridine SAM on Au(111) in H_2SO_4 0,1M. Scan rate: 5 mV/s

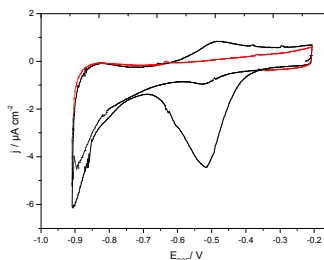


Figure 10. Cyclic voltammogram for 4-Mercaptopyridine SAM on Au(111) in NaOH 0,1M; first scan (solid line) and third scan (dotted line). Scan rate: 10 mV/s

4-Mercaptopyridine on a single Palladium layer on Au(111)

After Palladium Underpotential Deposition, the crystal was washed with water and immersed into a solution of 4,4'-Dithiodipyridine. Different modification procedures were performed for the STM analysis:

-6 and 12 min in 20 μM PySSPy solution

-20 min, 60 min and 19h in 100 μM PySSPy solution

The potential range in which the SAM is stable was detected by cyclic voltammetry. For all the modification procedures, the stability range in H_2SO_4 0,1M was from -0.2 to 0.5 V (Figure 11a). Extending the potential range towards the negative and the positive directions, Hydrogen evolution (Figure 11b) and Palladium oxidation (Figure 11c) were encountered respectively.

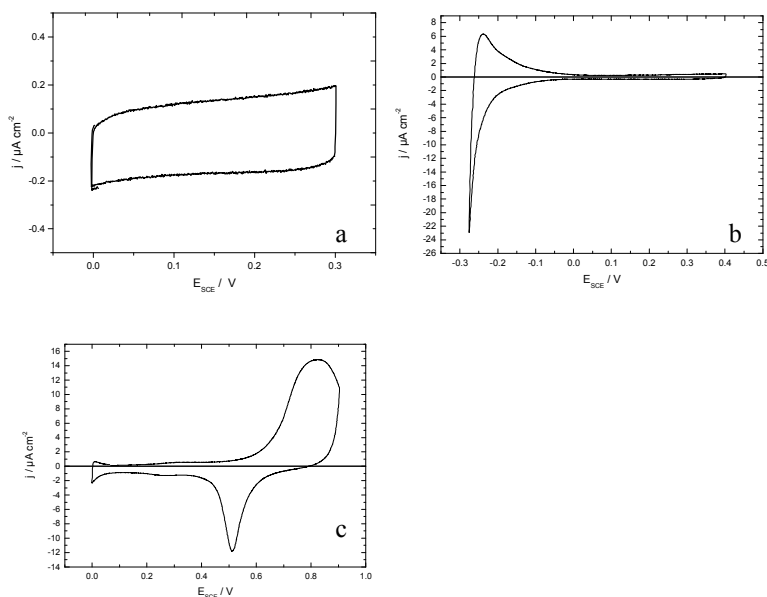


Figure 11. Cyclic voltammograms for 4-Mercaptopyridine modified Palladium monolayer on Au(111) in H_2SO_4 0,1M. Scan rate: 5 mV/s. Modification procedure: 6 min in $20\mu\text{M}$ PySSPy solution. They differ for their potential ranges: 0-0.3V (a); -0.28-0.4 (b); 0-0.9 (c).

STM analysis

STM of 4-Mercaptopyridine SAM on Au(111)/Pd

After the preparation of the SAM on Au(111)/Pd, the crystal was washed and connected in the STM cell with H_2SO_4 0,1M at a potential value comprising in the stability range.

The morphology of the surface was studied for surfaces modified with different procedures. Crystals modified for 6 and 12 minutes with $20\mu\text{M}$ 4,4'-Dithiodipyridine solution (Figures 12a and b) looked uniformly covered by the SAM that do not present ordered structures.

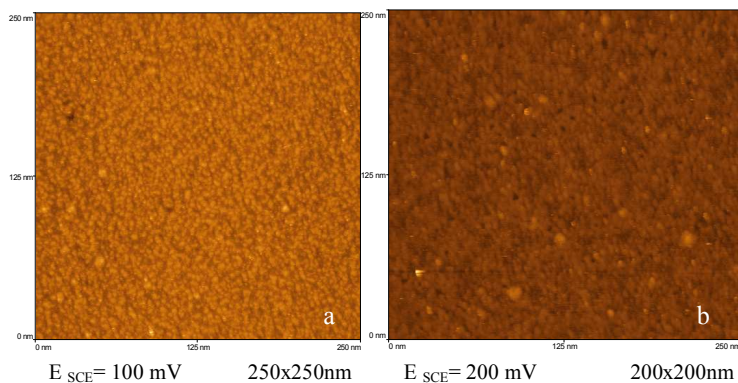
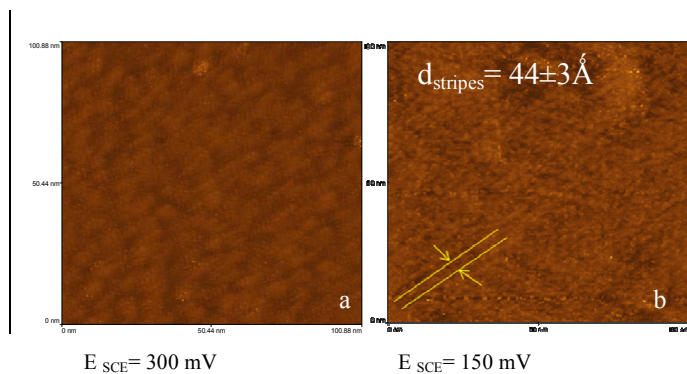


Figure 12. *in-situ* STM images of Au(111) covered by one layer of Palladium and a 4-Mercaptopyridine SAM in H_2SO_4 0,1M.. Procedure for SAM formation: 6 (Fig.a) and 12 (Fig.b) minutes in $20\mu M$ PySSPy solution.

An attempt to obtain ordered SAMs was done leaving the crystal in more concentrated solution for increasing times. A $100\mu M$ 4,4'-Dithiodipyridine solution was used with modification times of 20 minutes, 60 minutes and 19 hours, obtaining the three STM images of Figure 13, respectively.

While image 13a show the SAM still uniform but without molecular order, images 13b and c (corresponding to longer modification times of 1 and 19 hours) show a long-range order. Stripes observed in these images are about 40\AA distant.



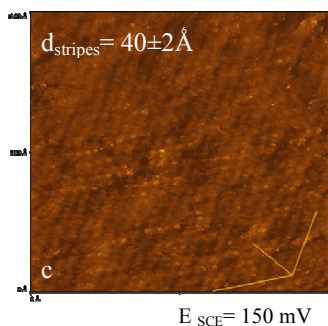


Figure 13. *in-situ* 100x100nm² STM images of Au(111) covered by one layer of Palladium and a 4-Mercaptopyridine SAM in H₂SO₄ 0,1M.. Procedure for SAM formation: 20 (Fig.a), 60 minutes (Fig.b) and 19 hours (Fig.c) in 100μM PySSPy solution.

Conclusion

4-Mercaptopyridine SAM on a single layer of Palladium on Au(111) was prepared and studied by cyclic voltammetry and EC-STM. Different procedures for SAM formation were performed changing the concentration of the thiol solution and the modification times. Within the stability potential range of the SAM in H₂SO₄ 0,1M (-0.2 ÷ 0.5V), *in-situ* STM images were registered. The microscopy investigation evidenced an uniform morphology of the SAM but without order at molecular level. Only with the use of longer modification times and higher concentrated thiol solution, STM images evidenced a long range order, in which stripes are 40 Å large. It is possible that the SAM needs longer time to organize and give ordered long range structures.

Therefore, a strong difference of behavior between the 4-Mercaptopyridine SAM on Au(111), where very ordered and compact structures are formed, and the same SAM on a Pd(111) layer has been evidenced. A possible cause of the different behavior could be due to the particular nature of the Palladium-SAM interface, that recent studies in literature hypnotize to contain both Sulfide and thiolate species. For this reason, a further investigation on the nature of the interface is demanded for a better understanding of the system.

3 CONCLUSIONS AND PERSPECTIVES

This thesis led to the realization, by means of electrodeposition, of nanometric and submicrometric materials with potential important applications.

The performance of surface limited electrodeposition methods, alone and combined with the use of appropriately designed templates, led to the obtainment of different types of nanostructures: monoatomic layers, nanostructured thin films and islands. These electrodeposition methods are Underpotential Deposition (UPD), Electrochemical Atomic Layer Epitaxy (ECALE), Surface Limited Redox Replacement (SLRR) and a new method that we called "Selective Electrodesorption Based Atomic Layer Deposition" (SEBALD), that is here presented for the first time and is still under study. Most of the work was done on Silver single crystals and is divided into three parts.

The first part deals with the electrodeposition of semiconductor thin films by the ECALE method. More precisely, a STM structural investigation was performed on the Sulfur layer deposited on Ag(100) and Ag(110) at underpotential, completing the overview of the Sulfur UPD on Silver low index faces. This Sulfur layer constitutes the first step of metal sulfide thin films preparation by ECALE. Then, compounds such as PbS and CdS have been obtained. Their preparation and their characterization by means of electrochemical techniques and AFM are described.

In the second part, different methods for metal electrodeposition controlled at atomic level are studied with the aim of preparing bimetallic catalysts with Silver. In fact, the possibility of synergic effects of some metals on the catalytic activity of Silver led us to study the way to perform controlled deposition. For those metals that do not give UPD on Silver, such as Cobalt or Iron, SEBALD and SLRR methods were used.

SEBALD is a novel electrochemical route to deposit monolayers of metals on Ag(111), here presented for the first time. It is based on the idea to exploit underpotential deposition of metals on Sulfur covered Silver, followed by the electrodesorption of Sulfur that leaves a monolayer of the metal. The method can also be used to obtain metal layers of controlled thickness. In fact, the basic ECALE cycle can also be repeated to increase the thickness of the sulfide, so that the successive selective desorption of Sulfur leaves increasing amounts of metals.

The method has been first examined using CdS, whose deposition conditions by ECALE on Ag(111) are well known. Thereafter, the method has been applied to the

deposition of Cobalt and Iron. A first morphological analysis of metal deposits obtained by SEBALD shows, at least in the cases under study, that they assemble in clusters.

Future investigation on SEBALD should verify the existence of a correlation between the number of ECALE cycles used to form the sulfide film and the dimensions of metal clusters remained after sulfur desorption. If this correlation exists, SEBALD would constitute a simple method to prepare surfaces with metal clusters of various sizes. Moreover, these resultant bimetallic nanostructures could be tested as catalysts towards Oxygen reduction, giving information on the influence of morphology at atomic level on this catalytic reaction.

The second way to perform controlled deposition at atomic level is constituted by the method known as Surface Limited Redox Replacement (SLRR), elaborated by Adžić et al.

According to this method, an ordered metal adlayer obtained by underpotential deposition is used as a template for deposition of a more noble metal. A replacement occurs via an irreversible and spontaneous redox process in which the UPD layer is oxidatively dissolved by cations of more noble metals, which are simultaneously reduced and deposited. Here, SLRR has been successfully used to deposit a single layer of Cobalt on Ag(111) by replacement of a Zinc monolayer previously formed at underpotential.

In the third part of the thesis, the same surface limited electrodeposition methods are performed on Silver surfaces covered by thiol based Self Assembled Monolayers used as templates. SAM are used as insulate layers that prevent deposition on Silver, except within their natural or artificial nanostructured holes. A first type of SAM patterned by μ Contact Printing was used to perform electrodeposition of CdS limited to stripes. A second type of pattern was originated by selective desorption of one component from a binary SAM. Two systems of binary SAMs (formed by 1-Octanethiol/3-Mercapto-1-propionic acid and 1-Dodecanethiol/3-Mercapto-1-propionic acid) were well characterized and samples of variable percentages of the single components were prepared. These templates were first characterized using CdS as an electrodeposition probe and then used for metal electrodeposition. The study of metallic nanostructures obtained on Silver with this method aims to design, develop and valuate a series of Platinum free catalysts for cathodes of Direct Alcohol Fuel Cells (DAFCs). Electrodeposition of nanolayers and nanoclusters of non-noble metals (Cobalt and Iron) on Silver, exploiting surface limited phenomena like underpotential deposition (UPD) and Surface Limited Redox Replacement (SLRR), was performed on the whole surface and on the surface covered by templates.

At the end of the thesis, two additional sections are dedicated to a project carried out during a period of research at the University of Ulm (Germany) under the

supervision of professor Kolb. It deals with electrodeposition on Gold single crystal and SAM formation.

First, Palladium Underpotential Deposition on Au(111) was studied by cyclic voltammetry and EC-STM. Then, a SAM of 4-Mercaptopyridine was prepared on a single layer of Palladium on Au(111) and studied by cyclic voltammetry and EC-STM. Different procedures for SAM formation were performed by changing the concentration of the thiol solution and the modification times. Within the stability potential range of the SAM in H_2SO_4 0,1M, in-situ STM images were recorded. The microscopy investigation evidenced an uniform morphology of the SAM but without order at molecular level. Only with the use of longer modification times and higher concentrated thiol solution, STM images evidenced a long range order, in which stripes are 40 Å large.

Therefore, a strong difference of behavior between the 4-Mercaptopyridine SAM on Au(111), where very ordered and compact structures are formed, and the same SAM on a Pd(111) layer has been evidenced. A possible cause of the different behavior could be due to the particular nature of the Palladium-SAM interface, that recent studies in literature hypotize to contain both sulfide and thiolate species. For this reason, a further investigation on the nature of the interface is demanded for a better understanding of the system.

4 REFERENCES

- ¹ Hodes, G., Ed. *Electrochemistry of Nanomaterials*; Wiley-VCH: Weinheim, 2001.
- ² K. Pandey, S. N. Sahu, S. Chandra, *Handbook of Semiconductors Electrodeposition*, Marcel Dekker, Inc, New York, 1996; Y. Golan, G. Hodes, I Rubinstein, *J. Phys. Chem.*, 100, 2220, 1996
- ³ R. Resh, T. Prohaska, G. Friedbacher, M. Grasserbauer, T. Kanninen, S. Lindroos, M. Leskelä, L. Niinistö, *Fres. J. Anal. Chem.* 53, 772, 1995
- ⁴ B. W. Gregory, J. L. Stickney, *J. Electroanal. Chem.*, 300, 543, 1991
- ⁵ Ceconi T.; Atrai A.; Bardi U.; Forni F.; Innocenti M.; Loglio F.; Foresti M. L.; Rovida G. *J. Electron Spectrosc. Rel. Phen.* 2001, 114-116, 563-568.
- ⁶ Innocenti, M.; Cattarin, S.; Cavallini, M.; Loglio, F.; Foresti, M. L. *J. Electroanal. Chem.* 2002, 532, 219-225.
- ⁷ Innocenti, M.; Cattarin, S.; Loglio, F.; Ceconi, T.; Seravalli, G.; Foresti, M. L. *Electrochim. Acta* 2004, 49, 1327-1337.
- ⁸ Foresti, M. L.; Pozzi, A.; Innocenti, M.; Pezzatini, G.; Loglio, F.; Salvietti, E.; Giusti, A.; D'Anca, F.; Felici, R.; Borgatti, F. *Electrochim. Acta*, 2006, 51, 5532-5539.
- ⁹ Riveros G, Gomez H, Henriguez R, Schrebler R, Maratti RE, Dalchiele EA (2001) *Sol Energy Mater Sol Cells* 70:255; Kumar V, Sharma TP (1998) *Opt Mater* 10:253.
- ¹⁰ Su B, Choy KL (2000) *Thin Solid Films* 102:361; Caicedo LM, Cediel G, Dussan A, Sandino JW, Calderon C, Gordillo G (2000) *Phys Status Soli B* 220:249.
- ¹¹ B.B. Blizanac, P.N. Ross and N.M. Markovic, *J. Phys. Chem. B* 110, 2006, 4735-4741.
- ¹² Markovic, N. M.; Ross, P. N. *Surf. Sci. Rep.*, 45, 2002, 117-230.
- ¹³ Blizanac, B. B.; Lucas, C.; Gallagher, M.; Arenz, M.; Ross, P. N.; Markovic, N. M. *J. Phys. Chem.*, 108, 2003, 625-634.
- ¹⁴ Adzic R. R. *Electrocatalysis*; Wiley-VCH: New York, 1998; pp197-242.
- ¹⁵ Schmidt, T. J.; Stamenkovic, V.; Ross, P. N.; Markovic, N. M. *Phys. Chem. Chem. Phys.* 5, 2003, 400-406.
- ¹⁶ B .B. Blizanac, P.N. Ross and N.M. Markovic, *Electrochim Acta*, 52, 2007, 2264-2271.
- ¹⁷ J.L. Fernandez, D. A. Walsh, A.J. Bard, *J. Am. Chem. Soc.*, 127, 2005, 357-365.
- ¹⁸ Y. Wang, P. B. Balbuena, *J. Phys. Chem. B* 109, 2005, 18902-18906
- ¹⁹ H.A. Hansen, J. Rossmeisl, J.K. Nørskov. *Phys. Chem. Chem. Phys.*, 2008, DOI: 10.1039/b803956a
- ²⁰ Zwetanova, A.; Juttner, K. *J. Electroanal. Chem.* 119, 1981, 149-164.

- ²¹ McIntyre, J. D. E.; Peck, W. F. *Electrochemistry at Single-Crystal Metal Electrodes. Electrocatalytic Effects on Surface Atomic Structure, Defects and Adatoms on Oxygen Reduction*; The Electrochemical Society: Pennington, NJ, 1984; pp 102-130.
- ²² T. Hurlen, Y. L. Sandler and E. A. Pantier, *Electrochim. Acta*, 11, 1966, 1463-1473
- ²³ Israel E. Wachs and Robert J. Madix, *Surf. Sci.*, 76, 1978, 531-558.
- ²⁴ L. Xiao, L. Zhuang, Y. Liu, J. Lu, H. D. Abruña, *J. Am. Chem. Soc.*, 2009, 131 (2), pp 602-608.
- ²⁵ D.M. Kolb, "Advances in Electrochemistry and Electrochemical Engineering", Gerischer, H., Tobias, H., Eds.; vol 11, John Wiley, New York, 1978, p.125.
- ²⁶ S. R. Brankovic, J.X. Wang and R.R. Adžić, *Surf. Sc.* 474, 2001, L173-L179.
- ²⁷ C. Thambidurai, Y.-G. Kim and J. L. Stickney, *Electrochim. Acta* 53, 2008, 6157-6164.
- ²⁸ Aloisi, G. D.; Cavallini, M.; Innocenti, M.; Foresti, M. L.; Pezzatini, G.; Guidelli, R. *J. Phys. Chem B* 1997, 101, 4774-4780.
- ²⁹ J. C. Love, L.A. Estroff, J.K. Kriebel, R. G. Nuzzo, G.M. Whitesides, *Chem. Rev.*, 2005, 105 (4), 1103-1170.
- ³⁰ Tour, J. M. *Acc. Chem. Res.* 2000, 33, 791.
- ³¹ Zehner, R. W.; Parsons, B. F.; Hsung, R. P.; Sita, L. R. *Langmuir* 1999, 15, 1121.
- ³² Baunach, T.; Kolb, D. M. *Anal. Bioanal. Chem.* 2002, 373, 743.
- ³³ Armstrong, F. A.; Hill, H.A.O.; Walton, N.J. *Acc Chem. Res.*, 1988, 21, 407.
- ³⁴ Cricenti A.; Scarselli M.A.; Paleari R.; Mosca A. *J. Vac. Sci. Technol.*, B 1994, 12, 1494.
- ³⁵ Mosca A.; Paleari R.; Arosio P.; Cricenti A.; Scarselli M.A.; Generosi R.; Selci S.; Rovida E. *J. Vac. Sci. Technol.*, B 1994, 12, 1486.
- ³⁶ S. Caporali, S. Bellandi, M. Innocenti, O. Lopilato, L. Romualdi and G. Pezzatini., *Gold Bulletin*, Volume 43 No 2, 2010, 122-130.
- ³⁷ T. Baunach, V. Ivanova, D. M. Kolb, H. Boyen, P. Ziemann, M. Büttner, P. Oelhafen, *Adv. Mater.* 2004, 16 (22), 2024.
- ³⁸ F. Eberle, M. Saitner, H.-G. Boyen, J. Kucera, A. Gross, A. Romanyuk, P. Oelhafen, M. D'Olieslaeger, M. Manolova and D.M. Kolb, *Angew. Chem. Int. Ed.* 49, 2009, 341-345.
- ³⁹ Kumar, A.; Whitesides, G. M. *Appl. Phys. Lett.* 1993, 63, 2002-2004
- ⁴⁰ Kumar, A.; Biebuyck, H. A.; Whitesides, G. M. *Langmuir* 1994, 10, 1498.
- ⁴¹ Cavallini M, Facchini M, Albonetti C, Biscarini F, Innocenti M, Loglio F, Salvietti E, Pezzatini G, Foresti ML. *J Phys Chem C* 2000;111(3):1061.
- ⁴² Salvietti E, Loglio F, Innocenti M, Cavallini M, Facchini M, Pezzatini G, Raiteri R, Foresti ML. *Electrochim Acta* 2007;52(19):6034.

- ⁴³ Bain C. D.; Whitesides, G. M., *J. Am. Chem. Soc.* 1988, 110, 6560. Laibinis P.E., Fox M.A; Folkers J.P; Whitesides, G. M; *Langmuir* 1991, 7, 3167.
- ⁴⁴ Bain, C. D.; Biebuyck, H. A.; Whitesides, G. M. *Langmuir* 1989, 5, 723.
- ⁴⁵ Bain, C. D.; Whitesides, G. M. *J. Am. Chem. Soc.* 1988, 110, 3665.
- ⁴⁶ Bain, C. D.; Whitesides, G. M. *J. Am. Chem. Soc.* 1989, 111, 7164.
- ⁴⁷ Bain, C. D.; Whitesides, G. M. *Langmuir* 1989, 5, 1370.
- ⁴⁸ Laibinis, P. E.; Fox, M. A.; Folkers, J. P.; Whitesides, G. M. *Langmuir* 1991, 7, 3167.
- ⁴⁹ Folkers, J. P.; Laibinis, P. E.; Whitesides, G. M. *Langmuir* 1992, 8, 1330.
- ⁵⁰ Laibinis, P. E.; Whitesides, G. M. *J. Am. Chem. Soc.* 1992, 114, 1990.
- ⁵¹ Laibinis, P. E.; Nuzzo, R. G.; Whitesides, G. M. *J. Phys. Chem.* 1992, 96.
- ⁵² Biebuyck, H. A.; Whitesides, G. M. *Langmuir* 1993, 9, 1766.
- ⁵³ Folkers, J. P.; Laibinis, P. E.; Whitesides, G. M.; Deutch, J. J. *J. Phys. Chem.* 1994, 98, 563.
- ⁵⁴ Munakata, H.; Kuwabata, S.; Ohko, Y.; Yoneyama, H. *J. Electroanal. Chem.* 2001, 496, 29–36.
- ⁵⁵ Imabayashi, S.; Hobara, D.; Kakiuchi, T.; Knoll, W. *Langmuir* 1997, 13.
- ⁵⁶ Munakata, H.; Kuwabata, S.; Ohko, Y.; Yoneyama, H. *J. Electroanal. Chem.* 2001, 496, 29–36.
- ⁵⁷ Takami, T.; Delamarche, E.; Michel, B.; Gerber, C.; Wolf, H.; Ringsdorf, H. *Langmuir* 1995, 11, 3876.
- ⁵⁸ Stranick, S.J.; Parikh, A. N.; Tao, Y.T.; Allara, D.L.; Weiss, P.S. *J. Phys. Chem.* 1994, 98, 7636.
- ⁵⁹ Sato, Y.; Yamada, R.; Mizutani, F.; Uosaki, K. *Chem. Lett.* 1997, 987.
- ⁶⁰ Hobara, D.; Ota, M.; Imabayashi, S.; Niki, K.; Kakiuchi, T. *J. Electroanal. Chem.* 1998, 444, 113.]
- ⁶¹ Imabayashi, S.; Hobara, D.; Kakiuchi, T.; Knoll, W. *Langmuir* 1997, 13.
- ⁶² Hobara, D.; Sasaki, T.; Imabayashi, S.; Kakiuchi, T. *Langmuir* 1999, 15, 5073–5078.
- ⁶³ Rovida, G.; Pratesi, F. *Surf. Sci.* 1981, 104, 609-624.
- ⁶⁴ Yu, M.; Woodruff, D.P.; Satterley, C. J.; Jones, R.G.; Dhanak, V.R. *J. Phys. Chem. C* 2007, 111, 3152-3162.
- ⁶⁵ Cavallini, M.; Bracali, M.; Aloisi, G.; Guidelli, R. *Langmuir* 1999, 15, 3003-3006.
- ⁶⁶ Wan, L. I.; Shundo, S.; Inumai, J.; Itaya, K. *Langmuir* 2000, 16, 2164-2168.
- ⁶⁷ Hatchett D. W.; White H. S. *J. Phys. Chem.* 1996, 100, 9854.
- ⁶⁸ Hatchett, D. W.; Ga, X.; Catron, S. W.; White, H. S. *J. Phys. Chem.* 1996, 100, 331.
- ⁶⁹ Lay, M. D.; Varazo, K.; Stickney, J. L. *Langmuir* 2003, 19, 8416-8427.

- ⁷⁰ Schlaup, C.; Friebel, D.; Broekmann, P.; Wandelt, K. *Surf. Sci.* 2008, 602, 864-870.
- ⁷¹ Spänig, A.; Broekmann, P.; Wandelt, K. *Electrochim. Acta* 2005, 50, 4289-4296.
- ⁷² Spänig, A.; Broekmann, P.; Wandelt, K. *Z. Phys. Chem.* 2003, 217, 459-477.
- ⁷³ Demir, U.; Shannon, C. *Langmuir* 1996, 12, 594-596.
- ⁷⁴ Foresti, M.L.; Capolupo, F.; Innocenti, M.; Loglio, F. *Cryst. Growth Des.* 2002, 2, 73.
- ⁷⁵ Hamelin, A. In *Modern Aspects of Electrochemistry*; Conway, B.E., White, R. E., Bockris J.O'M., Eds.; Plenum Press: New York, 1985; Vol. 16, p.1.
- ⁷⁶ T. Kurasawa (1960) Patent Japan 35:5619
- ⁷⁷ Innocenti, M.; Pezzatini, G.; Forni, F.; Foresti, M. L. *J. Electrochem. Soc.* 2001, 148(5), C357-C362.
- ⁷⁸ G. Valette, *J. Electroanal. Chem.* 1987, 224, 285-294.
- ⁷⁹ Innocenti, M.; Foresti, M. L.; Fernandez, A.; Forni, F.; Guidelli, R. *J. Phys. Chem. B* 1998, 102, 9667-9676.
- ⁸⁰ Maestre, M. S.; Rodríguez-Amaro, R.; Muñoz, E.; Ruiz, J. J.; Camacho L. *J. Electroanal. Chem.* 1994, 373, 1-2, 31-37.
- ⁸¹ Foresti, M. L.; Innocenti, M.; Forni, F.; Guidelli, R. *Langmuir* 1998, 14, 7008-7016.
- ⁸² Software Reflectivity Tool Parrat 1999, 32, HMI, Berlin.
- ⁸³ L.G.Parratt *Phys. Rev.* 1954, 95, 359.
- ⁸⁴ L.Nevot, P.Croce *Revue Phys.Appl.* 15, 761 (1980).
- ⁸⁵ E. Lastraioli, F. Loglio, M. Cavallini, F. Simeone, M. Innocenti, F. Carla', M. L. Foresti, *Langmuir*, 26 (22), 2010, 17679-17685.
- ⁸⁶ Meldrun F. C., Flath J., Knoll W. (1999) *Thin Solid Films* 348:188.
- ⁸⁷ Markov V. F., Maskaeva L. N. (2001) *J. Anal. Chem.* 56:754.
- ⁸⁸ Mady A. K., Girgis A., Mady A. H., Moustaf R. (1987) *Phys. Status Solidi A* 100:107.
- ⁸⁹ Sharon M., Ramaiah K. S., Kumar M., Neumann-Spallart M., Levy-Clement C. 1997, *J. Electroanal. Chem.* 436:49
- ⁹⁰ Puiso J., Lindroos S., Tamulevicius S., Leskela M., Snitka V. (2003) *Thin Solid Films*. 428:223.
- ⁹¹ Kannianen T., Lindroos S., Resch R., Leskela M., Friedbacher G., Grasserbauer M. (2000) *Materials Research Bulletin* 35:1045.
- ⁹² Gadave K. M., Jodgudri S. A., Lokhande C. D. (1994) *Thin Solid Films* 245:7
- ⁹³ Torimoto T., Takabayashi S., Mori H., Kuwabata S. *J. Electroanal. Chem* 2002, 522:33.
- ⁹⁴ Öznülür T., Erdoğan I., Şişman I., Demir Ü. *Chem. Mater.*, 2005, 17(5):935

- ⁹⁵ Fernandes, V.C., Salvietti E., Loglio F., Innocenti M., Mascaro L. H., Foresti M. L. *ECS Transactions*, 2007, 11(7):279.
- ⁹⁶ Toney M., Gordon J. G., Samant M. G., Borges G. L., Melroy O. R., Yee D., Sorensen L. *B.J. Phys. Chem.* 1995, 99:4733 and references therein
- ⁹⁷ Foresti M.L., Pezzatini G., Cavallini M., Aloisi G., Innocenti M., Guidelli R. *J. Phys. Chem. B* 1998, 102:7413.
- ⁹⁸ Innocenti M., Cattarin S., Cavallini M., Loglio F., Foresti M.L. *J. Electroanal. Chem.* 2002, 53: 2219.
- ⁹⁹ Loglio F., Innocenti M., Pezzatini G., Foresti M.L. *J. Electroanal. Chem.* 2004, 562:117.
- ¹⁰⁰ Innocenti M., Cattarin S., Loglio F., Cecconi T., Seravalli G., Foresti M.L. *Electrochim. Acta* 2004, 49:1327.
- ¹⁰¹ Sackmann J., Bunk A., Potschke R. T., Staikov G., Lorenz W. *Electrochim. Acta* 1998, 43:2863.
- ¹⁰² Nowak P., Laajalehto K. *Applied Surface Science.* 2000, 157:101
- ¹⁰³ Mikhlin Y. L., Romanchenko A. S., Shagaev A. A. *Applied Surface Science* 2006, 252:5645.
- ¹⁰⁴ Cavallini M, Facchini M, Albonetti C, Biscarini F, Innocenti M, Loglio F, Salvietti E, Pezzatini G, Foresti ML. *J Phys Chem C*
- ¹⁰⁵ Salvietti E, Loglio F, Innocenti M, Cavallini M, Facchini M, Pezzatini G, Raiteri R, Foresti ML. *Electrochim Acta* 2007;52(19):6034.
- ¹⁰⁶ Wilbur JL, Kumar A, Kim E, Whitesides GM. *Adv Mater* 1994;6:600.
- ¹⁰⁷ Kumar A, Whitesides GM. *Appl Phys Lett* 1993;63:2002.
- ¹⁰⁸ Kumar A, Biebuyck HA, Whitesides GM. *Langmuir* 1994;10:1498.
- ¹⁰⁹ Xia Y, Whitesides GM. *Angew Chem Int Ed* 1998;37:551.
- ¹¹⁰ Xia Y, Rogers JA, Paul KE, Whitesides GM. *Chem Rev* 1999;99:1823.
- ¹¹¹ Geissler M, Wolf H, Stutz R, Delmarche E, Grummt UW, Michel B, Bietsch A. *Langmuir* 2003;19:6301.
- ¹¹² Munakata, H.; Kuwabata, S.; Ohko, Y.; Yoneyama, H. *J. Electroanal. Chem.* 2001, 496, 29–3.
- ¹¹³ Laibinis, P. E.; Fox, M. A.; Folkers, J. P.; Whitesides, G. M. *Langmuir* 1991, 7, 3167.
- ¹¹⁴ Miller, C.; Cuendet, P.; Grätzel, M. *J. Phys. Chem.* 1991, 95, 877.
- ¹¹⁵ Finklea, H. O.; Avery, S.; Lynch, M.; Furtch, T. *Langmuir* 1987, 3, 409.
- ¹¹⁶ Amatore, C.; Saveant, J. M.; Tessier, D. J. *J. Electroanal. Chem.* 1983, 147, 39.
- ¹¹⁷ Ganesh, V.; Pandey, R. R.; Malhotra, B. D.; Lakshminarayanan, V. *J. Electroanal. Chem.* 2008, 619–620, 87.
- ¹¹⁸ N.M. Markovic, T.J. Schmidt, V. Stamenkovic and P.N. Ross, *Fuel Cells* 2001, 1, No 2, 105-116.

-
- ¹¹⁹ M. Innocenti, S. Bellassai, C. Bianchini, F. Carlà, F. Loglio, L. Polonia, F. Vizza, M. L. Foresti, *Elettrochimica Acta*, 2010, 55, 2550-2554.
- ¹²⁰ J. Guo, A. Hsu, D. Chu, R. Chen *J. Phys. Chem. C* 2010, 114, 4324-4330.
- ¹²¹ B.B. Blizanac, P.N. Ross and N.M. Markovic, *J. Phys. Chem. B* 2006, 110, 4735-4741.
- ¹²² J. Tang, M. Petri, L.A. Kibler, D.M. Kolb *Electrochim. Acta*, 51, 2005, 125-132.
- ¹²³ F.A. Armstrong, H.A.O. Hill, N.J. Walton *Acc. Chem. Res.*, 1988, 21, 407.
- ¹²⁴ A. Cricenti, M.A. Scarselli, R. Paleari, A. Mosca *J. Vac. Sci. Technol. B*, 1994, 12, 1494.
- ¹²⁵ A. Mosca, R. Paleari, P. Arosio, A. Cricenti, M.A. Scarselli, R. Generosi, S. Selci, E. Rovida *J. Vac. Sci. Technol. B* 1994, 12, 1486.
- ¹²⁶ P. Carro, G. Corthey, A.A. Rubert, G.A. Benitez, M.H. Fonticelli, R.C. Salvarezza *Langmuir* 2010, 26(18), 14655-14662.
- ¹²⁷ T. Baunach, V. Ivanova, D. M. Kolb, H. Boyen, P. Ziemann, M. Büttner, P. Oelhafen, *Adv. Mater.* 2004, 16 (22), 2024.